



# Ice-Ocean Exchange Processes in the Jovian and Saturnian Satellites

Krista M. Soderlund<sup>1</sup> · Klára Kalousová<sup>2</sup> · Jacob J. Buffo<sup>3</sup> · Christopher R. Glein<sup>4</sup> · Jason C. Goodman<sup>5</sup> · Giuseppe Mitri<sup>6,7</sup> · G. Wesley Patterson<sup>8</sup> · Frank Postberg<sup>9</sup> · Marc Rovira-Navarro<sup>10,11</sup> · Tina Rückriemen<sup>12,13</sup> · Joachim Saur<sup>14</sup> · Britney E. Schmidt<sup>3</sup> · Christophe Sotin<sup>15</sup> · Tilman Spohn<sup>13,16</sup> · Gabriel Tobie<sup>17</sup> · Tim Van Hoolst<sup>18,19</sup> · Steven D. Vance<sup>15</sup> · Bert Vermeersen<sup>10,11</sup>

Received: 16 July 2019 / Accepted: 9 June 2020  
© Springer Nature B.V. 2020

**Abstract** A growing number of satellites in the outer solar system likely have global oceans beneath their outer icy shells. While the presence of liquid water makes these ocean worlds compelling astrobiological targets, the exchange of heat and materials between the deep interior and the surface also plays a critical role in promoting habitable environments. In this article, we combine geophysical, geochemical, and geological observations of the Jovian satellites Europa, Ganymede, and Callisto as well as the Saturnian satellites Enceladus

---

Ocean Worlds

Edited by Athena Coustenis, Tilman Spohn, Rafael Rodrigo, Kevin P. Hand, Alexander Hayes, Karen Olsson-Francis, Frank Postberg, Christophe Sotin, Gabriel Tobie, Francois Raulin and Nicolas Walter

---

✉ K.M. Soderlund  
[krista@ig.utexas.edu](mailto:krista@ig.utexas.edu)

<sup>1</sup> Institute for Geophysics, Jackson School of Geosciences, The University of Texas at Austin, J.J. Pickle Research Campus, Bldg. 196, 10100 Burnet Road (R2200), Austin, TX 78758-4445, USA

<sup>2</sup> Charles University, Faculty of Mathematics and Physics, Department of Geophysics, Prague, Czech Republic

<sup>3</sup> Georgia Institute of Technology, Atlanta, GA, USA

<sup>4</sup> Southwest Research Institute, San Antonio, MA, USA

<sup>5</sup> Wheaton College, Norton, MA, USA

<sup>6</sup> International Research School of Planetary Sciences, Università d'Annunzio, Pescara, Italy

<sup>7</sup> Dipartimento di Ingegneria e Geologia, Università d'Annunzio, Pescara, Italy

<sup>8</sup> Johns Hopkins University Applied Physics Laboratory, Laurel, MD, USA

<sup>9</sup> Freie Universität Berlin, Berlin, Germany

<sup>10</sup> Technische Universiteit Delft, Delft, The Netherlands

<sup>11</sup> NIOZ Royal Netherlands Institute for Sea Research, Yerseke, The Netherlands

<sup>12</sup> TU Berlin, Berlin, Germany

<sup>13</sup> DLR Institute of Planetary Research, Berlin, Germany

<sup>14</sup> University of Cologne, Cologne, Germany

and Titan to summarize our current state of understanding of their interiors and surface exchange processes. Potential mechanisms for driving exchange processes upward from the ocean floor and downward from the satellite surface are then reviewed, which are primarily based on numerical models of ice shell and ocean dynamics and complemented by terrestrial analog studies. Future missions to explore these exo-oceans will further revolutionize our understanding of ice-ocean exchange processes and their implications for the habitability of these worlds.

**Keywords** Ice-ocean exchange · Europa · Ganymede · Callisto · Enceladus · Titan

A primary motivation for understanding ice-ocean exchange processes is to determine whether the conditions conducive to life exists (e.g., Hendrix et al. 2019). If life has developed, exchange between the ocean and ice shell also has practical implications for the search of biosignatures and planetary protection. In addition, this exchange may be a critical factor in explaining their surface geologies and origin/distribution of endogenic materials, as well as the satellite's overall evolution. Different manifestations across icy ocean worlds likely also contribute to the wide variety of satellite characteristics observed. Finally, by understanding these processes broadly across the solar system, we provide another natural laboratory to test physical, chemical, and biological hypotheses developed for Earth and other contexts.

In this article, we review ice-ocean exchange processes in outer solar system satellites that are the best candidates to host subsurface oceans: the icy Galilean satellites Europa, Ganymede, and Callisto and the Saturnian satellites Enceladus and Titan. While Neptune's satellite Triton and Kuiper belt objects such as Pluto may also have subsurface oceans (e.g., Hussmann et al. 2006; Nimmo et al. 2016), they are not as well studied nor considered explicitly here. Section 1 summarizes our current state of knowledge of the interiors of these moons, Sect. 2 describes surface exchange processes, Sect. 3 describes ice shell dynamics and exchange processes, Sect. 4 describes ocean dynamics and exchange processes, Sect. 5 describes terrestrial analogs, and Sect. 6 concludes with implications for habitability and future exploration.

## 1 Interiors of Icy Ocean Worlds

Most of what we know about the interiors of known icy ocean worlds comes from the *Galileo* (1989-2003) and *Cassini-Huygens* (1997-2017) missions. As reviewed by Hussmann et al. (2015) among others, the interiors of icy satellites are explored through the following data: radius and mass, gravity field, magnetic field, rotational state and shape/topography, surface temperatures and heat flow, composition of surface and atmosphere, activity at the surface,

---

<sup>15</sup> Jet Propulsion Laboratory-California Institute of Technology, Pasadena, USA

<sup>16</sup> International Space Science Institute, Bern, Switzerland

<sup>17</sup> Laboratoire de Planétologie et Géodynamique, UMR-CNRS 6112, Université de Nantes, Nantes, France

<sup>18</sup> Royal Observatory of Belgium, Brussels, Belgium

<sup>19</sup> Institute of Astronomy, KU Leuven, Leuven, Belgium

and knowledge of its formation and evolution including surface geology and tectonics, orbital dynamics, and chemical environment during accretion. Complementary to these observational data are laboratory and numerical data on the material properties of water/ice, rock, and metal, as well as their equations of state (e.g., Choukroun and Grasset 2010; Vance and Brown 2013; McDougall and Barker 2011; Lemmon et al. 2007; Connolly 2009; Balog et al. 2003). In this section, we first review the differentiation states and ocean existence, followed by more detailed descriptions of interior structures of the most prominent ocean worlds among the outer solar system satellites.

## 1.1 Differentiation and Ocean Existence

Mass and radius allow calculation of the mean density and an assessment of whether a satellite is rich in rock/iron or in ice. The gravity data, in particular the  $J_2$  and  $C_{22}$  components<sup>1</sup> (e.g., Anderson et al. 1996, 1998b,a, 2001), can be used to derive the moment of inertia factor (MoI) if the satellite can be assumed to be in hydrostatic equilibrium. Only for Titan have both gravitational coefficients been determined and this ratio of nearly 10/3 is compatible with hydrostatic equilibrium at  $2\sigma$  (Durante et al. 2019). Together with mass and radius, the MoI allows construction of simple, albeit non-unique, interior structure models that indicate whether or not a satellite has differentiated. The MoI factor of a homogeneous density sphere is 0.4, and a smaller value indicates an increase of density with depth, hence possible differentiation. Ice on the surface together with a low enough value of the moment of inertia factor allows speculation about a water/ice layer on top of a rock layer. Table 1 collects data on the mass, radii, and MoI of major icy satellites of the solar system.

The bulk densities of Ganymede, Callisto, Enceladus, and Titan suggest that their interiors contain 40 to 60% of ice/water, while Europa is a predominantly rocky body with a bulk ice/water mass fraction of only 6-9% (Hussmann et al. 2015). The level of differentiation of the interiors, however, likely differs between the satellites. Europa and Ganymede are thought to be fully differentiated into a central metallic core, a silicate mantle, and outer water ice-liquid shell (e.g., Anderson et al. 1996, 1998b). Enceladus is differentiated with a water ice-liquid outer shell and central rocky core that may be porous given the satellite's low mass and mean density, which prohibits a substantial metallic contribution (e.g., Iess et al. 2014; Roberts 2015; Ćadek et al. 2016; Beuthe et al. 2016). In contrast, Callisto and Titan may be only partially differentiated with an H<sub>2</sub>O layer overlying a core of ice mixed with rocks and metal up to significant depth, maybe up to the center (e.g., Anderson et al. 1998b; Sohl et al. 2003; Iess et al. 2010; Castillo-Rogez and Lunine 2010; Tobie et al. 2005; Gao and Stevenson 2013; Baland et al. 2014). A model of slow and incomplete differentiation of Callisto has been discussed by Nagel et al. (2004), while Barr and Canup (2010) suggest partial differentiation of Titan due to undifferentiated accretion and core formation due to impacts that allowed only some of Titan's rock to form a core.

It is widely agreed that these icy satellites have an outer ice I layer that is, in most cases, underlain by an ocean. The strongest observational evidence for the icy Galilean satellites

<sup>1</sup>  $J_2$  and  $C_{22}$  are coefficients in the spherical harmonic representation of the gravity field outside a satellite. If the satellite is a spherically symmetric rotating body, its equilibrium physical shape will be an oblate spheroid. In that case,  $J_0$  measures the mass of the satellite and  $J_2$  the flattening of its gravity field. In the case of a tidally deformed body, the equilibrium figure is triaxial and  $C_{22}$  is the dominant coefficient describing the deformation of the gravity field due to rotation and tidal deformation. If  $C > B > A$  are the principal moments of inertia of the satellite, then in case of the spherically symmetric rotating body  $A=B$  and  $Ma^2 J_2 = C - A$ , where  $M$  and  $a$  are the mass and equatorial radius of the satellite. For the tidally deformed body,  $4Ma^2 C_{22} = B - A$ .

**Table 1** Mass, radii, and moment of inertia of major icy satellites of the solar system. Data: Hussmann et al. (2015) for Europa, Ganymede, and Callisto; Iess et al. (2014), Roatsch et al. (2009), and Jacobson et al. (2006) for Enceladus; and Durante et al. (2019) for Titan

	Europa	Ganymede	Callisto	Enceladus	Titan
Mass ( $10^{22}$ kg)	4.8	14.8	10.8	0.01	13.5
Radius (km)	1565	2631	2410	252	2575
Mean density (kg)	2989	1942	1835	1609	1881
MoI	0.346	0.312	0.355	0.335	0.341

was the detection of magnetic induction signals counteracting the time-variable magnetic field of Jupiter in the satellites' rest frames (Khurana et al. 1998; Neubauer 1998; Zimmer et al. 2000; Kivelson et al. 2002). These signals are best explained by the presence of an electrically conducting fluid (i.e. a salty ocean) beneath the surface of the satellite. For Europa, strong geologic evidence for a global subsurface ocean also exists (e.g., Pappalardo et al. 1999), and observations of oscillations in auroral ovals by the *Hubble Space Telescope* have confirmed that Ganymede has a global subsurface ocean (Saur et al. 2015). The locations of the auroral ovals are controlled by Ganymede's magnetic field environment. Thus, a time-series of auroral images allows the evolution of the induction signals from Ganymede's interior to be monitored. In contrast, the case for Callisto is less clear since induction within the satellite's ionosphere may also explain the observed magnetic fields (Hartkorn and Saur 2017).

For satellites of Saturn, the same approach is not feasible since Saturn's magnetic field is not inclined with respect to the rotation axis, in contrast to Jupiter (dipole tilt of 9 degrees), and therefore the satellites do not sense a systematic time-periodic field in their rest frame. Instead, the existence of subsurface oceans and characterisation of their properties have relied on a variety of other methods. *Cassini* measurements of water vapour (e.g., Porco et al. 2006; Dougherty et al. 2006) and salty grains from geysers on Enceladus (e.g., Postberg et al. 2009) indicated the existence of water reservoirs beneath the surface, and the global character of the distribution of water as a subsurface ocean was demonstrated by gravity data (e.g., McKinnon 2015) and libration measurements (Thomas et al. 2016). Evidence for a subsurface ocean on Titan is based on the tidal Love number estimation from time-varying gravity field (Iess et al. 2012), detection of an electric perturbation by the *Huygens* probe during its descent through Titan's atmosphere that was interpreted as a Schumann resonance (Béghin et al. 2012), and precise measurements of the spin pole orientation (e.g., Baland et al. 2014).

Depending on the total amount of  $H_2O$  (solid or liquid), the bottom of the water layer may interface to a rocky layer as in the case of Europa and Enceladus or to a layer of high pressure ice phases that are denser than liquid and therefore decouple the ocean from the rocky layer. In case of Enceladus and Europa, whose hydrospheres are about 60 and 80–170 km thick, respectively (Čadek et al. 2016; Anderson et al. 1998b), the pressures at the hydrosphere-rock interface are  $\sim 7$  MPa and  $\sim 150$ – $200$  MPa, respectively, which is too low to crystallize high-pressure ice (note that the triple point of ice I, ice III, and liquid water is at  $\sim 210$  MPa). In case of large satellites, the pressures at the hydrosphere-rock interface are much higher with 1500–1700 MPa expected for Ganymede and 650–850 MPa for Titan (Vance et al. 2018a), thus leading to crystallization of ice VI (cf. also Fig. 1). For Callisto, the large uncertainty in the value of MoI results in the uncertainty of hydrosphere thickness. The corresponding hydrosphere-rock interface pressures can be either  $\sim 500$  MPa

( $\text{MoI} = 0.355$ ) or  $\sim 1000$  MPa ( $\text{MoI} = 0.32$ ) (Vance et al. 2018a) leading to ice V or ice VI layer crystallization, respectively. It is also possible that the underlying ice layer is mixed with rock as may be the case for Callisto and Titan if these are incompletely differentiated. More detailed discussions on the high-pressure ice layer can be found in Journaux et al. (2020).

The feasibility of subsurface oceans from energy balances of the satellites has been concluded by, for example, Spohn and Schubert (2003), Hussmann et al. (2006), and others (compare Sect. 3 below). Maintaining an ocean until the present day requires energy sources and/or the depression of the ice melting point due to the inclusion of other components such as salts or ammonia. Possible energy sources are internal heating coming from radioactive decay in the rocky part of the satellite (e.g., Spohn and Schubert 2003); dissipation of tidal energy in the rocky interior (e.g., Choblet et al. 2017a), the ocean (e.g., Tyler 2009; Wilson and Kerswell 2018), and/or the outer ice shell (e.g., Hussmann et al. 2006); and ohmic dissipation in the ocean (Gissinger and Petitdemange 2019). Tidal heating is likely important for Europa and Enceladus, but less so for Titan, Ganymede, and Callisto. This is because of Europa's proximity to Jupiter and the Laplace resonance and because Enceladus likely has a porous core that maintains strong tidal friction; both satellites also have the smallest pressure gradient, shifting the water ice triple point to greater depth. Ohmic dissipation is expected to be relatively weak, but can be enhanced locally (Gissinger and Petitdemange 2019, see Sect. 4.3). Another crucial factor in sustaining an ocean is heat transport in the ice I layer. Spohn and Schubert (2003) (see also references cited in Sect. 3 below) investigated various scenarios assuming a purely conductive and a convective ice I layer. They find that for pure water ice, convection might lead to complete freezing of the oceans, although the results depend on uncertain parameter values for the viscosity of the ice I layer and the scaling of convective vigor. A present-day global ocean for Enceladus has proven hard to explain based on thermal evolution models, which predict heat production rates given by present orbital conditions below the expected global heat flow (Roberts and Nimmo 2008; Tobie et al. 2008). The discrepancies between estimates of surface heat flow and tidal heating rates could potentially be explained if Enceladus formed relatively recently, if tidal heating and cooling were highly time variable rate (episodic or periodic), or if the effective rate of dissipation within Saturn is larger than the conventional value (O'Neill and Nimmo 2010; Lainey et al. 2012; Nimmo et al. 2018).

## 1.2 Internal Structure

With this general picture in mind, we will now review more detailed structures for each of the satellites. Interior models that represent possible internal structures of Jovian and Saturnian icy ocean worlds are shown in Fig. 1.

### 1.2.1 Europa

Gravity data in combination with the mass and radius constraints permit construction of density profiles with radius. These profiles typically take the form of three-layer interior models with an outer ice-liquid water layer, a rocky mantle, and a central metallic core for Europa. Hydrostatic equilibrium is also assumed because independent measurements of  $C_{22}$  and  $J_2$  are lacking (e.g., Schubert et al. 2004). For a three-layer model, the core and mantle radii can be determined if the density of each layer is assumed, leading to uncertainties in their values. In addition, solid ice and liquid water layers cannot be distinguished due to the small density contrast between them. These models suggest that Europa has an outer

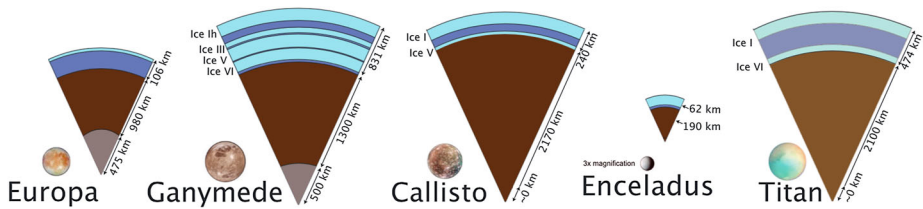


**Fig. 1** Spherically symmetric internal structure models that are consistent with geophysical constraints and use state-of-the-art equations of state and thermodynamic properties from Vance et al. (2018a). *Cassini* radio science and imaging measurements provide further details for the structures of Enceladus (Čadek et al. 2019; Hemingway and Mittal 2019) and Titan (Corlies et al. 2017; Durante et al. 2019), revealing that their ice shells are not uniform in thickness, likely owing to thermal or compositional heterogeneities. More yellowish shades for Titan were applied to highlight the likelihood of extensive organic content (see Sect. 1.2.5)

H<sub>2</sub>O layer that ranges from 80 km to 170 km (Anderson et al. 1998b; Sohl et al. 2002). Geologic and geodynamic arguments predict ice shell thicknesses that range from  $\sim 3$  km to  $>30$  km based on mechanical, thermal, cratering, and other methods (Billings and Kattenhorn 2005, see their Table 1 for a summary). The core radius depends on its assumed composition as well as the water layer thickness, ranging from 700 km for a Fe-FeS eutectic core composition and 100 km thick water layer to 200 km for a pure Fe core composition and 170 km thick water layer (Sohl et al. 2002). Mantle densities are consistent with an olivine-dominated mineralogy, becoming increasingly forsterite rich with decreasing water layer thickness (Sohl et al. 2002).

Magnetic field measurements add additional constraints on the interior structure and composition because their observational characterisation can, in principle, constrain the electrical conductivity, depth beneath the surface, and thickness of the ocean (e.g., Zimmer et al. 2000; Khurana et al. 2002; Seufert et al. 2011). Since the *Galileo* mission only observed induction from the main signal caused by Jupiter’s synodic period seen in the satellite’s rest frame, it was not possible to estimate these parameters individually. Schilling et al. (2007) found magnetic field data are best explained by electrical conductivity values of  $\gtrsim 0.5$  S/m with ocean thicknesses of  $\lesssim 100$  km. However, these numbers are subject to ambiguity because other values rendering the same product of conductivity and ocean thickness agree with the measurements comparably well. Observations at further inducing frequencies such as given by the orbital period of the moons, multiples of Jupiter’s synodic rotation frequency, or the solar rotation rate will break the degeneracy between ocean conductivity, ocean thickness, and depth (e.g., Seufert et al. 2011).

The composition—dissolved organic and inorganic speciation, salinity, and pH—of Europa’s ocean is poorly constrained. Most models and aqueous leaching experiments suggest that magnesium sulfate (MgSO<sub>4</sub>) is the dominant salt, in contrast to sodium chloride (NaCl) as in Earth’s ocean (Fanale et al. 2001; Kargel et al. 2000; Zolotov and Shock 2001; McKinnon and Zolensky 2003), although the concentration varies strongly between models and spans nearly five orders of magnitude across the literature. Recent spectroscopic observations from Earth (Fischer et al. 2015; Trumbo et al. 2019), which trade the higher spatial resolution of *Galileo* near-infrared imaging for better spectral resolution—reveal chlorides associated with active features. Recent interpretations of *Galileo* Near Infrared Mapping Spectrometer (NIMS) data in the light of new laboratory spectra find that perchlorates—oxidized Cl ostensibly from the internal ocean—can also match absorption features of surface materials (Hanley et al. 2014). The reddish tint of Europa’s non-icy materials surface materials has been attributed to radiation-induced flaws in crystalline sodium (e.g., Hand

and Carlson 2015). These many lines of evidence for endogenous chlorine do not rule out a sulfate dominated ocean. As noted by Zolotov and Kargel (2009), a highly oxidized ocean dominated by  $\text{Mg}^{2+}$  and  $\text{SO}_4^{2-}$  also has substantial  $\text{Na}^+$  and  $\text{Cl}^-$ . Equilibrium freezing of such an ocean yields a fractionated eutectic composition of mainly NaCl that is nearly identical to the result of applying the same method to seawater (Vance et al. 2019). Further complicating the interpretation of Europa's ocean composition based on the composition of its surface, the speciation of surface salts is influenced by radiation and by the speed at which freezing (or refreezing) occurs (Vu et al. 2016). Thus, more details regarding the ocean composition require firmer constraints on interior structure, ice thickness, surface composition, and potentially plume composition.

### 1.2.2 Ganymede

Models for Ganymede's internal structure, again constrained by mass and gravity data under the assumption of hydrostatic equilibrium, suggest an outer ice-liquid water layer between 600 to 900 km thick, with significant high-pressure ice phases; an intermediate mantle with thicknesses up to 1000 km and density consistent with an olivine-dominated, mostly dehydrated composition; and a central metallic core whose radius may extend from about 500 km to more than 1000 km depending on core composition (Anderson et al. 1996; Deschamps and Sotin 2001; Kuskov and Kronrod 2001; Sohl et al. 2002; Vance et al. 2014, 2018a). Multiple pressure-induced phase transitions are expected within Ganymede's outer water layer, and the outermost ice I shell is expected to be less than ~150 km thick (Vance et al. 2014, 2018a).

Measurements of the induced magnetic field by *Galileo* and auroral oval oscillations observed by the *Hubble Space Telescope* indicate that the ocean electrical conductivity is at least 0.09 S/m, which corresponds to a minimum salt concentration of 0.9 gram  $\text{MgSO}_4$  per kilogram of ocean water, for an ocean between 150 to 250 km depths (Saur et al. 2015). As for Europa, a bias towards a magnesium sulfate ocean composition for Ganymede is based firstly on models for the aqueous alteration of CI chondrites (Kargel 1991)—subsequently shown to be erroneous (McKinnon and Zolensky 2003)—that provided a good match to *Galileo* NIMS spectra that fit well to  $\text{MgSO}_4$ . The ocean's oxidation state, and thus the dominant ionic composition, remains to be confirmed. The intrinsic magnetic field of Ganymede further implies the formation of an iron-rich core that may itself be layered with a solid inner and fluid outer core (e.g., Rückriemen et al. 2018).

### 1.2.3 Callisto

The interior structure of Callisto, which may not be fully differentiated, is the least constrained of the Galilean satellites. Here, the interpretations of *Galileo* results are less clear because the satellite may not be in hydrostatic equilibrium (Gao and Stevenson 2013) and the induced magnetic field signal may be due to the ionosphere rather than a subsurface ocean (Hartkorn and Saur 2017). The MoI-factor assuming hydrostatic equilibrium (Anderson et al. 2001) prohibits a metallic core, requires low densities in the silicate interior, and corresponds to water layers that are  $\lesssim 250$  km thick (Vance et al. 2018a). Conversely, a significantly lower MoI estimate that does not assume hydrostatic equilibrium (Gao and Stevenson 2013) requires a central iron core and mantle densities that are consistent with an anhydrous pyrolite composition (Vance et al. 2018a). If an ocean is present, Zimmer et al. (2000) found that the magnetic field data are best explained by electrical conductivity values of  $\gtrsim 0.02$  S/m with ocean thicknesses of  $\lesssim 300$  km. Because Callisto formed farthest from

Jupiter of the Galilean satellites and thus received the least tidal heating, any ocean that is present may be nearly frozen, making the satellite an appealing target for studying the end stage dynamics of a large ocean world.

#### 1.2.4 Enceladus

Recent observational data from the *Cassini-Huygens* mission has shed new light on the interiors of Saturnian satellites. At Enceladus, measurements of the gravity field, the shape and rotational state, and direct sampling of plume material all provide constraints on internal structure and composition. Early shape and gravity measurements, in combination with geyser activity near the south pole, indicated the presence of a subsurface water reservoir (e.g., Porco et al. 2006; Dougherty et al. 2006; Thomas et al. 2007; Collins and Goodman 2007; Iess et al. 2014). The existence of a global ocean instead of a regional sea was determined decisively by detection of a significant physical libration (Thomas et al. 2016). The libration amplitude is about four times larger than expected for a solid Enceladus due to the decoupling of the rotational behaviour of the shell with respect to the deeper solid interior and indicates that the ocean is about 20 km beneath the surface on average and that the mean ocean thickness is between 21 and 67 km (Thomas et al. 2016; Van Hoolst et al. 2016). Independent confirmation of these results was obtained by gravity (Iess et al. 2014) and topography (Nimmo et al. 2011; Tajeddine et al. 2017) data that predict, assuming isostasy at the long wavelengths observed in the gravity field, a core radius of  $\sim 190$  km, an ocean thickness of  $\sim 40$  km, and a shell thickness of  $\sim 20$  km, on average (Beuthe et al. 2016; Čadek et al. 2016).

Large variations in ice shell thickness exist, with mean equatorial, north polar, and south polar thicknesses of approximately 30 km, 15 km, and 5 km, respectively (McKinnon 2015; Thomas et al. 2016; Beuthe et al. 2016; Čadek et al. 2016, 2019; Hemingway and Mittal 2019). A thinner ice shell at the south pole of Enceladus favors exchange between the rocky interior, where hydrothermal processes are likely occurring (Hsu et al. 2015; Choblet et al. 2017a), and the surface (see Sect. 2.4). However, ice shell thickness variations are likely not stable without active forcing, due to the re-accretion of ice filling in topographic variations on timescales of days to years (called marine ice, see Sect. 5), or flow of the ice from thick to thinner regions (Nimmo et al. 2007).

Out of all the water oceans that inevitably exist in the universe, Enceladus' is the one that we know about second best (Glein et al. 2018; Postberg et al. 2018a). Measurements of the composition of grains and gases erupted out of Enceladus in the form of a plume show that the satellite's ocean contains four classes of materials. The first class is soluble salts (Postberg et al. 2009, 2011) that are dominated by sodium chloride (NaCl) and sodium bicarbonate ( $\text{NaHCO}_3$ ) or carbonate ( $\text{Na}_2\text{CO}_3$ ). Potassium salts also appear to be present, but are  $\sim 10^2$  times less abundant than their sodium counterparts (Postberg et al. 2009). Second, *in situ* observations of dust in the inner Saturnian system (Hsu et al. 2015) indicate that some plume grains from Enceladus contain embedded nanometer-sized particles of nearly pure silica ( $\text{SiO}_2$ ). Third, the major plume volatiles are  $\text{H}_2\text{O}$ ,  $\text{H}_2$ ,  $\text{NH}_3$ ,  $\text{CO}_2$ , and  $\text{CH}_4$  (Waite et al. 2017). The presence of minor and trace species, including volatile organic compounds (VOCs), is also implied by the mass spectrometry data from *Cassini*, although identifying and quantifying individual minor and trace species is challenging because the insufficiently resolved mass spectra allow multiple degenerate solutions to the composition (Magee and Waite 2017). Two effects that may lead to more uncertainty in the volatile composition are chemical reactions induced by grain impacts onto instrument surfaces (Waite et al. 2009), and adsorption of VOCs onto ice grains in the plume (Bouquet et al. 2019). Indeed, VOCs

have been identified in emitted ice grains (Postberg et al. 2008), which preferably adsorb polar oxygen- and nitrogen-bearing volatile organic compounds (Khawaja et al. 2019). These effects can be partially mitigated by focusing on the most weakly adsorbing volatiles (e.g., hydrocarbons) during the slowest flybys. The fourth class of materials in the plume/ocean are macromolecular organic compounds (Postberg et al. 2018b). The data from *Cassini* suggest that these materials have high molecular masses (>200 u) and are carbon-rich (low H/C ratios) owing to an abundance of unsaturated carbon atoms in unfused benzene rings. These features can result in hydrophobic phase separation from water. The data also suggest the presence of further chemical complexity in the form of oxygen- and nitrogen-bearing functional groups in the observed organic matter.

The composition of the ocean should reflect processes occurring within it. An important process on Enceladus is water-rock interaction. This is how minerals in preexisting rocks react with water and other volatiles to produce new minerals and a modified aqueous solution composition. A key signature of water-rock interaction is a high concentration of  $\text{Na}^+$  (0.06–0.4 mol/kg  $\text{H}_2\text{O}$ ; Postberg et al. 2009). In primitive materials such as anhydrous chondrites, the chief carrier of Na is silicates such as feldspars or silicate glasses. When water reacts with this type of material, sodium can be leached into the aqueous solution. The presence of oceanic chloride indicates that the original rock contained primary grains of halite or another Cl-bearing mineral (Clay et al. 2017), or the original alteration fluid contained HCl (Dhooghe et al. 2017) or  $\text{NH}_4\text{Cl}$  (Altwegg et al. 2020). If the original alteration fluid was composed of melted cometary ices, then the presence of carbonate salts,  $\text{CO}_2$ , and  $\text{NH}_3$  in the plume can be easily explained. Carbon dioxide and ammonia are abundant in numerous comets (A'Hearn et al. 2012; Dello Russo et al. 2016) and could be inherited directly. Reactions of Na-bearing rocks with  $\text{CO}_2$  in water should produce some dissolved  $\text{NaHCO}_3$  or  $\text{Na}_2\text{CO}_3$  depending on the pH, which is thought to be mildly alkaline (pH  $\sim$ 9) in Enceladus' ocean (Glein and Waite 2020). Much of the chemistry described here may have taken place at low temperatures, perhaps during the early history of Enceladus when water separated from rock, or subsequently as a result of seafloor weathering. The observed high ratio of Na/K suggests that low-temperature reactions involving clay minerals are occurring today (Zolotov 2012).

Water-rock interaction can also occur at higher temperatures if the system is hydrothermally active. Choblet et al. (2017a) developed a model of tidal heating and fluid circulation showing that hydrothermal activity in Enceladus' core is plausible. This could explain observations of  $\text{SiO}_2$  nanoparticles (Hsu et al. 2015) and  $\text{H}_2$  gas (Waite et al. 2017). Higher temperatures lead to increased leaching of silica, and if the fluid is subsequently cooled conductively or by mixing with ocean water, then amorphous silica saturation can be exceeded, causing precipitation. Sekine et al. (2015) proposed that sufficient silica can be leached from primordial rocks dominated by pyroxenes and olivine, while Glein et al. (2018) argued that a larger source of silica may be needed, such as quartz-bearing rocks that formed from earlier weathering. The large flux of  $\text{H}_2$  emanating from Enceladus calls for a robust source, with the most likely being serpentinization of chondritic rock (Waite et al. 2017). Serpentinization is an alteration process that results in the hydration and partial oxidation of ultramafic (Mg- and Fe-rich) rocks. Undifferentiated chondritic rock is very rich in iron, and this provides substantial reducing potential to generate  $\text{H}_2$  from  $\text{H}_2\text{O}$ . However, a likely difference from  $\text{H}_2$  generation on Earth is that the source rock on Enceladus may have already been hydrated, as suggested by the low density of Enceladus' core (Iess et al. 2014). This is not particularly meaningful from a bulk composition point of view, but it implies complexity in a body that potentially experienced different types of alteration over space and time (see Glein et al. (2018)).

### 1.2.5 Titan

Multiple lines of evidence from the *Cassini-Huygens* mission also constrain Titan's interior. The observation of an Extremely Low Frequency (ELF) electromagnetic wave with a frequency of about 36 Hz by the *Huygens* probe during its descent through Titan's atmosphere requires the existence of a resonant cavity between Titan's stratospheric ionized layers and a conductive layer beneath the non-conductive surface. This lower reflecting boundary is best explained by the transition from ice to a conducting ocean at a depth of 55 to 80 km below the surface (Béghin et al. 2012). Gravity and topography also indicate an ocean that is, on average, about 100 km beneath the surface (Nimmo and Bills 2010). Measurements of the time-varying gravity field of Titan determining the tidal Love number ( $k_2 = 0.616 \pm 0.067$ ; Durante et al. 2019) also imply an ice shell thickness between 50–100 km (e.g., Mitri et al. 2014), which is consistent with thermal modeling results (Tobie et al. 2006; Mitri et al. 2010).

The gravitational constraints provide not only unambiguous evidence of a subsurface ocean close to the surface, but also indicate that Titan's subsurface ocean is likely much denser than pure water. The ocean appears to have a high bulk density, exceeding  $1100 \text{ kg/m}^3$ , based on the large value of the measured tidal Love number (Iess et al. 2012; Baland et al. 2014; Lefevre et al. 2014; Mitri et al. 2014; Vance et al. 2018a; Durante et al. 2019). Magnesium and ammonium sulfates have been proposed on the basis of chemical and physical models (Fortes et al. 2007) and in the context of experiments investigating the chemistry of these compounds (Hogenboom 1995; Hogenboom et al. 1997; Vance and Goodman 2013). The high density constraint could be met with 10 wt%  $\text{MgSO}_4$  (Vance et al. 2018a). A reducing ocean dominated instead by chlorides can obtain similar large densities, but equation of state data in the relevant pressure range are not yet available to demonstrate this. A saline ocean is not expressly required by the current uncertainty in the Love number, though, which permits densities as low as  $1100 \text{ kg/m}^3$ , consistent with the pure water or even 3 wt% ammonia ( $\text{NH}_3$ ) cases as described by Vance et al. (2018a). The high Love number could alternatively be explained by a significant viscous behavior of the interior below the ocean (Durante et al. 2019) or by a resonantly excited internal gravity mode, which would require the ocean to be stably stratified (Luan 2019).

Maintaining a dense salty ocean and thin ice requires a high heat flux, exceeding 800 GW ( $10 \text{ mW/m}^2$ ) (Vance et al. 2018a). Such a high heat flux would be consistent with recent geological activation of Titan, perhaps concurrent with the formation of Saturn's rings (Čuk et al. 2016). A dense ocean and thin ice shell only worsen the problem of accounting for the low density ( $2600 \text{ kg/m}^3$ ) of Titan's rocky interior. It thus seems likely that Titan is weakly differentiated, highly porous, or both. Alternatively, a differentiated Titan with a small metallic core ( $R < 400 \text{ km}$ ) would be permitted by the gravitational constraints if the low density layer under the ocean can be explained (Vance et al. 2018a). The presence of some dissolved electrolytes in Titan's ocean solutes is consistent with the model used for the ELF waves, and with a potential low temperature at the top ocean compatible with a likely rigid ice shell (Vance et al. 2018a). An intriguing possibility is that the low density of Titan's interior can be explained by the presence of organic materials. Geochemical modeling can reproduce the ratios of  $^{36}\text{Ar}/\text{N}_2$  and  $^{15}\text{N}/^{14}\text{N}$  as measured by *Huygens* in Titan's atmosphere, if the building blocks of Titan contained abundant organic materials that were subsequently heated and outgassed from the deep interior (Miller et al. 2019). This idea is challenging to model because it requires thermodynamic descriptions of organic-rich mineral assemblages that are rare or non-existent in Earth's geology. Recent progress in developing the needed

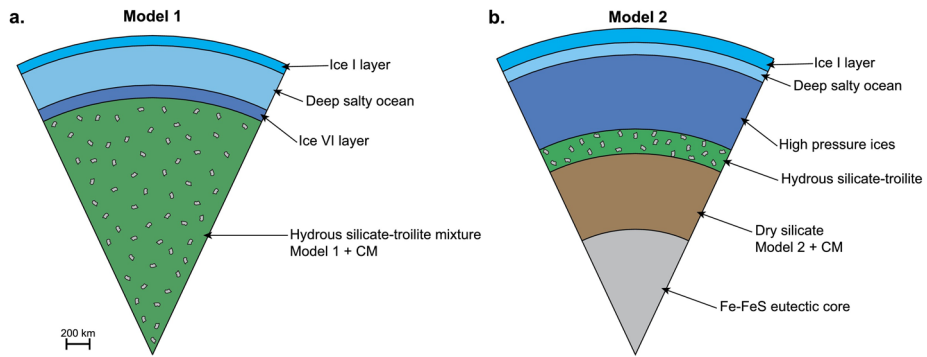


**Fig. 2** Possible interior structures of Titan including significant organic materials. From Néri et al. (2020)

petrological data allowed Néri et al. (2020) to construct models for Titan, based on CI chondrite compositions, that incorporate significant organic materials. The resulting Titan models have the low internal densities required to satisfy gravitational constraints (Fig. 2).

## 2 Surface Exchange Processes

Potential surface expressions of ice-ocean material exchange vary widely in morphology and age across the satellites. The mechanisms of exchange can be broadly categorized into those caused by impacts, tectonics, cryovolcanism/outgassing, and plumes; a unique morphology characterized by *in situ* surface disruption suggestive of lithospheric thinning, termed chaos, is observed on Europa and will be discussed separately since multiple processes may be responsible. Here, lithosphere refers to the strong upper layer of the ice shell. Europa exhibits global resurfacing with a surface age between 30 and 90 million years (Bierhaus et al. 2009), while Enceladus' surface exhibits both ancient terrains and ongoing geologic activity (e.g., Patterson et al. 2018). Titan's surface is also geologically active, with its thick atmosphere and hydrocarbon seas playing a significant role that will not be discussed in detail here (see Jaumann et al. (2009) for a review). Conversely, Ganymede and Callisto show older and more limited signs of surface exchange (Schenk et al. 2004).

### 2.1 Impact Processes

Multi-ringed structures observed on the icy worlds Callisto, Ganymede, and Europa range in size from the ~2000 km diameter Valhalla basin ring system on Callisto (Fig. 3a) (McKinnon and Melosh 1980; Moore et al. 2004; Schenk et al. 2004) to the ~300 km diameter Tyre multi-ringed structure on Europa (Schenk et al. 2004; Schenk and Turtle 2009). They all share morphological characteristics that suggest impact into a relatively thin brittle lithosphere underlain by a ductile or liquid subsurface (McKinnon and Melosh 1980; Melosh 1989). The scale of multi-ring basins on Callisto and Ganymede suggests the possibility of direct exchange between the ice shell and ocean of the satellites. However, the depth to the ice-ocean interface at the time of formation for these basins is not known, leaving open the possibility that their ice shells were not breached during the formation of these features. An abrupt transition from complex crater morphologies to multi-ring morphologies observed on Europa indicates a similarly abrupt transition from ice to water may occur at depths of 10

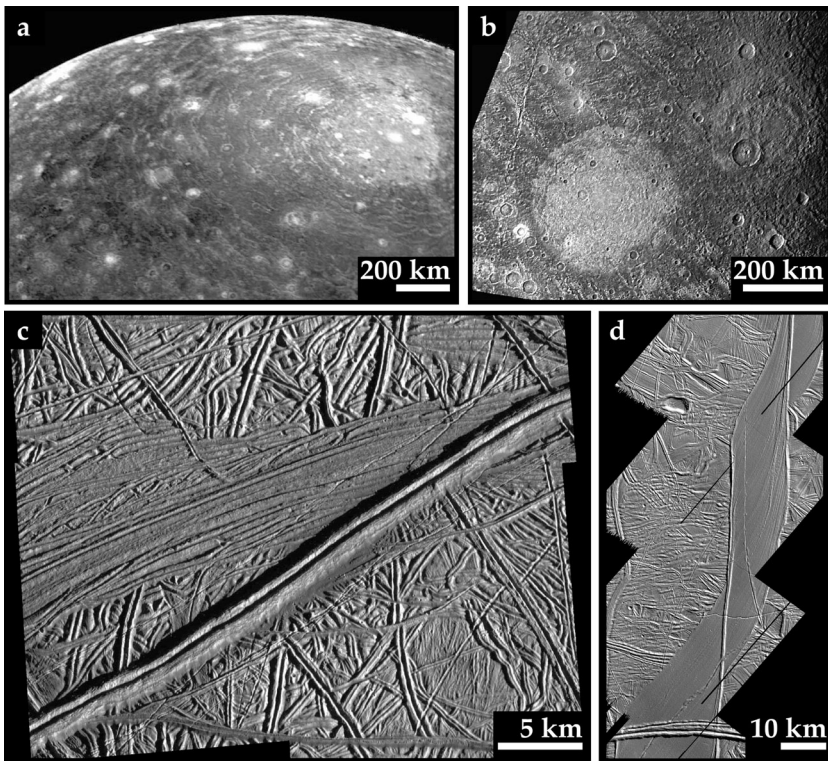


**Fig. 3** Impact and tectonic features of icy ocean worlds. **(a)** The prominent impact basin Valhalla on Callisto. The circular region is 300 km in diameter and basin rings extend 1500 km from the basin center. **(b)** The 340 km diameter palimpsest Memphis Facula on Ganymede. **(c)** An archetype double ridge on Europa, Antheos Linea. **(d)** A dilational band, Astypalaea Linea, on Europa

to a few 10s of km (Schenk et al. 2004) and suggests impacts that formed multi-ring structures could have sampled the satellite's subsurface ocean. However, a lack of radial faulting associated with the formation of multi-ring structures on Europa argues that they may not have breached its ice shell (Turtle 1998; Kadel et al. 2000). While clear evidence for direct ice-ocean material exchange is not present in association with this process, the potential for convection within the ice shells of Callisto, Ganymede, and Europa (Shoemaker et al. 1982; Schubert et al. 2004; Barr and Showman 2009) indicates that indirect ice-ocean exchange could still occur.

Palimpsests are impact features that appear to be unique to Callisto and Ganymede (Fig. 3b). They are generally circular to slightly elliptical albedo features that leave a barely discernable topographic imprint and are characterized by faint concentric lineations and, often, a central smooth region (Schenk et al. 2004; Patterson et al. 2010). Their diameters are measured in 100s of km and, similar to the older multi-ring basins, their formation has been attributed to impact into a relatively thin brittle lithosphere (Shoemaker et al. 1982). As with multi-ring basins, it is possible that direct ice-ocean exchange could have occurred when these features formed, but not clearly so. However, as with the multi-ring basins and structures, indirect exchange of material is also a possibility.

Several numerical studies using hydrocodes have been performed to investigate under which conditions melt may be generated upon impact and impact cratering may excavate

oceanic water to the surface (e.g., Artemieva and Lunine 2003; Kraus et al. 2011; Senft and Stewart 2011). For thin ice shells ( $\leq 10$  km), a projectile of a few kilometers in diameter is sufficient to break the entire shell and expose water to the surface (e.g., Turtle and Pierazzo 2001; Lunine et al. 2010). For thicker ice shells, exposure of oceanic water is still possible if the projectile size is about half the ice shell thickness (e.g., Artemieva and Lunine 2005; Lunine et al. 2010). Large impacts such as the one that formed the Menrva crater on Titan, for example, should have brought a large volume of water to the surface and temporarily changed the climate of Titan by potentially rising the surface temperature by 80 K (Zahnle et al. 2014). Monteux et al. (2016) also showed that an impactor of 25 km in radius at moderate velocity ( $\sim 2$  km s<sup>-1</sup>) was able to totally disrupt the ice shell and excavate a huge volume of oceanic water to the surface. Even if such large impact events remain rare during the moon's history, they have the potential to induce resurfacing from regional to global scales, for sufficiently large impacts.

## 2.2 Tectonic Processes

Ridges on Europa come in a variety of morphological forms, are observed on length scales of up to 1000s of kilometers, and can range from linear to cycloidal to anastomosing in plan-form (Prockter and Patterson 2009). Double ridges are by far the most common ridge type and are observed over most of the satellite's visible surface history (Figueredo and Greeley 2000, 2004). Numerous models have been suggested for the formation of European ridges, all of which appeal to the exploitation of a pre-existing fracture in the ice shell. The most widely accepted model of ridge formation suggests that cyclical strike-slip motion on a pre-existing fracture will dissipate heat and cause the warmer, now more buoyant, ice flanking the fracture to uplift and form a double ridge (Nimmo and Gaidos 2002; Han and Showman 2008; Kalousová et al. 2016). This process could also create melt that would migrate down the fracture and, provided the fracture penetrates the brittle lithosphere, could provide a direct or indirect path of bringing surface material to Europa's subsurface ocean. The path taken would depend on the thickness and rheology of the shell. Other models of ridge formation suggest they could be pathways for fissure eruptions (Kadel et al. 1998), dike intrusions (Turtle et al. 1998), linear diapirism (Head et al. 1999), or melt squeezed to the surface via cyclical tidal (Greenberg et al. 1998). More recently, subsurface sills feeding cryoclastic eruptions have been proposed (Dombard et al. 2013; Craft et al. 2016). In contrast with the shear heating model, these models imply that ocean material would be brought to the surface or near surface.

Some double ridges (Fig. 3c) and ridge complexes (another morphological feature class) on Europa are flanked by deposits that are relatively low albedo and extend for up to 10 km on either side of the feature they are associated with (Lucchitta and Soderblom 1982; Belton et al. 1996). The dark material is likely a relatively thin surficial deposit that drapes over the preexisting terrain (Geissler et al. 1998; Fagents et al. 2000). These deposits may be continuous along the flanks of a ridge, or spaced in discrete subcircular regions along the margins of a ridge (Prockter and Patterson 2009). Observations by the *Galileo* NIMS instrument suggest that low albedo deposits associated with tectonic features on Europa are composed of sulfates (McCord et al. 2002) or MgCl<sub>2</sub> (Brown and Hand 2013; Ligier et al. 2016) that are converted into magnesium sulfates through radiolytic processes. The proposed compositions of low albedo deposits suggest that they were initially emplaced by an endogenic process and have subsequently been affected by exposure to the local radiation environment.

Ridges on Enceladus also come in a variety of forms (Patterson et al. 2018), but the most relevant of them for discussing ice-ocean exchange are the 'tiger stripes' of the South Polar



**Fig. 4** False-color mosaic showing the very young surface of Enceladus' South Polar Terrain with the four parallel 'tiger stripe' fractures centered around the south pole of the moon. Credit: NASA/JPL/Space Science Institute

Terrain (SPT) (Fig. 4). The SPT is a pervasively fractured, geologically young, and low-lying region bound by a quasi-polygonal circumpolar system of scarps that are intermittently broken by Y-shaped structures (Porco et al. 2006; Helfenstein 2014). Within this terrain are the ridges Damascus Sulcus, Baghdad Sulcus, Cairo Sulcus, and Alexandria Sulcus, collectively referred to as tiger stripes. These features are associated with anomalously high heat flows and are geologically active, as evidenced by eruptive jets (see Sect. 2.4) of water and other constituents (e.g., Porco et al. 2006; Hansen et al. 2008) that are likely sourced directly from Enceladus' subsurface ocean (Spencer et al. 2018).

Bands on Europa are another class of tectonic feature whose formation could facilitate ice-ocean material exchange (Fig. 3d). This feature can be subdivided into three morphological classes: dilational bands, bright bands, and subsumption bands. Dilational bands, also referred to as pull-apart bands, are the more commonly observed feature type (Figueredo and Greeley 2000, 2004). These bands have margins that can be easily reconstructed (Schenk and McKinnon 1989; Pappalardo and Sullivan 1996; Sullivan et al. 1998), indicating that their interiors consist of subsurface material that has been emplaced at the surface of Europa (e.g., Howell and Pappalardo 2018). Dilational band formation represents a significant process by which Europa's crust has been resurfaced (Schenk and McKinnon 1989; Pappalardo and Sullivan 1996; Prockter et al. 2002).

Two end-member models have been proposed for the formation of pull-apart bands. One is the tidal pumping model proposed by Tufts et al. (2000), which suggests that bands are part of a continuum process that begins with the formation of a fracture, progresses to a ridge, and ultimately ends in the formation of a dilational band. This mechanism proposes direct exchange of ocean material with the surface of Europa. The second model, by Prockter et al. (2002), proposes that band formation is distinct from that of ridges and involves solid-state material rising to fill the separating margins of a preexisting fracture in a manner analogous to terrestrial mid-ocean ridges. This mechanism would imply indirect exchange of ocean material with the surface. Analog wax experiments have indicated that oblique

opening and shearing commonly associated with the formation of dilational bands is best explained with the latter model of formation (Manga and Sinton 2004).

Bright bands are linear features that disrupt preexisting terrain and have internal textures reminiscent of dilational bands. However, unlike that feature type, bright bands are far less common and have margins that do not appear as if they can be reconstructed. Formation mechanisms relying on dilational, contractional, and/or lateral deformation have all been proposed to explain the unique characteristics of this type of band (Prockter and Patterson 2009). Depending on the formation mechanism used (or combination thereof), ice-ocean exchange is possible, but without additional data to test the proposed formation models, the potential importance of this feature type for material exchange is not as clear as it is with dilational bands.

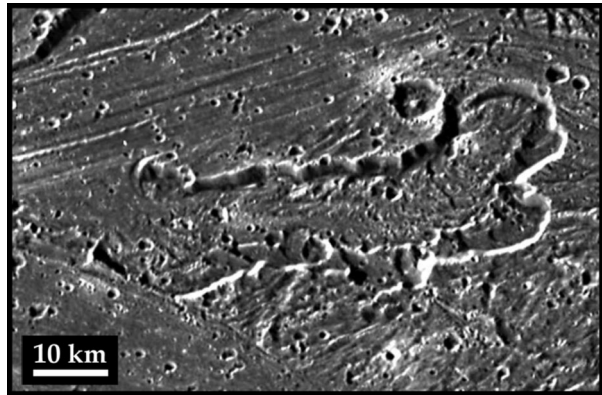
Recent work has introduced a new band feature class: subsumption bands (Kattenhorn and Prockter 2014). This feature type has been observed within Falga Regio on Europa and is associated with the loss of surface material. It is not clear, however, if material subducted in this manner would reach the ice-ocean interface (e.g., Johnson et al. 2017; Howell and Pappalardo 2019).

### 2.3 Cryovolcanic and Outgassing Processes

The potential for cryovolcanic activity on Ganymede has changed significantly between analyses conducted using *Voyager* versus *Galileo* data. Based on *Voyager* images, dark material on Ganymede was interpreted to have been modified by cryovolcanic activity (Murchie and Head 1989; Croft et al. 1994). This interpretation was supported by an apparent absence of small craters, embayment relationships observed in association with large craters, and smooth areas associated with tectonic and impact features (Casacchia and Strom 1984; Murchie et al. 1990; Schenk and Moore 1995). Groove lanes that pervasively disrupt dark material on Ganymede were interpreted to represent regions of resurfacing by cryovolcanic flows, which were subsequently tectonized in some areas to form grooves (Golombek and Allison 1981; Golombek 1982; Shoemaker et al. 1982; Allison and Clifford 1987). However, higher-resolution *Galileo* image data of Ganymede revealed no unequivocal observation of lobate materials with an identifiable source vent or any other identifiable morphology related to cryovolcanism associated with dark material (Prockter et al. 2000). Candidate cryovolcanic units identified from *Voyager* data at lower resolution on the basis of embayment and texture instead appeared to be the result of fluidized impact ejecta (Pappalardo et al. 2004) and dark smooth materials in topographic lows appeared to have accumulated by downslope movement of loose material, instead of by some cryovolcanic mechanism (Prockter et al. 1998). Higher-resolution *Galileo* image data of groove lanes on Ganymede have also lacked clear morphological evidence for flow fronts, source vents, embayment relationships, or any other evidence suggestive of cryovolcanic emplacement. However, indirect evidence for volcanic resurfacing has been identified in the form of small isolated caldera-like features (Fig. 5) (Lucchita 1980; Schenk and Moore 1995; Spaun et al. 2001) and smooth, topographically low bright lanes (Schenk et al. 2001).

For Titan, the only ocean world with a dense atmosphere, evidence of outgassing comes from the presence of  $^{40}\text{Ar}$  in Titan's atmosphere (Niemann et al. 2005; Waite et al. 2005; Atreya et al. 2006) because  $^{40}\text{Ar}$  is produced by the decay of  $^{40}\text{K}$  that is initially contained in the silicate fraction. The amount of  $^{40}\text{Ar}$  in Titan's atmosphere was measured by the Gas Chromatograph Mass Spectrometer (GCMS) onboard the *Huygens* probe in 2005 (Niemann et al. 2005) and by the *Cassini* Ion and Neutral Mass Spectrometer (INMS) (Waite et al. 2005). The value was revised to  $3.39 (\pm 0.12) \times 10^{-5}$  mole fraction by Niemann et al.

**Fig. 5** Oblique view of a depression found within Sippar Sulcus, Ganymede, and acquired during the G8 encounter at 179 m/pixel, where south is up. This feature has a surface texture that may be indicative of flow toward its open end, consistent with it being a source region for icy volcanic material. From Patterson et al. (2010)



(2010). Depending on the elementary composition of the silicate fraction, the outgassing corresponds to 5 to 20% of the total amount of  $^{40}\text{Ar}$  produced by the decay of  $^{40}\text{K}$ . Another clue for the existence of exchange processes comes from the presence of methane in Titan's atmosphere because methane is destroyed by photolysis. Current models (Wilson and Atreya 2000; Bézarard et al. 2014) suggest that the present amount of methane would disappear in less than 30 Myr, which is short relative to geological timescales. Therefore, methane has to be resupplied into the atmosphere, and endogenic (e.g., cryovolcanic) processes have been proposed as a possible process (Tobie et al. 2006). Potential cryovolcanic features on Titan are relatively young, not widely distributed across the surface, and include flow fields near Hotei Arcus, Tui Regio, and Ganesa Macula (see Jaumann et al. (2009) for a review).

## 2.4 Plume Processes

As described in Sect. 2.2, there are tectonic processes on Enceladus and Europa that can provide potential (in the case of Europa) or actual (in the case of Enceladus) conduits for ice-ocean exchange relating to plume activity.

For Enceladus, approximately 100 supersonic jets of gas and ice grains have been observed to erupt from the four SPT tiger stripes to form a large plume towering above the south pole (Spahn et al. 2006; Porco et al. 2006; Hansen et al. 2008; Porco et al. 2014; Spitale et al. 2015). Observed plume emission rates vary, with an average of about 300 kg/s of water vapour (Hansen et al. 2019). The vapour redeposits onto the vent's ice walls or condenses to tiny ice grains (e.g., Ingersoll and Pankine 2010; Schmidt et al. 2008; Yeoh et al. 2015), and a substantial part of the ice grains appear to be frozen ocean spray entrained in the flow that might directly sample the composition of the ocean (Postberg et al. 2009, 2011). Estimates for the gas to ice ratio in the plume vary greatly, although recent estimates suggest an average value of  $\sim 10$  (Kempf et al. 2018; Postberg et al. 2018a). While the ejection speeds for plume vapour are generally above Enceladus' escape speed (Goldstein et al. 2018), only a fraction of the ice grains escape the moon's gravity to form Saturn's E ring (Kempf et al. 2018) and a greater part falls back to form surface deposits (Scipioni et al. 2017; Southworth et al. 2019).

The jets and plume are temporally and spatially variable. Jets appear to turn on and off on typical time scales of years, indicating occasional opening / sealing of certain ice vents (Nimmo et al. 2014), and systematic variations observed across the fissures suggest trends in the composition of the plume material and/or variations in the plumbing connecting these reservoirs to the surface (Hedman et al. 2018). In contrast, plume activity is coupled

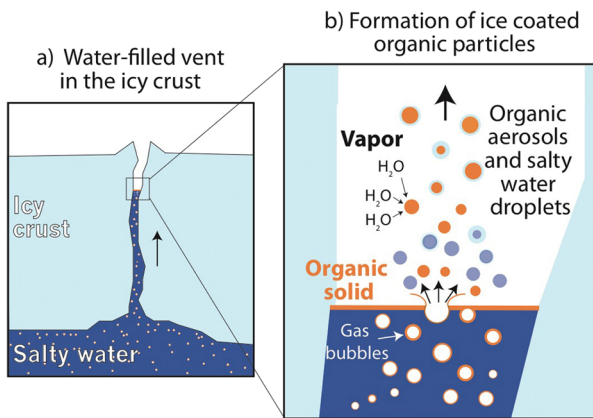


**Fig. 6** Schematic of the formation of ice grains from heterogeneous nucleation (not to scale). **(a)** Ascending gas bubbles in the ocean efficiently transport organic material into water-filled cracks in the south polar ice crust. **(b)** Organics ultimately concentrate in a thin organic layer on top of the water table inside the icy vents. When gas bubbles burst, they form aerosols made of insoluble organic material that later serve as efficient condensation cores for the production of an icy crust from water vapor, thereby forming organic-rich particles. Another effect of the bubble bursting is that larger, pure saltwater droplets form, which freeze and are later detected as salt-rich ice particles in the plume and the E ring. The figure implies the parallel formation of both organic and saltwater spray, but their formation could actually be separated in space (e.g., at different tiger stripe cracks) or time (e.g., dependent on the varying tidal stresses). From Postberg et al. (2018b)

most prominently to the moon's orbital period (e.g., Hurford et al. 2012), with brightness variations on the order of years as well (Hedman et al. 2013; Nimmo et al. 2014; Ingersoll and Ewald 2017); variations in the integrated emitted gas flux over time seem to be milder (Hansen et al. 2017; Teolis et al. 2017; Hansen et al. 2019).

The detection of silica nano particles (Hsu et al. 2015), salts, and large organic molecules in the erupted ice grains (Postberg et al. 2009, 2011, 2018b) in combination with  $\text{CH}_4$  and  $\text{H}_2$  measured in the plume (Waite et al. 2017) suggests that material originating from the moon's rocky core enters the plume. This indicates that the tiger stripe fractures penetrate the entire thickness of the ice shell, tapping into the global ocean underneath (Porco et al. 2006; Kite and Rubin 2016; Spencer et al. 2018). From buoyancy arguments, water should fill large parts of these fractures and the level of neutral buoyancy should be situated at  $\sim 90\%$  of the distance from the ocean to the moon's surface, above which the fractures would be vapor-filled. With an apparent ice shell thickness locally of not more than 5 km (e.g., Čadek et al. 2019), it seems plausible that liquid water could be situated at only a few hundred meters depth within the fractures with some variability ( $\sim 10$ s of meters) due to flushing from tidal flexing of the crust (Kite and Rubin 2016). *Cassini* measurements constrain the outlet diameters to be  $< 10$  m (Goguen et al. 2013), and models suggest that the average width of cracks narrows to less than a few 10s of centimeters above the water surface (Schmidt et al. 2008; Postberg et al. 2011; Nakajima and Ingersoll 2016) and is on the order of 1 m for the water filled portion (Kite and Rubin 2016; Spencer et al. 2018).

The mechanical and thermodynamic driver of the plume is evaporation of ocean water from the water surface inside back-pressured ice vents (Spencer et al. 2018). There, temperatures and pressures are close to the triple point of water, which allows water to evaporate efficiently. Together with volatile gases emerging from depth or exsolving from the ocean water, vapor is quickly accelerated by the pressure gradient to nearby open space and even becomes supersonic in some jets, thereby exceeding velocities of 1 km/s (Hansen et al. 2008;

Goldstein et al. 2018). During this ascent, the gases cool substantially and, depending on their composition, will partially condense onto walls and into ice grains (Waite et al. 2017; Bouquet et al. 2019; Khawaja et al. 2019). Almost pure water ice grains and most of the likewise salt poor, but organic-bearing grains are thought to form in this way from supersaturated vapor inside (Schmidt et al. 2008; Postberg et al. 2009) and at the outlets (Yeoh et al. 2015) of ice vents. The majority of ice grains in the plume are in a crystalline state (Dhingra et al. 2017), indicative of formation temperatures above 135 K.

The apparent heterogeneity of ice grain compositions strongly argues for different grain formation mechanisms (Fig. 6). Salty ice grains are thought to be frozen ocean spray generated when bubbles burst at the water surface inside the vertical cracks (Postberg et al. 2009, 2011). These bubbles might be formed from either mildly boiling water close to its triple point or upwelling volatile gases (e.g., CO<sub>2</sub>, CH<sub>4</sub>, or H<sub>2</sub>). Consequently, these grains seem to be samples of oceanic near-surface waters (Postberg et al. 2009). A similar mechanism has been proposed to form ice grains containing complex organic substances in high concentrations. In analogy to similar processes on Earth's oceans (e.g., Wilson et al. 2015), this solid organic material might have accumulated as part of an organic film near the oceanic surface. Upon bubble bursting, these organics become aerosolized and then serve as condensation cores to form a water ice crust that is entrained in the vapor flow rising through Enceladus' ice vents (Postberg et al. 2018b).

For Europa, the first tentative telescopic detection of a plume occurred during a *Hubble Space Telescope* observation in December 2012. Localized ultraviolet line emission of hydrogen and oxygen were attributed as dissociative products of H<sub>2</sub>O vapor (Roth et al. 2014). Using off-limb observations while absorbing background light during Europa transits in front of Jupiter, Sparks et al. (2016, 2017) twice found indications for a plume at identical positions. However, both authors also report non-detections on several occasions, indicating sporadic or at least highly variable activity. In a reanalysis of *Galileo* magnetometer data recorded below 400 km altitude during the spacecraft's closest Europa flyby, Jia et al. (2018) reported anomalies consistent with plume activity close to the position of the Sparks et al. (2016, 2017) observations. Direct searches with the *Keck Observatory* found water vapour in only one of 17 observations, further suggesting that outgassing events are localized and sporadic (Paganini et al. 2020). Each of the individual observations does not provide unequivocal proof of a plume. However, the sum of all observations with multiple different techniques argues strongly for some level of at least intermittent venting activity. The origin of these putative plumes, however, remains an open question. Although a similar interpretation has been invoked for Europa as Enceladus (Southworth et al. 2015), the absence of correlation with true anomaly (Sparks et al. 2017; Paganini et al. 2020) and the much larger gravity on Europa challenge this interpretation.

## 2.5 Chaos Terrain

A terrain unique to Europa, and covering approximately a quarter of its surface, is termed chaos. Chaotic terrain is formed by disruption of the preexisting surface into isolated plates, coupled with the development of lumpy matrix material between the plates. Models for the formation of chaotic terrain that have been proposed in the literature fall into 1 of 5 categories – melt-through, diapirism, brine mobilization, sill injection, or impact – and are reviewed in Collins and Nimmo (2009). The melt-through model for chaos formation was born from the visible similarity of plates in chaotic terrain to terrestrial pack ice (Carr et al. 1998; Greeley et al. 1998). In this model, a heat source at the base of the icy shell facilitates melting of the overlying ice, exposing the ocean below and leading to the formation of

plates equivalent to icebergs that float in a matrix of refrozen ocean material (Greenberg et al. 1999; Thomson and Delaney 2001). The diapirism model for chaos formation proposes that the morphology of chaotic terrain and pits, spots, and domes (collectively termed lenticulae) represents the surface expression of rising diapirs (Pappalardo et al. 1998; Rathbun et al. 1998; Figueredo et al. 2002; Mével and Mercier 2007). Such diapirs would develop due to either thermal or compositional buoyancy within the ice shell (Barr and Showman 2009). In another model of chaos formation, Head and Pappalardo (1999) and Collins et al. (2000) suggest that the formation of matrix material arises from partial melting of non-water-ice, low-melting-point materials and the mobilization of resulting briny liquids within the ice shell. Another way to deliver liquid into the icy shell of Europa is to inject it directly from the ocean. In this formation model, sills of melt form within Europa's icy shell from pressurized water injected from fractures that penetrate its base (Crawford and Stevenson 1988; Collins et al. 2000; Manga and Wang 2007). Once water is emplaced, ice-water interactions and freeze out of the liquid can describe the unique morphological and topographic characteristics of chaos on Europa (Schmidt et al. 2011). Finally, morphological similarities between chaotic terrain on Europa and terrestrial explosion craters (Billings and Kattenhorn 2003) have led to the suggestion of an impact origin for the formation of chaos (Cox et al. 2008; Cox and Bauer 2015). In this model, floating plates of the original ice surface are preserved in a slushy matrix, filling an irregular hole in the ice left by the explosion crater.

### 3 Ice Shell Dynamics and Exchange Processes

Exchange processes between the deep ocean and the surface can provide key information about the chemistry and organic content of the ocean, including the chemical processes at work at the rocky core/ocean interface, as has been demonstrated for Enceladus. Similarly important is assessing the downward transfer from the surface to the ocean since surface material may provide compounds, such as oxidants, required to maintain the chemical disequilibrium between the ocean and possible hydrothermal fluids in the rocky core, a process that seems required for life (Hand et al. 2007). Exchange between the ocean and the surface involves transport through the icy shell.

#### 3.1 Thermal State of the Ice Shell

The thickness of the outer ice shell is the principal characteristic that influences potential exchanges between the interior and the surface (Chyba and Phillips 2002). It is controlled by thermal equilibrium between the shell and the subsurface ocean, which depends on how the energy from internal heating (radiogenic and/or tidal) is transported through the ice shell – both conduction and subsolidus convection are suitable heat transport mechanisms (e.g., Spohn and Schubert 2003; Mitri and Showman 2005; Tobie et al. 2006). The temperature profile is quite different between a conductive (colder) and a convective (warmer) shell. Moreover, various studies have shown that the convective processes can be separated into different regimes (e.g., Moresi and Solomatov 1995). In the stagnant lid regime, a thick conductive lid is present on top of the convective layer which effectively slows down the heat transfer and possibly limits the exchange between the ocean and the surface, while in the mobile lid regime, which represents plate tectonics, the lid is thinner and more heat and/or material can be transferred (Fig. 7a).

Subsolidus convection is an efficient way to transport material between the deep interior and the surface. On Earth, this process is coupled with plate tectonics that leads to the major

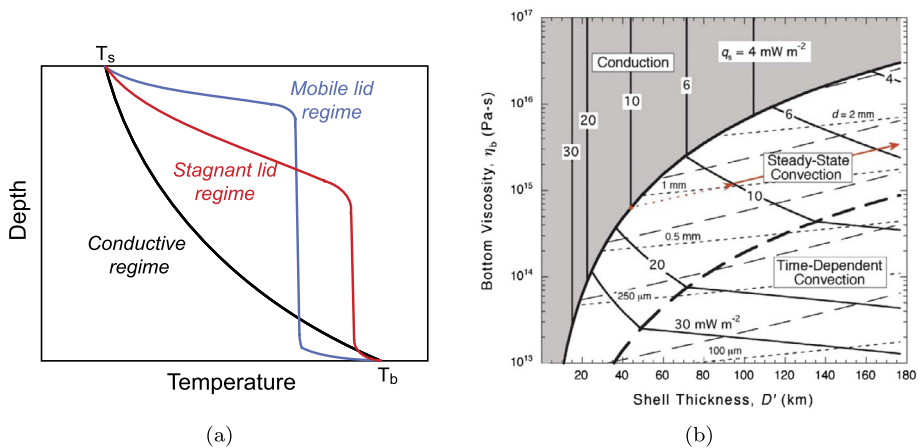


**Fig. 7** (a) Conductive (black) and convective thermal profiles in the stagnant (red) or mobile (blue) lid regime in the ice shell and (b) occurrence of convection (stationary or time-dependent) as a function of ice shell thickness and bottom viscosity in the stagnant lid regime (McKinnon 2006)

tectonic features such as mid-ocean ridges, subduction zones, and transform faults. It also produces most of the volcanism. Terrestrial convection is also characterized by the presence of hot plumes that form at a hot thermal boundary layer or are triggered by the presence of partial melt (Ogawa 2014). Although it is controlled by the same physical processes, thermal convection in icy shells differs significantly from terrestrial mantle convection for several reasons. First, silicate mantles are heated from within by radiogenic decay while icy mantles are mostly heated from below and, in some cases, from within by tidal heating. Second, internal melting creates a negative buoyancy due to the high density of liquid water relative to ice, while in silicate mantles, it favors the rise of hot thermal upwellings. Third, in the case of an icy crust above an internal ocean, the bottom interface is not fixed as for silicate mantles but evolves depending on crystallization/melting processes.

Thermal evolution models have provided some constraints on the ice shell thickness of ocean worlds in our solar system although more information is needed to obtain accurate present-day estimates. According to models, the outer ice shells can undergo large thickness variations during their evolution (Hussmann et al. 2002; Sotin et al. 2009; Mitri et al. 2010; Peddinti and McNamara 2019) and potentially produce multiple transitions between conductive and convective states (Mitri and Showman 2005). The coupling between the thermal and orbital evolution of Europa and Ganymede together with Io in the Laplace resonance could have produced multiple heat pulse events, potentially producing tectonic activity such as grooved terrains on Ganymede and internal melting in the crusts (Showman and Malhotra 1997; Bland et al. 2009). The Laplace resonance is a three-body resonance with a 1:2:4 orbital period ratio between Io, Europa, and Ganymede. Due to this resonance, orbital energy is transferred from Io to Europa and Ganymede through gravitational interactions, which forced the orbital eccentricity of the moons and which, under some circumstances, can increase the heat produced by tidal friction (Hussmann and Spohn 2004).

For most satellites, except probably Enceladus (Choblet et al. 2017a), tidal heating mainly occurs in the ice shell, where the visco-elastic timescale can be of the order of the orbital period of the tidal forcing (Tobie et al. 2003; Sotin et al. 2009; Beuthe 2013). As a consequence, modulation in the tidal forcing due to orbital resonances, such as the Laplace resonance, can lead to significant time variations in average ice shell thickness. Tidal heating

may also vary spatially. Tidal heating in thin ice shells is larger at the poles than at equatorial regions by a factor of about four (Tobie et al. 2003; Beuthe 2013) and also strongly depends on regional shell structure (e.g., the presence of faults) and thickness variations, since the tidal stress is approximately inversely proportional to the local shell thickness (Souček et al. 2016, 2019; Běhouňková et al. 2017; Beuthe 2018).

Although the question of thickness and thermal state of the ice shells is not satisfactorily resolved, various models of solid state convection have been developed. Consolmagno and Lewis (1978) initiated these studies, and more realistic models have subsequently been developed (e.g., Deschamps and Sotin 2000; Tobie et al. 2003; Barr and Pappalardo 2005; Mitri and Showman 2005; Barr and McKinnon 2007; Han and Showman 2010; Běhouňková et al. 2015; Weller et al. 2019) once it was discovered that taking into account the variability of viscosity was key to a good description of heat transfer by convection (Davaille and Jaupart 1993; Moresi and Solomatov 1995). The vigor of convection is measured through the non-dimensional Rayleigh number, which compares the driving mechanism (e.g., gravitationally induced thermal buoyancy) with the resistive mechanisms – diffusion of heat (described by heat diffusivity) and momentum (described by the fluid viscosity) (e.g., Ricard 2007). The Rayleigh number is defined as

$$Ra = \frac{\alpha \rho g \Delta T d^3}{\eta \kappa}$$

where  $\alpha$  is the thermal expansivity,  $\rho$  the fluid density,  $g$  the gravitational acceleration,  $\Delta T$  the typical temperature contrast over the fluid layer,  $d$  the characteristic size of the layer (typically the ice shell thickness),  $\eta$  the dynamic viscosity, and  $\kappa$  the thermal diffusivity. The main parameters that control how heat is transferred are the ice shell thickness and the ice viscosity. If the Rayleigh number exceeds a critical value ( $\sim 10^3$ ), ice starts to flow and heat is transferred by convection, which is more efficient than conduction since the conductive heat flux is inversely proportional to the thickness of the shell. For values of parameters appropriate to ice shells ( $\alpha \sim 10^{-4} \text{ K}^{-1}$ ,  $\rho \sim 920 \text{ kg m}^{-3}$ ,  $g \sim 1 \text{ m s}^{-2}$ ,  $\Delta T \sim 160 \text{ K}$ ,  $d \sim 10\text{--}100 \text{ km}$ ,  $\kappa \sim 10^{-6} \text{ m}^2 \text{ s}^{-1}$ ,  $\eta \sim 10^{14}\text{--}10^{16} \text{ Pa s}$ ), Rayleigh numbers can vary between  $10^3$  and  $10^8$  and it thus seems likely that many of the thicker ice shells may be convecting at the present time. The critical value of the thickness at which convection starts has been investigated by a number of studies that included different complexities in the viscosity laws applicable to ice (e.g., Deschamps and Sotin 2000; Mitri and Showman 2005; Barr and McKinnon 2007) and showed that the likelihood of subsolidus convection in the icy shells of ocean worlds depends strongly on the deformation properties of ice.

The creep behavior of ice I has been studied in laboratory (e.g., Durham and Stern 2001; Goldsby and Kohlstedt 2001; De La Chapelle et al. 1999) and observed on terrestrial glaciers (e.g., Hudleston 2015). Several mechanisms can occur to accommodate the deformation rate of ice: propagation of dislocations, diffusion, grain boundary sliding, and basal slip, each of them dominating in certain conditions. The deformation rate can be expressed as a combination of these different processes (Goldsby and Kohlstedt 2001) and depends on pressure ( $P$ ), temperature ( $T$ ), shear stress ( $\tau$ ), and grain size ( $d$ ), which also depends on the  $P$ - $T$ - $\tau$  conditions. Although each process has been well characterized, the grain size is poorly constrained for icy moons (Barr and McKinnon 2007). Yet its knowledge is crucial to determine the icy shells' thermal states since the smaller the grain size, the lower the value of viscosity and thus the thinner the layer at the onset of convection. Barr and McKinnon (2007) suggest that the minimum thickness for convection to initiate in large ocean worlds such as Ganymede would be between 35 and 66 km for grain sizes of 3 to 8 mm, respectively. In

a study applied to Callisto, McKinnon (2006) proposes maps showing the conditions for convection to exist as a function of the viscosity at the ice/ocean interface and the thickness of the ice layer (Fig. 7b). Although the domain for convection seems large and suggests that convection would be dominant for thicknesses larger than 20 km, note that the value of the corresponding grain size is less than 1 mm, which is more than an order of magnitude smaller than the values predicted in Barr and McKinnon (2007). Note also that the grain size evolution model predicts an increase in grain size after convection starts, leading to increased viscosity and less vigorous convection. Finally, the presence of impurities would affect the grain size of ice as it has been observed and modeled in cold ice sheets on the Earth (Durand et al. 2006). Convection processes in the icy crust may have been intermittent on Ganymede, Titan (Tobie et al. 2005, 2006), Europa (Husmann et al. 2002), and Enceladus (Barr 2008), and a definite answer has to await measurements by future missions.

### 3.2 Global Dynamics of the Ice Shell

Long-wavelength topography and gravity can be used to constrain the lateral variations in shell thickness. Its amplitude and pattern provide insights on the thermal state and global dynamics of the ice shell as well as on the coupling with the underlying ocean (e.g., Nimmo et al. 2011). In combination with heat production within the ice shell, strong heat flux anomalies coming from the seafloor and heat flux patterns due to oceanic circulation can lead to a modulation of the ice/ocean interface. The 3D structure of the ice shell and its global dynamics thus result from a balance between the heat transfer through the ice shell, melting/crystallization processes at the base and within the ice shell, and lateral ice flow (Čadek et al. 2017; Kvorka et al. 2018) (Fig. 8).

From the inversion of the topography and gravity data collected by *Cassini*, maps of ice shell thickness have been inferred by several studies on Titan (Lefevre et al. 2014; Mitri et al. 2014; Kvorka et al. 2018) and Enceladus (Čadek et al. 2016, 2019; Beuthe et al. 2016; Hemingway and Mittal 2019). On Titan, the long-wavelength topography is associated with small gravity anomalies indicating a high degree of compensation (e.g., Durante et al. 2019). The observed topography, characterized by relatively small amplitudes (about 1 km peak to peak) and an anomalous equatorial bulge (the poles are about 300 m lower than the equator) can be explained either by a deflection of the ocean/ice interface (Nimmo and Bills 2010; Hemingway et al. 2013; Lefevre et al. 2014) or by density variations in the upper crust, likely due to heavy hydrocarbon clathrates (Choukroun and Sotin 2012). Assuming that surface topography is due to ice/ocean interface deflection, the inferred deflection amplitude ( $\pm 5$  km) indicates a very slow ice flow at the base of the ice shell. It also implies a conductive and highly viscous ice shell above a relatively cold ocean ( $T < 250$  K) (Lefevre et al. 2014; Kvorka et al. 2018). By modeling the shape evolution of Titan's ice shell including diffusive heat transfer through the ice shell, heterogeneous tidal heating in the ice shell, heat flux anomalies from the ocean and basal ice flow, Kvorka et al. (2018) show that the observed topography is not consistent with tidal heating pattern in the ice shell and rather indicates heat flux anomalies in the ocean (Fig. 9a). The anomalous topographic bulge would be consistent with lateral variations of ocean heat flux on the order of 0.1–1 mW/m<sup>2</sup>, characterized by upwelling of warm water in polar regions and downwelling of cold water at low latitudes (Kvorka et al. 2018) that may result from convective flows in the ocean (Soderlund 2019; Amit et al. 2020) (see Sect. 4).

Using a similar approach, Čadek et al. (2019) estimated the heat flux anomalies at the bottom of Enceladus' ice shell in order to explain the observed topography (Tajeddine et al. 2017) and gravity (Iess et al. 2014). Compared to Titan, the ice shell thickness variations are

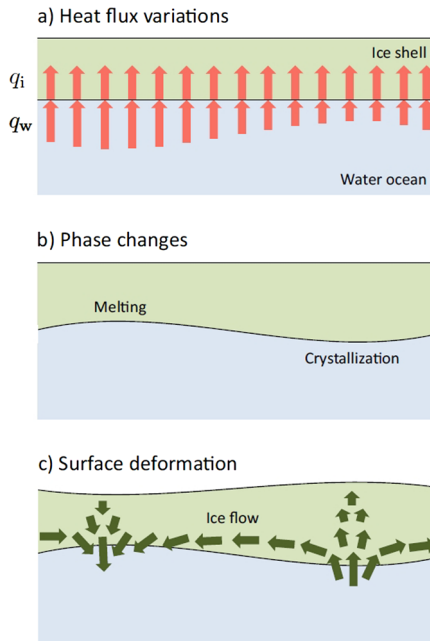


**Fig. 8** Sketch of the processes occurring at the ice/water interface and their consequences for the ice shell evolution (Kvorka et al. 2018). **(a)** The normal component of heat flux is not generally continuous at a phase interface. Melting occurs in regions where heat flux from the ocean is larger than heat flux in the ice shell. The opposite situation leads to crystallization. **(b)** In regions of melting, the ice shell loses mass and its thickness decreases. Crystallization is accompanied by ice mass gain and ice shell thickening. Both processes tend to restore the heat flux balance at the boundary. **(c)** Undulations of the ice/water interface generate pressure gradients that induce flows in the ice shell. These flows deform the upper boundary of the shell. Depressions develop above the regions of melting, while the surface tends to rise above the regions of crystallizations

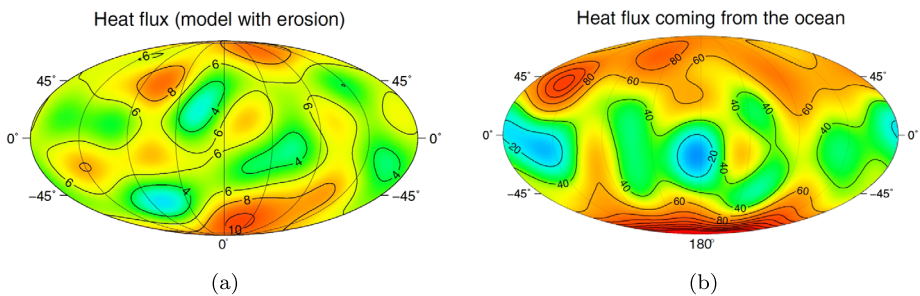


**Fig. 9** Heat flux anomalies from the ocean derived from the ice shell thickness variations, assuming a conductive ice shell, on **(a)** Titan for a model including surface mass redistribution by erosion (Kvorka et al. 2018) and **(b)** Enceladus (Čadek et al. 2019)

much larger, ranging from 5 km at the south pole to 35 km at the equator that are associated with heat flux anomalies about ten times larger than on Titan (Fig. 9b). By modelling the ice flow driven by variations in hydrostatic pressure on the ice/water interface, Čadek et al. (2019) demonstrated that Enceladus' ice shell is in a steady state, with melting located in polar regions and crystallization occurring in the equatorial region. The observed pattern is

consistent with the heat flux pattern predicted by tidally-heated water flow in the porous core of Enceladus (Choblet et al. 2017a), likely modulated by oceanic flow (Soderlund 2019).

The global shape data of Europa retrieved from *Galileo* limb profiles indicate that, if variations exist, they should be relatively small, thus implying an efficient ice flow at the base of the shell (Nimmo et al. 2007) or redistribution of topography through pressure-induced melting and freezing (Soderlund et al. 2014). The absence of significant ice shell thickness variations does not imply that there is no significant heat flow anomaly at the base of the ice shell. As shown by Čadek et al. (2017), any ice/ocean deflection relaxes much faster in Europa's conditions than in Enceladus' case because of its larger size. For the same ice shell thickness and viscosity structure, the relaxation rate is 100 times faster on Europa than on Enceladus, requiring a large heat flux anomaly to build up significant long-wavelength topography. Ashkenazy et al. (2018) modeled the global meridional ice flow in Europa's ice shell due to pressure gradients associated to equator-to-pole ice thickness variations. They show that the thickness variations barely exceed a few kilometers and are limited by ice flow and oceanic heat transport.

### 3.3 Melt Transport

While the observations of plumes at Enceladus and Europa support the possibility of liquids present within their ice shells, the physical processes leading to near-surface melting and liquid accumulation within the crust or their emplacement on the surface are still subject to discussion. Generation of liquids within the icy crust requires a heat source, such as tidal heating, and/or the presence of a secondary phase depressing the melting point. Two geodynamical contexts have been proposed for generation of melts by enhanced tidal heating inside the ice shell: either in hot upwelling plumes as a result of thermally-reduced viscosity (e.g., Sotin et al. 2002; Tobie et al. 2003; Běhounková et al. 2010) or along the faults due to tidally-activated strike-slip motions (e.g., Gaidos and Nimmo 2000; Nimmo and Gaidos 2002). Alternative sources of liquids would be a direct connection from the subsurface ocean through water-filled cracks (Fig. 10a, Sect. 2.4) and impact cratering (Fig. 10b, Sect. 2.1).

Contrary to the analogous setting on the Earth (silicate solids being denser than their melts), the negative buoyancy of water with respect to ice I is often seen as an obstacle to maintaining englacial water (Tobie et al. 2003; Kalousová et al. 2016). However, several possibilities have been proposed to overcome the negative buoyancy of water (e.g., Fagents 2003; Hammond et al. 2018): (i) volatiles such as CO<sub>2</sub>, CO, or SO<sub>2</sub> may be exsolved in water thus significantly increasing the fluid buoyancy, (ii) non-ice substances may be present in water or ice which will modify the density contrast between the two phases—either by decreasing the fluid density (e.g., NH<sub>3</sub>, CH<sub>4</sub>, N<sub>2</sub>) or by increasing the ice density (silicate particles, clathrates), (iii) compaction and associated low permeability of ice that allows an accumulation of melts within the shell, and (iv) partial freezing of a discrete liquid reservoir will lead to its overpressurization, which may further promote cracking and lead to water ascent.

Over long timescales, oceanic materials – either in the form of melt pockets or solid phases (salts, clathrate) – can be advected from the ice/ocean interface to the surface by thermal convection. The conductive lid separating the convective part from the surface (Fig. 7a) acts as a barrier for chemical exchanges. Rupture of the conductive lid, either by large-scale tectonic stresses and melt-induced collapse (Fig. 10c-d), is required to allow the exposure of materials brought by convective upwellings. Rupture of the lid also provides a means to recycle surface materials to the subsurface and potentially to advect them to the ocean

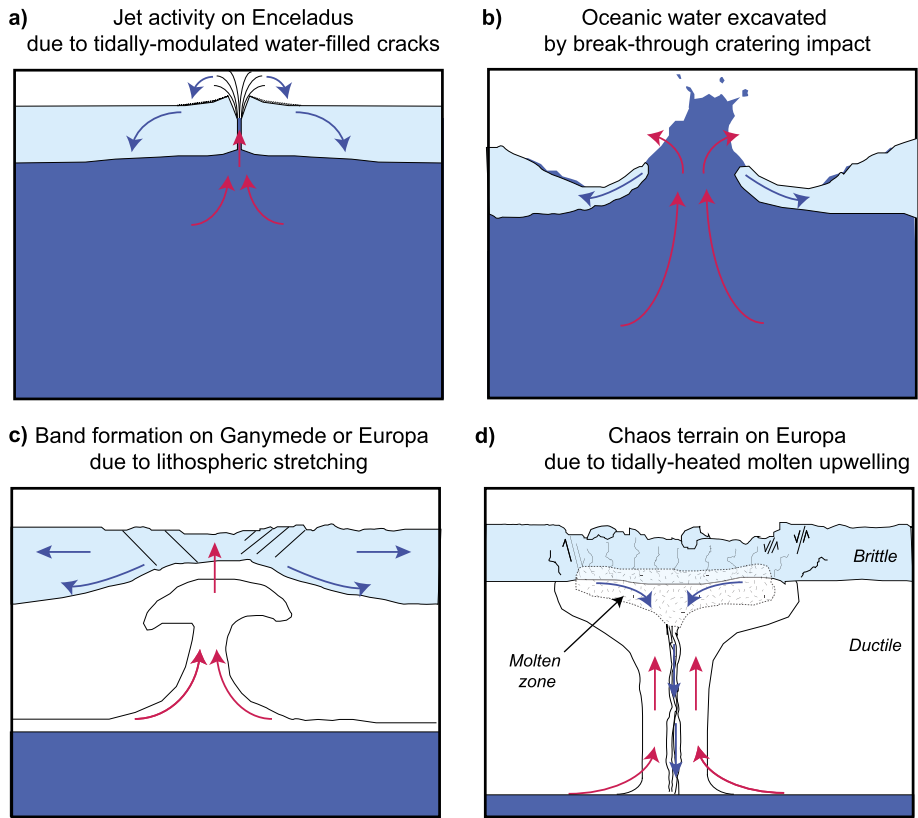


**Fig. 10** Four possible mechanisms leading to exchange between the subsurface ocean and the surface, which are mostly controlled by the ice shell thickness and the force acting on it: (a) oceanic water injection and associated jet activity requiring relatively thin shells ( $\lesssim 5$  km) and strong tidal forces (after Postberg et al. 2018b); (b) oceanic water excavation due to break-through cratering impact requiring ice shell thickness and impactor radius to be of comparable size (after Lunine et al. 2010); (c) indirect transport of oceanic materials by upwelling ices from the ocean/ice interface to shallow depths, associated with band formation and lithospheric stretching, occurring in 10–20 km thick shells under the action of significant tectonic stress (after Howell and Pappalardo 2018); (d) ice melting at shallow depths by tidally-heated thermal plumes and potential percolation of meltwater to the ocean, occurring for relatively thick ice shells ( $\gtrsim 25$  km) subjected to significant tidal forcing (after Sotin et al. 2002)

(Kattenhorn and Prockter 2014; Johnson et al. 2017; Klaser et al. 2019). In numerical simulations of thermal convection in icy shells, melting of water and its transport is often completely neglected (e.g., Han and Showman 2005, 2010) or highly simplified (Běhouňková et al. 2012). Some authors, however, have included water generation and considered its dynamic effect on the ice flow (Tobie et al. 2003; Kalousová et al. 2016). In these studies, the water content (porosity) is computed but the ice is considered to be effectively impermeable to the interstitial water transport (percolation) and water is thus simply advected by the flowing ice. These authors found that the occurrence of a few percents of water leads to fast (with respect to convection time scales) destabilization of the partially molten region, thus not supporting the long term stability of liquid water bodies. Let us note however, that only pure ice was considered and that the addition of salts may promote the melting process while the addition of volatiles may improve the buoyancy of the liquid. Alternatively, the

water transport by interstitial percolation has been modeled by using a two-phase mixture formalism by Kalousová et al. (2014) for Europa and Hammond et al. (2018) for Neptune's moon Triton. The drawback of these studies is that they only consider a one-dimensional geometry and thus neglect water advection by flowing ice (cf. above). The only simulations that took into account both water transport mechanisms, i.e. advection by ice and interstitial percolation, have been performed for the high-pressure ice layers of Ganymede (Kalousová et al. 2018; Kalousová and Sotin 2018) and Titan (Kalousová and Sotin 2020). More details can be found in Journaux et al. (2020). On the basis of the effect of melt on the dynamics and structure of the high-pressure ice layer, one can predict that a temperate layer (i.e. with temperature following the melting curve) would be present at the icy crust/ocean interface but details on its characteristics must await dedicated work.

Models have also been constructed to assess the possibility of cryolava ascent on the surfaces of icy satellites. Manga and Wang (2007) found that overpressure generated by freezing a few kilometers of ice is not sufficient for liquid water to erupt on the surface of Europa, while it may be sufficient on smaller satellites such as Enceladus. However, Quick and Marsh (2016) and Quick et al. (2017) found that cryolava may reach Europa's surface at temperatures as high as 250 K and undergo rapid cooling to form cryovolcanic domes. Even if the liquids do not reach the surface, they may be placed in the shallow subsurface where processes such as impact cratering can transport the deposited material on the surface.

The presence of near-surface liquid reservoirs was proposed to explain some ocean world surface morphologies in comparison with Earth-like processes. Michaut and Manga (2014) and Manga and Michaut (2017) investigated thermo-mechanical constraints on the emplacement and evolution of liquid water sills and proposed that Europa's pits, domes, and small chaos morphology could result from the evolution of these sills located at depths of 1 to 5 kilometers. Moreover, they suggest that the pits should be located above bodies of liquid water, which is in agreement with Schmidt et al. (2011) who proposed that Europa's chaos terrains form above liquid water lenses  $\sim 3$  kilometers below the surface. Walker and Schmidt (2015) investigated the effects of a subsurface liquid water body on the flexural response of an ice shell and the resulting topography. Their results reproduce the observed geology of Europa's chaos terrains as well as Enceladus' SPT, suggesting that they both formed by the ice collapse above a liquid water body. Similarly, sills and dikes have also been implicated for the formation of ridges on Europa (Dombard et al. 2013; Johnston and Montési 2014; Craft et al. 2016).

## 4 Ocean Dynamics and Exchange Processes

Oceans are an essential component of the ice-ocean exchange process as the intermediary layer between the outer ice shell and the underlying mantle/high pressure ice layer. Moreover, because the oceans are nearly inviscid and strong currents are expected, heat and materials are transported relatively quickly across them. Fluid motions within icy satellite oceans are driven by convection due to thermo-compositional density anomalies, mechanical forcings (e.g., tides, libration, and orbital precession), and magnetic forcing due to electromagnetic pumping. The resulting flows will promote mixing within the bulk ocean, which will influence the distribution of thermo-compositional gradients, especially along the seafloor and ice-ocean interface, and potentially have important implications for the ice shell and habitability.

## 4.1 Convection

### 4.1.1 Hydrothermal Plumes

The earliest efforts to understand ocean dynamics within icy worlds focused on local circulation driven by hydrothermal plumes upwelling from the rocky interior (Thomson and Delaney 2001; Goodman et al. 2004). The goal of these efforts was to explore connections between localized seafloor heating and geological features on the surface of Europa's ice crust. Initial work in this area (Thomson and Delaney 2001) argued that Coriolis forces would constrain the outward spread of the turbulent buoyant plume, creating a narrow "chimney" of warm fluid which could potentially deliver hydrothermal heat to a narrow patch of ice despite the depth of the ocean, and speculated that they could form the 5-20 km diameter lenticulae (Greenberg et al. 1999) or pits, domes, and spots (Pappalardo et al. 1998) commonly seen on Europa's surface. They further noted that these forces would create anticyclonic (counter-clockwise in the northern hemisphere) currents at the ice-water interface, which were consistent with the apparent motion of ice rafts in the large Conamara Chaos (Spaun et al. 1998).

Later work based on theoretical scaling laws for point-source plumes (Fernando et al. 1998), supplemented with laboratory tank experiments (Goodman et al. 2004) and numerical simulations (Goodman and Lenferink 2012), demonstrated that while the plumes would have a narrow aspect ratio, they would still be at least 20-50 km in diameter, far wider than the common sizes of pits, domes, and spots, suggesting that these features were more likely created by internal ice dynamics. However, the plume size was found to be compatible with the largest chaos regions on Europa. Temperature anomalies were found to be very small (mK) and flow velocities very weak (mm/s), making it unlikely that hydrothermal plumes would have any direct mechanical effect on the overlying ice layer. Mantle heat transport calculations by Lowell and DuBose (2005) also support the lack of melt-through events by hydrothermal plumes.

More recent work by Farber and Goodman (2014) included a better treatment of planetary rotation in these plumes and studied their implications for astrobiology. As a result of conservation of angular momentum and the Taylor-Proudman Theorem (Pedlosky 1987), rapid planetary rotation tends to inhibit shear flow along the axis of rotation (that is,  $(\boldsymbol{\Omega} \cdot \nabla)\mathbf{u} \rightarrow 0$ ). The flow is organized so that "Taylor columns" oriented parallel to the rotation axis do not deform. As a result, buoyant hydrothermal plumes tend to rise parallel to the planetary rotation axis (i.e. diagonally) rather than radially. This diagonal-ascent effect is typically ignored on the Earth (where the oceans are shallow and flows are typically much wider than they are deep), but it cannot be ignored in deep icy world ocean convection where ocean depth is a significant fraction of the satellite's radius. The diagonal ascent of a plume would cause its projection onto the ice surface to be an ellipse with the long axis oriented toward the pole. Hydrothermal plumes are also astrobiologically significant, both in providing a route for metabolically significant molecules to move from seafloor to surface, and for delivering potential biosignatures to the ice. Farber and Goodman (2014) also showed that tracer particles require thousands of years to move from top to bottom of Europa's ocean.

One important caveat remains, however. Local convective plumes will rise through a background ocean whose properties are determined by the ocean composition and global circulation. Compositional modification of these results is discussed below, and global convective flows are discussed in Sect. 4.1.2.

The extent to which hydrothermal plumes will buoyantly rise depends on the ocean composition. In a freshwater ocean, buoyancy of the plumes depends on its temperature relative

to the surrounding ocean water; since the warmer plumes are less dense, they are expected to reach the ice-ocean interface. However, the thermal expansion coefficient of water is negative between 0 and 3.98 °C (at 1 bar) such that the maximum fluid density is reached below at a temperature above the freezing point. As a result, the ocean would have a stable “stratosphere” beneath the ice-ocean interface that would prohibit further rising of the plume (Melosh et al. 2004). Increased pressure and ocean salinity move the temperature of maximum density towards the freezing temperature, reducing this effect. These temperatures coincide at pressures exceeding 27 MPa and salinities exceeding ~3 wt% for both seawater and magnesium sulfate compositions (Feistel and Hagen 1995; Melosh et al. 2004; Vance and Brown 2005). Further, considering a saline ocean, if the salt content is larger near the seafloor due to interactions with the underlying mantle or precipitates, its entrainment into the plumes would increase their density and cause them to reach the point of neutral density before reaching the ice-ocean interface (Vance and Brown 2005). However, Travis et al. (2012) argue that this initial salinity gradient would eventually become homogenized such that thermal buoyancy would regain dominance.

#### 4.1.2 Global Circulations

Heat flow from the seafloor combined with heat loss through the overlying ice shell is expected to drive thermal convection globally in the oceans, modulated by compositional buoyancy associated with salinity gradients that may enhance the vigor of convection (positive gradient) or have a stabilizing effect (negative gradient). The resulting fluid flows are governed by the Navier-Stokes equations where the most prominent forces are inertia, Coriolis, pressure gradient, and buoyancy, in combination with the ocean geometry and boundary conditions (e.g., Taubner et al. 2020). The hydrothermal plume studies above generally assume the ocean to be geostrophic, meaning a balance between the Coriolis and pressure gradient forces that effectively organizes the convective flows into quasi-two-dimensional Taylor columns that are aligned with the rotation axis (Fig. 11a). On a global scale, non-linear stresses associated with these columns will drive an eastward jet at low latitudes with multiple, alternating jets towards the poles, reminiscent of the jets in Jupiter’s atmosphere (Fig. 11b; e.g., Heimpel et al. 2015; Soderlund et al. 2014). The ocean is warmest at high latitudes due to the efficiency of vertical convection columns there and strong equatorial shear associated with the zonal jet (Fig. 11c; Aurnou et al. 2008). If zonal flows are weak, heat flow out of the ocean instead peaks at low latitudes (Amit et al. 2020).

As convection becomes more vigorous, however, the Taylor columns break down and fluid flows become three-dimensionalized. Here, mixing of absolute angular momentum will instead drive a westward equatorial jet and eastward jets at high latitudes (Fig. 11d; e.g., Aurnou et al. 2007; Gastine et al. 2013). A large-scale meridional overturning circulation also develops with upwelling flow near the equator and downwelling flow at higher latitudes in each hemisphere (Fig. 11e; Soderlund et al. 2013). This circulation brings warm ocean water preferentially toward the ice-ocean interface at low latitudes (Fig. 11f; Soderlund et al. 2014). Amit et al. (2020) find the opposite behavior for more vigorous convection with peak heat flow near the poles, which may again be attributable to zonal flow differences due to stress-free versus no-slip mechanical boundary conditions.

The transition between these convective regimes is an active area of research subject to considerable debate (e.g., Gastine et al. 2016; Cheng et al. 2018). Although the oceans are traditionally assumed to be strongly organized by rotation, Soderlund et al. (2014) postulated that Europa’s ocean is characterized by quasi-3D turbulence by estimating the convective regime following several potential scaling laws. These arguments are updated and extended

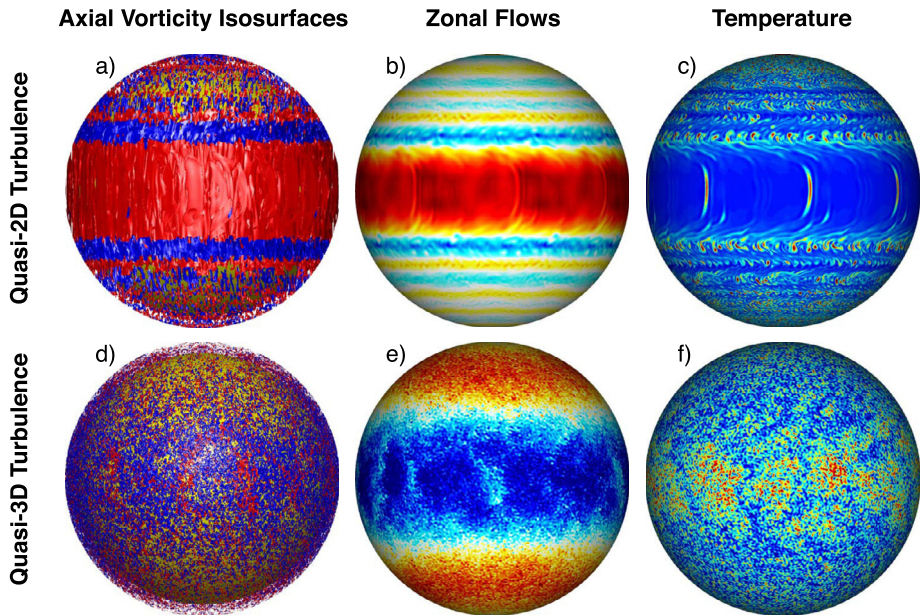


**Fig. 11** Flow structures, zonal flows, and temperature fields in convection models at a snapshot in time. Top row: Simulation with quasi-2D turbulence. Bottom row: Simulation with quasi-3D turbulence. Left column: axial vorticity isosurfaces,  $\omega_z = (\nabla \times \mathbf{u}) \cdot \hat{\mathbf{z}}$ . Red (blue) indicates cyclonic (anticyclonic) circulations aligned with the vertical  $\hat{\mathbf{z}}$  direction; the yellow sphere represents the seafloor. Middle column: zonal flows along the outer boundary; red (blue) indicates eastward (westward) flow. Right column: superadiabatic temperature fields below the outer boundary; red (blue) indicates warm (cool) fluid. Adapted from Soderlund et al. (2014)

to the oceans of Enceladus, Titan, and Ganymede in Soderlund (2019), who predicts thermal convection in the oceans of Europa, Ganymede, and Titan to all behave similarly (Fig. 11, bottom row). Rotation is predicted to play a more significant role for Enceladus. Considering the satellites collectively, peak zonal flow speeds are predicted to reach at least 10s of cm/s (up to meters per second) and mean (i.e. averaged over both time and all longitudes) radial flows span the mm/s to cm/s range (Soderlund 2019).

Complementary to the formation of individual chaos features through hydrothermal plumes, global convection models have focused the distribution of chaos terrains across Europa. Soderlund et al. (2014) hypothesized that the low latitude enhancement of ocean heating promotes the formation of these terrains through increased melting of the ice shell and subsequent accretion of relatively pure marine ice. Considering the other satellites, heat flux anomalies from the ocean derived recently for Enceladus (Čadek et al. 2019) and Titan (Kvorka et al. 2018) provide useful constraints for models of these oceans (see Fig. 9). The models of Soderlund (2019) are consistent with these heat flow patterns only if salinity effects are taken into account (cf. Amit et al. 2020). However, the distribution of heating from the underlying mantle/high pressure ice layer may be spatially heterogeneous (Travis et al. 2012; Choblet et al. 2017a,b; Kalousová et al. 2018) and these effects have not yet been taken into account.

Ocean composition and its thermodynamic properties may have a significant impact on global circulations due to the presence of a stable stratosphere if the thermal expansion coefficient is negative (Melosh et al. 2004) or if salinity gradients are maintained across the ocean. If salinity increases towards the seafloor, the thermal and compositional gradients op-

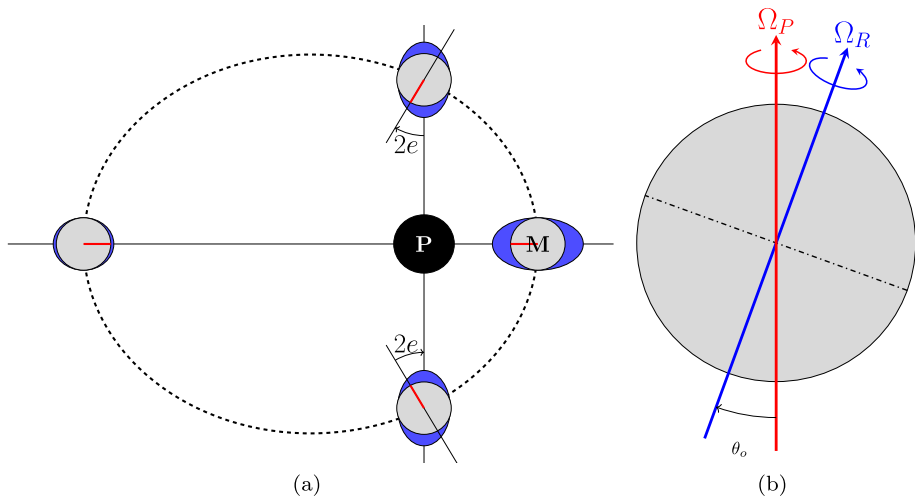


**Fig. 12** (a) Schematic representation of a tidally locked moon's eccentric orbit; the equilibrium tidal bulge is indicated in blue, and the  $0^\circ$  meridian is marked with a red line. Note the change of the tidal bulge amplitude and the longitudinal libration of the subplanet point. (b) A moon's rotation axes, where the moon rotates around its rotational axis with angular velocity  $\Omega_R$  and precesses with angular velocity  $\Omega_P$ , separated by the moon's obliquity  $\theta_o$

pose each other and double-diffusive convection may be expected (Vance and Brown 2005; Bouffard et al. 2017) with layering that can evolve into a 'staircase' configuration with well-mixed layers that are characterized by steps in salinity and temperature (e.g., Schmitt 1994). Conversely, if salinity increases toward the ice-ocean interface, both thermal and compositional gradients are unstable, leading to more vigorous convection. Melting and freezing along the ice-ocean interface will also lead to regions that are locally enhanced with fresher (i.e. stably stratified) and saltier (i.e. unstably stratified) water, respectively, that may drive additional circulations (Jansen 2016; Ashkenazy et al. 2018; Zhu et al. 2017). Moreover, if heterogeneous melting/freezing leads to large-scale topographic variations along the ice-ocean interface, they may also impact the characteristics of convection and promote mechanically driven flows (see Sect. 4.2).

## 4.2 Mechanical Forcings

The icy satellites are tidally locked, meaning that their rotational periods equal their orbital periods. This results in the moons having triaxial ellipsoid shapes with their longer axes pointing towards the planet. If the moons' orbits were perfectly circular and their rotational axis aligned with their orbital axis, there would not be any mechanical forcing. However, their orbits are eccentric and their rotational axes are tilted with respect to their orbital axes, resulting in time-changing tidal bulges, librations, and precessions (Fig. 12) that can drive ocean currents.

A common approach for studying ocean tides is to use the Laplace Tidal Equations (LTE) that control the barotropic ocean response (Hendershott 1981). The LTE assume a shallow ocean of constant density, and radial (vertical) ocean currents are considered to be negligible with respect to horizontal currents such that the problem becomes 2D. The resulting equations, which allow for surface gravity waves and planetary Rossby waves (e.g.,

Longuet-Higgins 1968), have been used to study the response of an ice-free ocean of constant thickness (e.g., Tyler 2008, 2009; Chen et al. 2014; Hay and Matsuyama 2017). The ocean response depends highly on the surface gravity wave speed. For thick oceans, the surface gravity wave speed is high, the ocean adjusts quickly to the perturbing tidal potential, and its response is given mainly by the equilibrium tide; this is the case of tides raised by a satellite's eccentricity (Fig. 13a). However, a high surface gravity wave speed does not hamper the propagation of tangentially non-divergent Rossby waves as they do not involve up and down motions (Fig. 13b).

The satellite's obliquity can excite planetary Rossby waves of sufficient amplitude to maintain a liquid ocean in Europa (Tyler 2014), but is insufficient to prevent Enceladus' ocean from freezing (e.g., Chen and Nimmo 2011; Matsuyama 2014). For thin oceans, gravity wave resonances can also occur. Nevertheless, characteristic ocean thicknesses for which these resonances occur are far from those inferred from observations; as an example, the thickest ocean for which a resonance occurs in Enceladus is around 350 m. If an ocean eventually begins to freeze out, it will necessarily go through resonant states where enhanced heat production prevents further freezing. Recently, Beuthe (2016), Matsuyama et al. (2018), and Hay and Matsuyama (2019) considered the effect of the overlying ice layer and showed that obliquity-forced dissipation is enhanced but the eccentricity tide is significantly dampened in satellites with high effective rigidity (Enceladus) and enhanced in satellites with low effective rigidity (Ganymede, Europa, Titan).

The LTE hold as long as the ratio of the characteristic vertical and horizontal length scales is small (Miles 1974). However, this may not be sufficiently accurate for icy satellite oceans. Using the ocean thickness and body's radius as a measure of vertical and horizontal length scales, higher ratios are obtained for Europa and Enceladus than for Earth ( $\sim 0.06$  and  $\sim 0.15$  versus  $\sim 0.001$ ), suggesting that 3D effects are relevant in the icy moons. Without the shallow water approximation, internal inertial waves can be excited. These waves have properties markedly different from shallow water waves. Upon reflection, an internal wave packet can change its wavelength. Depending on the ocean geometry, this can lead to the focusing of energy along internal shear layers (e.g., Rieutord et al. 2011; Maas 2005).

Rovira-Navarro et al. (2019) used the linearized Navier-Stokes equations to study the three dimensional response of an unstratified ocean of constant thickness to tidal forcing. They observed patterns of periodic inertial waves that take energy from the global tidal forcing and focus it along internal viscous shear layers that propagate in the ocean (see Fig. 13c). These shear layer fluid flows can have an amplitude of a few cm/s, but the dissipation due to inertial waves in an ocean of constant thickness is not sufficient to prevent a European or Enceladan ocean from freezing. Requier et al. (2019) extended this work to study the excitation of inertial waves by Enceladus' libration and concluded that this mechanism generates more dissipation than tidal forcing.

Rovira-Navarro et al. (2019) and Requier et al. (2019) ignored the advection terms in the Navier-Stokes equations, which otherwise can result in flow instabilities and the development of turbulence. Flow instabilities in spherical and ellipsoidal containers have been widely studied (e.g., Malkus 1994; Kerswell and Malkus 1998; Rieutord 2004). In a librating sphere, the viscous boundary layer at the solid-liquid interface can become unstable and break down to small scale turbulence. Wilson and Kerswell (2018) estimated the amount of tidal dissipation due to boundary layer instabilities and suggested that it should be potent enough to explain Enceladus' heat flux. If the container is ellipsoidal, the interaction of inertial waves with the mean flow excited by libration, precession, or tides can lead to the well-known elliptical instability, which also results in a turbulent flow regime similar to that shown in Fig. 13d (e.g., Kerswell 2002; Le Bars et al. 2015). Experimental and numerical work shows that Enceladus and Europa are likely unstable to libration-driven elliptic

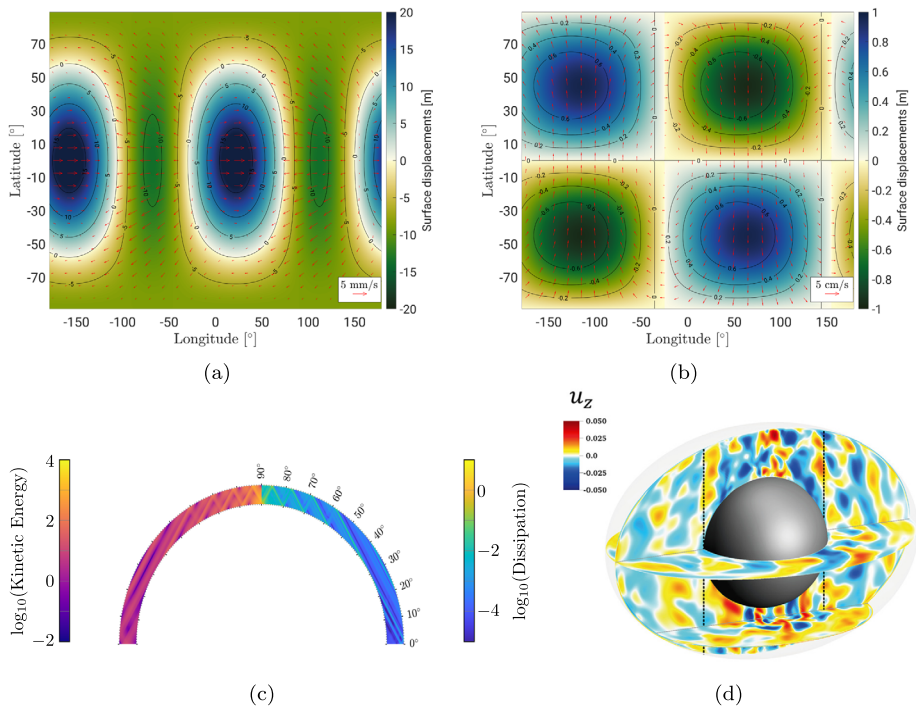


**Fig. 13** Characteristic flow fields for mechanical forcings. Flow field and surface displacements excited in Europa by the (a) eccentricity and (b) obliquity tide. The ocean is assumed to be 80 km and covered by a 20 km thick ice shell. Overlaid are contours corresponding to the equilibrium tide. The flow pattern propagates towards the east and west for the eccentricity and obliquity tides, respectively. Credit: M. Rovira-Navarro. (c) Internal waves excited by the eccentricity tide in an ice-free 30 (185) km thick Enceladus (European) ocean; the left and right quadrants respectively show the amplitude of kinetic energy and viscous dissipation. A logarithmic non-dimensional scale is used for both quantities with the maximum kinetic and viscous energy corresponding to 4.7 (0.65)  $\text{J/m}^3$  and 0.50 (0.026)  $\mu\text{W/m}^3$  for Enceladus (Europa), respectively (Rovira-Navarro et al. 2019). (d) Turbulent flow regime attained due to the libration-driven elliptical instability, where the vertical component of the non-dimensional velocity ( $u_z$ ) is shown. For more details, see Lemasquerier et al. (2017)

instability, while Titan, Ganymede and Callisto are probably not (Grannan et al. 2014, 2017; Lemasquerier et al. 2017). So far, ocean currents excited by mechanical forcing and convection (Sect. 4.1.2) have been studied separately. The interaction of mechanically driven and convective currents requires further attention.

The previous discussion assumed the ocean to be unstratified and contained within ellipsoidal or spherical shells devoid of topographical features. On Earth, stratification and ocean topography play a crucial role in shaping the ocean's response to tides by controlling the barotropic ocean response and the conversion of the barotropic tide to the (internal) baroclinic tide (Munk 1997; Egbert and Ray 2000). In icy ocean worlds, we expect the ocean floor and the basal ice shell topography to deviate from the idealized shapes explored so far in mechanically driven flow studies. For instance, Enceladus' ice shell thickness varies from  $\sim 5$  km at the south pole to  $\sim 30$  km at the equator (Sect. 1.2). Additionally, under certain circumstances a subsurface ocean might be stratified (Sect. 4.1.2). The study of mechanically-excited flows for complex ocean geometries and stratified subsurface oceans is an exciting topic for future research.

### 4.3 Magnetic Forcing

Jupiter's magnetic field is offset by  $\sim 10^\circ$  with respect to the orbital plane of the Galilean satellites. As a result, the satellites experience a time-varying magnetic field that induces electrical currents in the ocean. Akin to an induction electromagnetic pump, the salty ocean water is electromagnetically pumped by these variations of the Jovian magnetic field to drive a retrograde oceanic jet and weaker upwelling/downwelling motions at low latitudes (Gissinger and Petitdemange 2019). Because this induction pump is not very efficient, as indicated by the small Lorentz force ( $\sim 10^{-13}$  N/m<sup>3</sup> for Europa), the jet speeds are weak compared with the velocity of the Jovian field but large enough to still be significant oceanographically. Mean flow speeds of the equatorial jet are expected to reach a few cm/s in Europa's ocean, reducing to a few mm/s for Ganymede and  $< 1$  mm/s for Callisto where the Jovian magnetic field is weaker. This process is not expected to be significant for the Saturnian satellites due to the planet's nearly axisymmetric magnetic field.

Magnetic pumping leads to Ohmic dissipation within the oceans of  $\lesssim 10^8$  W (at Europa), which is several orders of magnitude weaker than both radiogenic and tidal heating. However, the dissipation may still be significant if it is spatially concentrated at high latitudes in a thin layer below the ice-ocean interface due to the skin effect (Gissinger and Petitdemange 2019). Moreover, because the zonal jet is characterized only by retrograde flow, it may contribute to the reorientation of Europa's ice shell (i.e. non-synchronous rotation) and the associated formation of lineaments (e.g., Helfenstein and Parmentier 1985).

## 5 Terrestrial Analogs

While a great amount of the work on ocean worlds has focused on geologic processes analogous to those seen within the solid Earth, studies of ice and ocean processes on Earth are equally important for understanding physical and biological processes on these moons. Here, we will show how analogs for the freezing and geochemical properties of planetary ice shells can draw from knowledge of sea ice and marine ice on Earth (e.g., Buffo 2019) as well as models of Snowball Earth (e.g., Ashkenazy et al. 2018).

### 5.1 Terrestrial Ice-Ocean Interfaces

The outer shells of icy satellites likely formed through top-down freeze-out of their oceans. On Earth, the majority of thick ice (ice sheets/shelves) is meteoric, forming via the compaction of snow. However, sea ice and marine ice on Earth form directly from the ocean and thus are analogous to what is expected on ocean bearing satellites. While forming under different environmental pressures, the thermal gradient is the main controller of ice chemistry in both sea ice and marine ice (e.g., Buffo et al. 2018; Buffo 2019). Analogously, it is likely that the ice-ocean interfaces of ice shells will be in either a high or low thermal gradient state, depending on shell thickness and age, where the high thermal gradient regime is similar to that observed in sea ice and the low thermal gradient to marine ice formed at the base of ice shelves.

Representative of the high thermal gradient regime, sea ice is easy to observe, both in the field and with remote sensing, and thus much is known about its structure and formation. The majority of sea ice is composed of granular and columnar ice (Dempsey and Langhorne 2012; Dempsey et al. 2010) driven by turbulent and quiescent ice-ocean interface conditions, respectively. However, in ice-shelf-adjacent sea ice in Antarctica, another process occurs

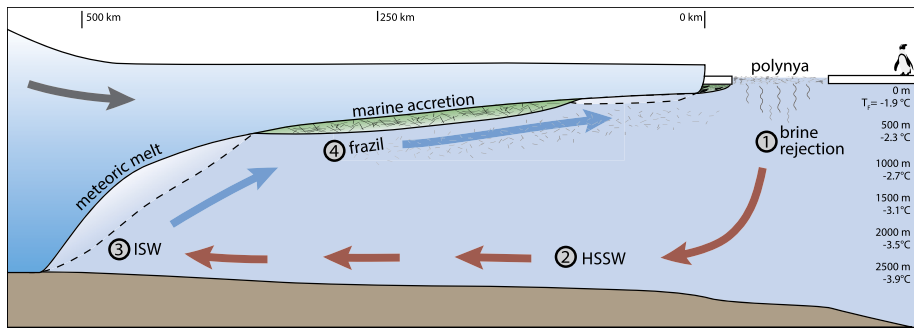


**Fig. 14** The ice pump, or how a slope in submerged ice interacts with the oceans to influence water mass formation and ice redistribution. On Earth, dense High Salinity Shelf Water (HSSW) forms via brine rejection in polynyas (1) and sinks, flowing into the shelf cavity (2). At the deep ice near the grounding zone, the *in situ* freezing point ( $T_f$ ) is lowered due to increased pressure. The HSSW formed at the warmer surface is above  $T_f$ , resulting in melting. This produces a fresh, buoyant Ice Shelf Water (ISW) plume (3). The ISW rises and  $T_f$  increases as the pressure decreases, resulting in the ISW becoming supercooled. Frazil ice crystals precipitate and release heat into the plume to relieve supercooling. The frazil ice accretes along the basal surface of the shelf and continues to grow, forming a layer of marine ice (4). Length and thickness approximately scaled to Amery Ice Shelf in West Antarctica (2.5 km thick grounding zone, 500 km length). Image modified from Lawrence et al. (2018)

that may be relevant to icy satellites: platelet ice accretion. Through a process known as the ice pump (e.g., Lewis and Perkin 1986), deep ice is melted at high pressures, creating a plume of fresher water that rises buoyantly along the shelf and out below the sea ice (Fig. 14). As the plume rises, depressurization causes the water to become supercooled (having temperatures below its *in situ* freezing point) and ice crystals called frazil or platelets form in the water column, rise up to the ice surface, and form a layer of poorly organized and highly porous ice. Under ice shelves, this layer can grow to immense thicknesses (> 100 m) and becomes marine ice (Fricker et al. 2001; Craven et al. 2005, 2009; Galton-Fenzi et al. 2012). Under sea ice, this platelet layer can be incorporated into the growing sea ice or remain unconsolidated. At the base of actively forming first year sea ice with low current velocities, transient brine drainage into supercooled water can additionally form brinicles (icicles that form around brine drainage channels), but these become inactive once the sea ice growth slows or platelet accretion takes over (Fig. 15).

Two lessons can be gained from sea ice and applied to icy satellites. First, thermal gradients are critical to the structure and composition of the ice. The thermal gradient within forming columnar sea ice is  $\sim 10$  K/m, for which the salinity is  $\sim 4$ –5 ppt (freezing from 34 ppt ocean), and it exhibits a critical porosity of 4–5% beyond which no brine drainage is observed (e.g., Dempsey et al. 2010; Golden et al. 2007). High thermal gradient conditions are only relevant for very shallow ice (< 1 km) on icy satellites, or if ocean water is injected rapidly from depth into the upper regions of their ice shells (Buffo 2019). In areas where rapid ice growth does occur, there could be important gradients in rheological properties that might make these regions more probable to fracture or re-melt (Buffo 2019). Second, ice accretion forced by melting of deep draft ice affects the thickness and properties of distant ice, which is key to consider as an interface process for other ice-ocean worlds. The thickness of the platelet ice layer is determined not by ice formation rate through surface cooling, but by the conditions of the ocean – very thick in large supercooling plumes to non-existent where the ocean is not supercooled. This layer can be efficiently modeled as

an upward sedimented layer of platelets whose crystal size is controlled by the degree of supercooling and the layer thickness by the lifetime of the plume (Buffo et al. 2018).

Representative of the low thermal gradient regime, marine ice is found in areas where supercooled water drives ice accretion onto the base of ice shelves (10s of meters to kilometers thick meteoric ice). This regime is characterized by very low thermal gradients,  $\ll 1$  K/m. The thickest marine ice observed on Earth is  $\sim 500$  m thick, comprising about half the thickness of the Amery ice shelf at its midpoint (Fricker et al. 2001). Borehole observations showed a many tens of meters thick unconsolidated platelet layer forming at the bottom of the marine ice (Craven et al. 2005). The marine ice in Amery demonstrates nearly complete brine rejection with salinities of 0.03–0.56 ppt (Craven et al. 2009), suggesting compaction driven desalination. Observations of accreting columnar marine ice at the bottom of the Ross Ice Shelf can be reproduced using sea ice models and lower thermal gradients: 5% critical porosity at 0.08 K/m yields a theoretical salinity of 1.7 ppt, while 1.95 ppt is estimated using constitutive equation based model results (Buffo 2019), which agrees well with field observations of 2.32 ppt (Zotikov et al. 1980).

The thermal gradient expected for most ice shells is squarely within the low-thermal gradient regime (e.g., 0.02 K/m for Europa (McKinnon 1999)). Once an ice shell reaches its diffusive limit ( $< 1$  km thick ice), the bulk salinity is unlikely to appreciably change, meaning that while the ice still contains some salt through accretion, the properties at the ice ocean interface do not change significantly with regards to the rate or properties of ice accreted (Buffo 2019), in the absence of platelet ice accretion. This diffusive limit marks how much ocean material the ice could deliver to the upper shell through convection or diapirism. These values are robust if the critical porosity is the physical limit past which brines are trapped within the ice, which is the observed limit in sea ice (Golden et al. 1998, 2007) and brine layers in ice shelves (Kovacs and Gow 1975) and matches observations of sub-ice shelf columnar ice (Buffo 2019).

Preliminary work by Buffo (2019) suggests that multiphase, hydraulically connected layers at the base of planetary ice shells are likely a stable, and thus common, phenomenon. Furthermore, the environmental pressures these layers are subject to (i.e., gravity, thermal gradient, ocean composition) likely dictate their thicknesses and structural properties. As the exchange boundary for energy and mass between the underlying ocean and ice shell, the structure and dynamics of these regions will substantially impact the thermochemical evolution of planetary cryospheres. Additionally, in the analogous terrestrial environments (sea ice), the porous nature of the ice-ocean interface provides a gradient rich substrate that supports a diverse biome.

## 5.2 Snowball Earth

At least two extreme glaciations occurred on Earth during the late Neoproterozoic era (750–580 Ma) (Hoffman and Schrag 2002). The Snowball Earth hypothesis proposes that the oceans froze over entirely during these episodes, so that the Earth was an icy ocean world. While debate continues over whether ice cover was total or partial (Liu and Peltier 2010), this episode may provide our best terrestrial proxy for ice covered oceans on a global scale. As with icy worlds in the outer solar system, a Snowball Earth ocean would be geothermally heated but isolated from direct solar heating or wind forcing. However, differential solar heating would still create variations in thickness that would drive global ice flow from pole to equator (Goodman and Pierrehumbert 2003). This flow would be balanced by melting and freezing into the ocean, leading to variations in salinity that would drive ocean circulations and close the glaciological cycle through the ocean (Ashkenazy et al. 2013). All of these

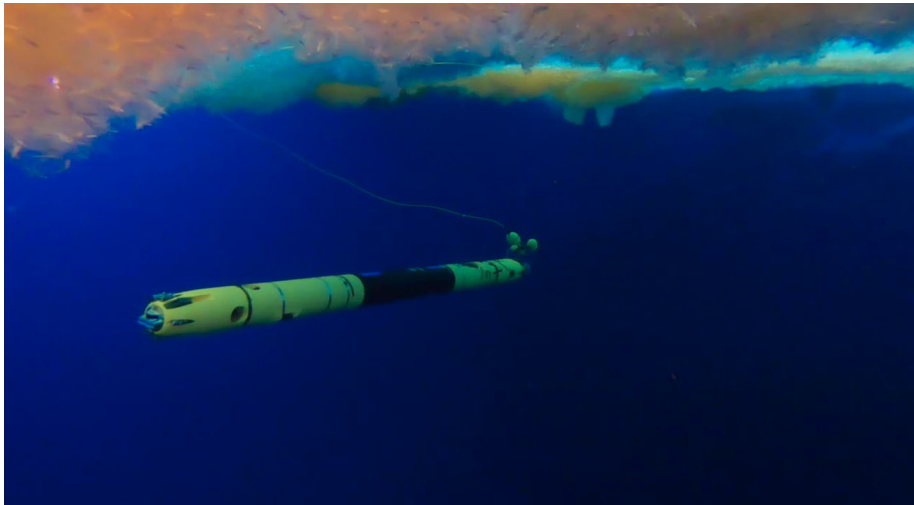


**Fig. 15** Platelet ice accreting under sea ice in McMurdo Sound. These ice crystals form in supercooled water below the adjacent McMurdo ice shelf and accrete onto the sea ice base. Brinicles can be seen in the background, extending downward from the ice-ocean interface. In some places beneath the shelf, these crystals accrete and compact to become marine ice, which may also be a process relevant to planetary ice-ocean interfaces. For scale, the underwater vehicle Icefin, at center, is approximately 12 feet in length. Credit: B. E. Schmidt/Icefin/RISEUP

dynamics are similar to predictions for the ice-covered oceans of the outer solar system, particularly the coupled interaction of global ice flow and haline-driven ocean circulation (Collins and Goodman 2007; Ashkenazy et al. 2018; Zhu et al. 2017). Interestingly, the unsolved question “Was the liquid ocean ever exposed at the surface?” is of key importance to both fields.

However, there are three key differences. First and most obviously, Earth’s oceans are relatively shallow and interrupted by continents. Their depth lessens the importance of planetary rotation (especially its horizontal component; Farber and Goodman 2014). The continents block global east-west flows of the type explored by Soderlund et al. (2014). On the other hand, coastlines allow fluid parcels to change their vorticity, enabling strong north-south currents that would otherwise be limited by angular momentum constraints (Pedlosky 1987).

A second difference between Snowball Earth and the icy worlds of the outer solar system is that Snowball Earth’s surface temperatures would have been far warmer, leading to a totally different pattern of ice flow dynamics. On Earth, modern-day and Snowball ice sheets flow via uniform strain, gradually spreading and thinning while maintaining constant flow velocity with depth (Weertman 1957; Goodman and Pierrehumbert 2003). However, this model does not work in the outer solar system: ice near the surface is too cold to flow at all. Instead, ice moves by vertical shear flow: warm ice near the base of the ice shell flows horizontally beneath a rigid upper shell (e.g., Collins and Goodman 2007; Ashkenazy et al. 2018). Relatedly, another distinction is that the tidal heating distribution between Snowball Earth and icy satellites would be different since the latter tend to be tidally locked with their host planets (e.g., Tobie et al. 2005).

Third, Snowball Earth would have had much thinner ice than the icy ocean worlds. Models of the Snowball Earth ice thickness typically predict ice 200–1000 m thick (Goodman and Pierrehumbert 2003), though local regions where clear ice allows solar penetration could

be as thin as a few meters (Warren et al. 2002). In contrast, ice shell thicknesses in the outer solar system range from  $\sim 5$  km at Enceladus' SPT to hundreds of kilometers for large satellites (e.g., Vance et al. 2018a). Many of these moons are then likely to be experiencing solid-state convection, while heat flow through Snowball Earth's ice shell probably occurred by conduction only. The thickness and weak thermal gradients within ice shells of ocean worlds also promotes the horizontal movement of ice via vertical shear rather than uniform strain, as discussed above.

Other important differences also abound, including greater uncertainties about solutes and seafloor heating distribution in the oceans of the outer solar system, but the similarities provide ample ground for collaboration between investigators in both fields.

## 6 Discussion and Perspectives

### 6.1 Habitability of Icy Ocean Worlds

The potential habitability of ocean worlds is an exciting prospect that has been commonly discussed for the past three decades, with increasing sophistication (e.g., Reynolds et al. 1983, 1987; Chyba 2000; Chyba and Phillips 2001; Hand et al. 2009; Vance et al. 2016; Barge and White 2017; Russell et al. 2017; Schmidt 2020), mirroring progress in astrobiology towards understanding the requirements to maintain a habitable planet. During this time, the direction of progress has been towards systems science, which is important for ocean worlds given that while they share many similarities with the Earth, conditions may be quite different. In particular, capturing coupled interactions between the geophysical and geochemical evolution of planets is needed given that the Earth and its biosphere coevolved (e.g., Des Marais et al. 2008; Hays et al. 2015).

Understanding the energy to support life in a given planetary system is the central organizing principle of the study of habitability. For the ocean worlds, this is a chance to understand not just what inventory of material they may have, but which processes continually supply energy for life. Here, the state of the interior, implied thermal and chemical evolution, and modern exogenic processes all couple together. Since light transmission even through pure glacial ice ceases at  $< 10$  m (Christner et al. 2014), photosynthesis is not a viable energetic pathway for the ocean worlds. Thus, understanding potential pathways for chemosynthesis (Zolotov and Shock 2003, 2004; Russell et al. 2017; Barge and White 2017), especially through serpentinization (Vance and Melwani Daswani 2020), is critical for understanding the habitability of icy ocean worlds.

Europa's global ocean, coupled with a potentially reducing interior (e.g., Zolotov and Shock 2001; Lowell and DuBose 2005; Vance et al. 2007, 2016) and oxidized surface (e.g., McCord et al. 2002; Paranicas et al. 2009) may provide a source of redox energy for a sub-surface biosphere. Life on Earth may have begun in relatively anoxic conditions potentially similar to conditions on Europa (Barge and White 2017; Russell et al. 2017). The surface of Europa is littered with spectrally detected salts that include  $\text{MgSO}_4$ ,  $\text{NaCl}$ , and  $\text{SO}$  compounds as well as sulfur implanted from the Io torus (see Carlson et al. (2009) for review), and  $\text{CO}$  and  $\text{CO}_2$  have been observed on the other moons but are likely unstable on Europa's surface (Hibbitts et al. 2000, 2003). Whether the ocean is highly reduced through interactions between the ocean and the seafloor (e.g., Zolotov and Shock 2001; Vance et al. 2007, 2016) or acidic due to downward transmission of oxidants from the surface (Pasek and Greenberg 2012) depends heavily on surface geology and the exchange rate with the ocean. However, it is unclear how much of the surface is actually drawn down into the interior and

how efficient surface-subsurface mixing could be. Determining what fraction of the surface is recycled or reprocessed in place, and how, will be important to constrain, alongside the elemental composition of surface materials. In particular, relative age dating of surface units with high resolution images combined with subsurface structural information from ice penetrating radar can constrain the nature and timescales of subduction/subsumption and other ice shell overturn processes. Overall, conditions of Europa's formation and later bombardment, as well as its past and potentially present activity, suggest the ingredients for life and present day energy to support it may exist.

For Enceladus, direct measurements of its ocean composition have been made by the *Cassini* mission. The ocean likely contains compounds that suggest ongoing interaction between the seafloor and ocean, as well as potential fuel for chemosynthetic life. Ocean-derived material erupting from Enceladus' south pole contains both simple and complex organics, ice crystals, and salts (Waite et al. 2006, 2009, 2017; Postberg et al. 2011, 2018b), while Hsu et al. (2015) demonstrated the presence of silica nanoparticles that are interpreted as evidence for extensive hydrothermalism and a well-mixed ocean. Waite et al. (2017) demonstrated the presence of molecular hydrogen that would be available energy for metabolism; however, it bears questions as to whether hydrogen would be detected if the ocean were inhabited since hydrogen could be consumed by metabolic processes. Nonetheless, Enceladus' ocean geochemistry is the only one measured to date and contains products known to support life on Earth, and therefore is habitable by current standards. A mission that would return to Enceladus and search for higher chained organics and organic complexity *in situ* within the plume could reveal strong indications as to whether life is present on Enceladus (e.g., Lunine et al. 2018).

For Ganymede and Titan, where high pressure ice phases become important, the most pertinent question is whether any interaction can be maintained between the silicate layer and the oceans. Though Ganymede's outer shell is presently inactive at the surface, its deeper ice layers may overturn under basal heating from the deeper interior (e.g., Kalousová et al. 2018). Vance et al. (2014) showed that the phase behavior of water-MgSO<sub>4</sub> salt mixtures under Ganymede conditions can form multiple ocean layers separated by high pressure ice layers, potentially with a deep reservoir of saline liquid above the silicate core that may argue for the possibility of serpentinization. Similar conditions could be possible at Titan, where clathrates may also play a role (Castillo-Rogez and Lunine 2010) and the ice shell may not be convecting (e.g., Nimmo and Bills 2010). It is unclear whether sources of oxidants could exist within ocean planets with outer ice shells in the stagnant lid regime, like Ganymede and Titan. However, if mixing between these reservoirs is possible, or if the decomposition of clathrates can deliver new sources of energy, these moons could be habitable. Titan's surface habitability is a different question all together; with liquid ethane and methane across the surface, Titan could support exotic kinds of habitability, fueled by different chemical compounds, including benzene (see Lunine et al. (2019) for a review).

## 6.2 *In Situ* Exploration of Terrestrial Habitats

Ice on Earth is rich with life both within the ice and along its interfaces (e.g., Prisco and Christner 2004; Deming and Eicken 2007). Analog habitats in Antarctica include perennially ice-covered lakes (e.g., Prisco et al. 1998; Murray et al. 2012) and subglacial lakes such as Vostok and Whillians (Christner et al. 2014; Mikucki et al. 2016). Although communities are supported primarily by the silicate materials at the bed, most of the communities are chemosynthetic, or rely on the oxidation and reduction of species such as iron, sulfur, nitrogen and methane as metabolisms. In the Arctic, subglacial volcanos in Iceland (e.g.,

Gaidos et al. 2004) and sulfur-rich subglacial springs expressed at the surface of Borup Fjord (Gleeson et al. 2011, 2012) power similar communities.

A growing amount of research is conducted via field studies with analog mission technologies, from *in situ* and remote sensing instrumentation to full vehicle platforms. Drilling vehicles are being developed for future missions as well as deep glacial access. In addition to ocean gliders (e.g., Lee and Rudnick 2018) and open ocean autonomous underwater vehicles (AUVs) (e.g., Jenkins 2010; Dutrieux et al. 2014) that have been developed for oceanographic operations on Earth, vehicles developed with ocean world exploration beyond Earth in mind include BRUIE (Buoyant Rover for Under-Ice Exploration (Berisford et al. 2013), ENDURANCE (Environmentally Non-Disturbing Under-ice Robotic ANtartic Explorer: Hovering Autonomous Underwater Vehicle) (Gulati et al. 2010), ARTEMIS (Autonomous Rovers/airborne-radar Transects of the Environment beneath the McMurdo Ice Shelf) (Kimball et al. 2018), Nereid Under Ice (German and Boetius 2019), and Icefin (Meister et al. 2018). These vehicles have operated under lake ice, sea ice and/or ice shelves and are returning data about oceanographic and ice-ocean exchange processes and their links to biological communities under the ice.

Analog missions on Earth feed forward into our understanding of planetary processes as well as how to one day explore these bodies *in situ*. Data from underwater vehicles inform everything from how ice-ocean exchange processes occur (e.g., Dutrieux et al. 2014) to how seafloor communities operate on Earth, such as the discovery of the Lost City hydrothermal field (Kelley et al. 2001). Scientifically, these missions contribute to exploring regions of our own planet that are challenging to observe with traditional means (Schmidt et al. 2020), revealing the physical underpinnings of ocean and ice processes across a wide variety of scales. The best analogs for icy ocean worlds are deep and/or covered by thick ice, such that they are only recently becoming accessible with robotic platforms (e.g., Shank et al. 2018; Schmidt 2020; Aguzzi et al. 2020). As these observations mature, so too do the technologies that make the observations possible, such as advancements in navigation, machine learning, and autonomous decision making that will be required for these vehicles to one day operate under the ice on ocean worlds.

### 6.3 Future Mission Exploration

Future missions can investigate ice-ocean exchange in the outer solar system. NASA's planned *Europa Clipper* mission will conduct multiple science investigations (Buffington et al. 2017): (i) *In situ* sampling of Europa's atmosphere will look for compositional and isotopic signatures of ocean pH and water-rock interactions. (ii) Remote sensing from the ultraviolet to mid-infrared will provide global mapping of 95% of the surface. (iii) Ice-penetrating radar will sound through kilometers of ice to characterize ice shell structure and search for the ice-ocean interface. (iv) Gravity science, magnetometer/plasma, and altimetry investigations will constrain the thickness of the ocean and underlying silicate layer, as well as the vigor of tidal heating, to understand the workings of the ice relative to the underlying materials (Pauer et al. 2010; Verma and Margot 2018; Steinbrügge et al. 2018). A complementary suite of instrument investigations is planned to fly on ESA's *Jupiter ICy moon Explorer (JUICE)* spacecraft (Grasset et al. 2013), which is anticipated to orbit Ganymede in the early 2030's.

Landed geophysical investigations on Europa (Pappalardo et al. 2013; Hand et al. 2017) could more precisely evaluate the satellite's radial density structure, rheological and thermal state of its mantle, and extent of seafloor hydration (Vance et al. 2018a,b). At the time of this writing, the *InSight* mission is conducting a geophysical investigation of Mars, using

seismometers and heat probes to further characterize the radial structure, composition, and temperature of the interior (Smrekar et al. 2018). The *Dragonfly* concept, selected as NASA's next New Frontiers class mission, will include seismic and mass spectrometer investigations that could reveal the hydration state of silicates in Titan's interior and the degree of ice-ocean exchange (Turtle et al. 2017).

The long term goals of ocean world exploration are the detection of life and the exploration of the oceans under the ice (e.g., Hendrix et al. 2019). Ultimately, the tools used for exploring the ice and ocean on Earth could be sent to exo-ocean worlds. As a result, missions that drill through the ice and those that would navigate water pockets and oceans under the ice are being developed by many groups (e.g., Dachwald et al. 2014; Stone et al. 2014; Winebrenner et al. 2016; Zacny et al. 2018; Cwik et al. 2019; Schmidt et al. 2020), and technology programs in this area are being funded by NASA (for example, SESAME program selections (2019)). From sampling actively during ice descent, to profiling the ocean, to surveying the underside of the ice shell, to one day accessing the seafloor, a number of potential missions to the ocean worlds exist just beyond the reach of current technology.

**Acknowledgements** The authors thank two anonymous reviewers for their thoughtful comments. K.M.S. was supported by NASA Grant NNX14AR28G. K.K. was supported by the Czech Science Foundation through project No. 19-10809S and by Charles University Research Program No. UNCE/SCI/023. C.R.G. was supported by NASA through the Cassini Project. G.M. acknowledges support from the Italian Space Agency (2018-25-HH.0). Work by F.P. was funded by the European Research Council (ERC) Consolidator Grant 724908-Habitat OASIS. M.R.N. has been financially supported by the Space Research User Support program of the Netherlands Organization for Scientific Research (NWO) under contract number ALW-GO/16-19. T.R. was supported by the Helmholtz Association (project VH-NG-1017). Work by JPL co-authors was partially supported by strategic research and technology funds from the Jet Propulsion Laboratory, Caltech, and by the Icy Worlds and Titan nodes of NASA's Astrobiology Institute (13-13NAI7\_2-0024 and 17-NAI8-2-017). The authors thank the European Space Agency (ESA) and the Belgian Federal Science Policy Office (BELSPO) for their support in the framework of the PRODEX programme. This is UTIG contribution number 3659.

**Publisher's Note** Springer Nature remains neutral with regard to jurisdictional claims in published maps and institutional affiliations.

## References

- J. Aguzzi, M.M. Flexas, S. Flögel, C. Lo Iacono, M. Tangherlini, C. Costa, S. Marini, N. Bahamon, S. Martini, E. Fanelli et al., Exo-ocean exploration with deep-sea sensor and platform technologies. *Astrobiology* (2020). <https://doi.org/10.1089/ast.2019.2129>
- M.F. A'Hearn, L.M. Feaga, H.U. Keller, H. Kawakita, D.L. Hampton, J. Kissel, K.P. Klaasen, L.A. McFadden, K.J. Meech, P.H. Schultz et al., Cometary volatiles and the origin of comets. *Astrophys. J.* **758**(1), 29 (2012)
- M.L. Allison, S.M. Clifford, Ice-covered water volcanism on Ganymede. *J. Geophys. Res., Solid Earth* **92**(B8), 7865–7876 (1987). <https://doi.org/10.1029/JB092iB08p07865>
- K. Altwegg, H. Balsiger, N. Hänni, M. Rubin, M. Schuhmann, I. Schroeder, T. Sémon, S. Wampfler, J.J. Berthelier, C. Briois et al., Evidence of ammonium salts in comet 67P as explanation for the nitrogen depletion in cometary comae. *Nat. Astron.* **4**, 533–540 (2020).
- H. Amit, G. Choblet, G. Tobie, F. Terra-Nova, O. Čadek, M. Bouffard, Cooling patterns in rotating thin spherical shells—Application to Titan's subsurface ocean. *Icarus* **338**, 113509 (2020)
- J.D. Anderson, E.L. Lau, W.L. Sjogren, G. Schubert, W.B. Moore, Gravitational constraints on the internal structure of Ganymede. *Nature* **384**(6609), 541 (1996)
- J.D. Anderson, G. Schubert, R.A. Jacobson, E.L. Lau, W.B. Moore, W.L. Sjogren, Distribution of rock, metals, and ices in Callisto. *Science* **280**(5369), 1573–1576 (1998a). <https://doi.org/10.1126/Science.280.5369.1573>
- J.D. Anderson, G. Schubert, R.A. Jacobson, E.L. Lau, W.B. Moore, W.L. Sjogren, Europa's differentiated internal structure: inferences from four Galileo encounters. *Science* **281**, 2019–2022 (1998b)

- J.D. Anderson, R.A. Jacobson, T.P. McElrath, W.B. Moore, G. Schubert, P.C. Thomas, Shape, mean radius, gravity field, and interior structure of Callisto. *Icarus* **153**(1), 157–161 (2001)
- N. Artemieva, J. Lunine, Cratering on Titan: impact melt, ejecta, and the fate of surface organics. *Icarus* **164**, 471–480 (2003). [https://doi.org/10.1016/S0019-1035\(03\)00148-9](https://doi.org/10.1016/S0019-1035(03)00148-9)
- N. Artemieva, J.I. Lunine, Impact cratering on Titan II. Global melt, escaping ejecta, and aqueous alteration of surface organics. *Icarus* **175**, 522–533 (2005). <https://doi.org/10.1016/j.icarus.2004.12.005>
- Y. Ashkenazy, H. Gildor, M. Losch, F.A. Macdonald, D.P. Schrag, E. Tziperman, Dynamics of a Snowball Earth ocean. *Nature* **495**, 90–93 (2013). <https://doi.org/10.1038/nature11894>
- Y. Ashkenazy, R. Sayag, E. Tziperman, Dynamics of the global meridional ice flow of Europa's icy shell. *Nat. Astron.* **2**(1), 43–49 (2018). <https://doi.org/10.1038/s41550-017-0326-7>
- S.K. Atreya, E.Y. Adams, H.B. Niemann, J.E. Demick-Montelara, T.C. Owen, M. Fulchignoni, F. Ferri, E.H. Wilson, Titan's methane cycle. *Planet. Space Sci.* **54**(12), 1177–1187 (2006). <https://doi.org/10.1016/j.pss.2006.05.028>
- J.M. Aurnou, M.H. Heimpel, J. Wicht, The effects of vigorous mixing in a convective model of zonal flow on the Ice Giants. *Icarus* **190**, 110–126 (2007)
- J.M. Aurnou, M.H. Heimpel, L. Allen, E.M. King, J. Wicht, Convective heat transfer and the pattern of thermal emission on the gas giants. *Geophys. J. Int.* **173**, 793–801 (2008)
- R.M. Baland, G. Tobie, A. Lefevre, T. Van Hoolst, Titan's internal structure inferred from its gravity field, shape, and rotation state. *Icarus* **237**, 29–41 (2014)
- P.S. Balog, R.A. Secco, D.C. Rubie, D.J. Frost, Equation of state of liquid Fe-10 wt% S: Implications for the metallic cores of planetary bodies. *J. Geophys. Res. Solid Earth* **108**(B2) (2003). <https://doi.org/10.1029/2001JB001646>
- L.M. Barge, L.M. White, Experimentally testing hydrothermal vent origin of life on Enceladus and other icy/ocean worlds. *Astrobiology* **17**(9), 820–833 (2017)
- A.C. Barr, Mobile lid convection beneath Enceladus' south polar terrain. *J. Geophys. Res., Planets* **113**(E7) (2008). <https://doi.org/10.1029/2008JE003114>
- A.C. Barr, R.M. Canup, Origin of the Ganymede–Callisto dichotomy by impacts during the late heavy bombardment. *Nat. Geosci.* **3**(3), 164 (2010)
- A.C. Barr, W.B. McKinnon, Convection in ice I shells and mantles with self-consistent grain size. *J. Geophys. Res., Planets* **112**(E2) (2007). <https://doi.org/10.1029/2006JE002781>
- A.C. Barr, R.T. Pappalardo, Onset of convection in the icy Galilean satellites: Influence of rheology. *J. Geophys. Res., Planets* **110**(E12) (2005). <https://doi.org/10.1029/2004JE002371>
- A.C. Barr, A.P. Showman, Heat transfer in Europa's icy shell, in *Europa*, ed. by R.T. Pappalardo, W.B. McKinnon, K.K. Khurana (University of Arizona Press, Tucson, 2009), pp. 405–430
- C. Béghin, O. Randriamboarison, M. Hamelin, E. Karkoschka, C. Sotin, R.C. Whitten, J.J. Berthelier, R. Grard, F. Simões, Analytic theory of Titan's Schumann resonance: constraints on ionospheric conductivity and buried water ocean. *Icarus* **218**(2), 1028–1042 (2012)
- M. Běhounková, G. Tobie, G. Choblet, O. Čadek, Coupling mantle convection and tidal dissipation: applications to Enceladus and Earth-like planets. *J. Geophys. Res., Planets* **115**(E14), E09011 (2010). <https://doi.org/10.1029/2009JE003564>
- M. Běhounková, G. Tobie, G. Choblet, O. Čadek, Tidally-induced melting events as the origin of south-pole activity on Enceladus. *Icarus* **219**, 655–664 (2012). <https://doi.org/10.1016/j.icarus.2012.03.024>
- M. Běhounková, G. Tobie, O. Čadek, G. Choblet, C. Porco, F. Nimmo, Timing of water plume eruptions on Enceladus explained by interior viscosity structure. *Nat. Geosci.* **8**, 601–604 (2015). <https://doi.org/10.1038/ngeo2475>
- M. Běhounková, O. Souček, J. Hron, O. Čadek, Plume activity and tidal deformation on Enceladus influenced by faults and variable ice shell thickness. *Astrobiology* **17**(9), 941–954 (2017). <https://doi.org/10.1089/ast.2016.1629>
- M.J.S. Belton, J.W. Head, A.P. Ingersoll, R. Greeley, A.S. McEwen, K.P. Klaasen, D. Senske, R. Pappalardo, G. Collins, A.R. Vasavada, R. Sullivan, D. Simonelli, P. Geissler, M.H. Carr, M.E. Davies, J. Veverka, P.J. Gierasch, D. Banfield, M. Bell, C.R. Chapman, C. Anger, R. Greenberg, G. Neukum, C.B. Pilcher, R.F. Beebe, J.A. Burns, F. Fanale, W. Ip, T.V. Johnson, D. Morrison, J. Moore, G.S. Orton, P. Thomas, R.A. West, Galileo's first images of Jupiter and the Galilean Satellites. *Science* **274**(5286), 377–385 (1996). <https://doi.org/10.1126/science.274.5286.377>
- D.F. Berisford, J. Leichty, A. Klesh, K.P. Hand, Remote under-ice roving in Alaska with the buoyant rover for under-ice exploration, in *AGU Fall Meeting Abstracts* (2013)
- M. Beuthe, Spatial patterns of tidal heating. *Icarus* **223**, 308–329 (2013)
- M. Beuthe, Crustal control of dissipative ocean tides in Enceladus and other icy moons. *Icarus* **280**, 278–299 (2016)
- M. Beuthe, Enceladus's crust as a non-uniform thin shell: I tidal deformations. *Icarus* **302**, 145–174 (2018). <https://doi.org/10.1016/j.icarus.2017.11.009>

- M. Beuthe, A. Rivoldini, A. Trinh, Enceladus's and Dione's floating ice shells supported by minimum stress isostasy. *Geophys. Res. Lett.* **43**(19), 10,088–10,096 (2016)
- B. Bézard, R.V. Yelle, C.A. Nixon, The composition of Titan's atmosphere, in *Titan: Interior, Surface, Atmosphere, and Space Environment*, ed. by I. Müller-Wodarg, C.A. Griffith, E. Lellouch, T.E. Cravens (Cambridge University Press, Cambridge, 2014), p. 158
- E.B. Bierhaus, K. Zahnle, C.R. Chapman, R.T. Pappalardo, W.B. McKinnon, K.K. Khurana, Europa's crater distributions and surface ages, in *Europa* (University of Arizona Press, Tucson, 2009), p. 161
- S.E. Billings, S.A. Kattenhorn, Comparison between terrestrial explosion crater morphology in floating ice and European chaos, in *Lunar and Planetary Institute Science Conference Abstracts*, vol. 34 (2003), p. 1955
- S.E. Billings, S.A. Kattenhorn, The great thickness debate: Ice shell thickness models for Europa and comparisons with estimates based on flexure at ridges. *Icarus* **177**(2), 397–412 (2005)
- M.T. Bland, A.P. Showman, G. Tobie, The orbital–thermal evolution and global expansion of Ganymede. *Icarus* **200**(1), 207–221 (2009)
- M. Bouffard, S. Labrosse, G. Choblet, A. Fournier, J. Aubert, P.J. Tackley, A particle-in-cell method for studying double-diffusive convection in the liquid layers of planetary interiors. *J. Comput. Phys.* **346**, 552–571 (2017)
- A. Bouquet, C.R. Glein, J.H. Waite Jr., How adsorption affects the gas–ice partitioning of organics erupted from Enceladus. *Astrophys. J.* **873**(1), 28 (2019)
- M.E. Brown, K.P. Hand, Salts and radiation products on the surface of Europa. *Astrophys. J.* **145**, 110 (2013)
- B. Buffington, T. Lam, S. Campagnola, J. Ludwinski, E. Ferguson, B. Bradley, C. Scott, M. Ozimek, A. Haapala Chalk, F. Siddique, Evolution of trajectory design requirements on NASA's Planned Europa Clipper Mission, in *68th International Astronautical Congress (IAC)*, IAC-17-C1.7.8 (2017)
- J.J. Buffo, Multiphase reactive transport in planetary ices. PhD thesis, Georgia Institute of Technology (2019)
- J.J. Buffo, B.E. Schmidt, C. Huber, Multiphase reactive transport and platelet ice accretion in the sea ice of McMurdo sound, Antarctica. *J. Geophys. Res.*, *Oceans* **123**(1), 324–345 (2018)
- O. Čadek, G. Tobie, T. Van Hoolst, M. Massé, G. Choblet, A. Lefèvre, G. Mitri, R.M. Baland, M. Běhouňková, O. Bourgeois et al., Enceladus's internal ocean and ice shell constrained from Cassini gravity, shape, and libration data. *Geophys. Res. Lett.* **43**(11), 5653–5660 (2016)
- O. Čadek, M. Běhouňková, G. Tobie, G. Choblet, Viscoelastic relaxation of Enceladus's ice shell. *Icarus* **291**, 31–35 (2017). <https://doi.org/10.1016/j.icarus.2017.03.011>
- O. Čadek, O. Souček, M. Běhouňková, G. Choblet, G. Tobie, J. Hron, Long-term stability of Enceladus' uneven ice shell. *Icarus* **319**, 476–484 (2019)
- R.W. Carlson, W.M. Calvin, J.B. Dalton, G.B. Hansen, R.L. Hudson, R.E. Johnson, T.B. McCord, M.H. Moore, Europa's surface composition, in *Europa* (2009), pp. 283–327
- M.H. Carr, M.J.S. Belton, C.R. Chapman, M.E. Davies, P. Geissler, R. Greenberg, A.S. McEwen, B.R. Tufts, R. Greeley, R. Sullivan, J.W. Head, R.T. Pappalardo, K.P. Klaasen, T.V. Johnson, J. Kaufman, D. Senske, J. Moore, G. Neukum, G. Schubert, J.A. Burns, P. Thomas, J. Veverka, R. Greeley, Evidence for a subsurface ocean on Europa. *Nature* **391**, 363–365 (1998)
- R. Casacchia, R.G. Strom, Geologic evolution of Galileo Regio, Ganymede. *J. Geophys. Res.*, *Solid Earth* **89**(S02), B419–B428 (1984)
- J.C. Castillo-Rogez, J.I. Lunine, Evolution of Titan's rocky core constrained by Cassini observations. *Geophys. Res. Lett.* **37**(20) (2010). <https://doi.org/10.1029/2010GL044398>
- E.M.A. Chen, F. Nimmo, Obliquity tides do not significantly heat Enceladus. *Icarus* **214**(2), 779–781 (2011)
- E.M.A. Chen, F. Nimmo, G.A. Glatzmaier, Tidal heating in icy satellite oceans. *Icarus* **229**, 11–30 (2014)
- J.S. Cheng, J.M. Aurnou, K. Julien, R.P.J. Kunnen, A heuristic framework for next-generation models of geostrophic convective turbulence. *Geophys. Astrophys. Fluid Dyn.* **112**(4), 277–300 (2018)
- G. Choblet, G. Tobie, C. Sotin, M. Běhouňková, O. Čadek, F. Postberg, O. Souček, Powering prolonged hydrothermal activity inside Enceladus. *Nat. Astron.* **1**(12), 841 (2017a)
- G. Choblet, G. Tobie, C. Sotin, K. Kalousová, O. Grasset, Heat transport in the high-pressure ice mantle of large icy moons. *Icarus* **285**, 252–262 (2017b). <https://doi.org/10.1016/j.icarus.2016.12.002>
- M. Choukroun, O. Grasset, Thermodynamic data and modeling of the water and ammonia–water phase diagrams up to 2.2 GPa for planetary geophysics. *J. Chem. Phys.* **133**, 144502 (2010)
- M. Choukroun, C. Sotin, Is Titan's shape caused by its meteorology and carbon cycle? *Geophys. Res. Lett.* **39**(4) (2012). <https://doi.org/10.1029/2011GL050747>
- B.C. Christner, J.C. Priscu, A.M. Achberger, S.P. Carter, K. Christianson, A.B. Michaud, J.A. Mikucki, A.C. Mitchell, M.L. Skidmore et al., A microbial ecosystem beneath the West Antarctic ice sheet. *Nature* **512**(7514), 310 (2014)

- C.F. Chyba, Energy for microbial life on Europa. *Nature* **403**(6768), 381 (2000)
- C.F. Chyba, C.B. Phillips, Possible ecosystems and the search for life on Europa. *Proc. Natl. Acad. Sci.* **98**(3), 801–804 (2001)
- C.F. Chyba, C.B. Phillips, Europa as an abode of life. *Orig. Life Evol. Biosph.* **32**(1), 47–67 (2002). <https://doi.org/10.1023/A:1013958519734>
- P.L. Clay, R. Burgess, H. Busemann, L. Ruzié-Hamilton, B. Joachim, J.M.D. Day, C.J. Ballentine, Halogens in chondritic meteorites and terrestrial accretion. *Nature* **551**(7682), 614 (2017)
- G.C. Collins, J.C. Goodman, Enceladus' south polar sea. *Icarus* **189**(1), 72–82 (2007)
- G.C. Collins, F. Nimmo, Chaotic terrain on Europa, in *Europa*, ed. by R.T. Pappalardo, W.B. McKinnon, K.K. Khurana (University of Arizona Press, Tucson, 2009), pp. 259–281
- G.C. Collins, J.W. Head, R.T. Pappalardo, N.A. Spaun, Evaluation of models for the formation of chaotic terrain on Europa. *J. Geophys. Res.* **105**, 1709–1716 (2000)
- J.A.D. Connolly, The geodynamic equation of state: what and how. *Geochem. Geophys. Geosyst.* **10**(10) (2009). <https://doi.org/10.1029/2009GC002540>
- G.J. Consolmagno, J.S. Lewis, The evolution of icy satellite interiors and surfaces. *Icarus* **34**(2), 280–293 (1978). [https://doi.org/10.1016/0019-1035\(78\)90168-9](https://doi.org/10.1016/0019-1035(78)90168-9)
- P. Corlies, A.G. Hayes, S.P.D. Birch, R. Lorenz, B.W. Stiles, R. Kirk, V. Poggiali, H. Zebker, L. Iess, Titan's topography and shape at the end of the Cassini Mission. *Geophys. Res. Lett.* **44**(23), 11–754 (2017)
- R. Cox, A.W. Bauer, Impact breaching of Europa's ice: constraints from numerical modeling. *J. Geophys. Res., Planets* **120**(10), 1708–1719 (2015)
- R. Cox, L.C.F. Ong, M. Arakawa, K.C. Scheider, Impact penetration of Europa's ice crust as a mechanism for formation of chaos terrain. *Meteorit. Planet. Sci.* **43**(12), 2027–2048 (2008).
- K.L. Craft, G.W. Patterson, R.P. Lowell, L. Germanovich, Fracturing and flow: investigations on the formation of shallow water sills on Europa. *Icarus* **274**, 297–313 (2016). <https://doi.org/10.1016/j.icarus.2016.01.023>
- M. Craven, F. Carsey, A. Behar, J. Matthews, R. Brand, A. Elcheikh, S. Hall, A. Treverrow, Borehole imagery of meteoric and marine ice layers in the Amery Ice Shelf, East Antarctica. *J. Glaciol.* **51**(172), 75–84 (2005)
- M. Craven, I. Allison, H.A. Fricker, R.C. Warner, Properties of a marine ice layer under the amery ice shelf, East Antarctica. *J. Glaciol.* **55**(192), 717–728 (2009)
- G.D. Crawford, D.J. Stevenson, Gas-driven water volcanism and the resurfacing of Europa. *Icarus* **73**(1), 66–79 (1988). [https://doi.org/10.1016/0019-1035\(88\)90085-1](https://doi.org/10.1016/0019-1035(88)90085-1)
- S.K. Croft, R. Casacchia, R.G. Strom, (US) GS, Geologic map of the tiamat sulcus quadrangle (jg-9) of ganymede. U S Geol Surv Map I-1548 (1994)
- M. Čuk, L. Dones, D. Nesvorný, Dynamical evidence for a late formation of Saturn's moons. *Astrophys. J.* **820**(2), 97 (2016)
- T. Cwik, W. Zimmerman, M. Smith, An architecture for a nuclear powered cryobot to access the oceans of icy worlds, in *Nuclear and Emerging Technologies for Space, American Nuclear Society Topical Meeting* (2019), pp. abstract–122
- B. Dachwald, J. Mikucki, S. Tulaczyk, I. Digel, C. Espe, M. Feldmann, G. Francke, J. Kowalski, C. Xu, IceMole: a maneuverable probe for clean in situ analysis and sampling of subsurface ice and subglacial aquatic ecosystems. *Ann. Glaciol.* **55**(65), 14–22 (2014)
- A. Davaille, C. Jaupart, Transient high-Rayleigh-number thermal convection with large viscosity variations. *J. Fluid Mech.* **253**, 141–166 (1993). <https://doi.org/10.1017/S0022112093001740>
- S. De La Chapelle, H. Milsch, O. Castelnau, P. Duval, Compressive creep of ice containing a liquid intergranular phase: rate-controlling processes in the dislocation creep regime. *Geophys. Res. Lett.* **26**(2), 251–254 (1999). <https://doi.org/10.1029/1998GL900289>
- N. Dello Russo, H. Kawakita, R.J. Vervack Jr., H.A. Weaver, Emerging trends and a comet taxonomy based on the volatile chemistry measured in thirty comets with high-resolution infrared spectroscopy between 1997 and 2013. *Icarus* **278**, 301–332 (2016)
- J.W. Deming, H. Eicken, *Life in Ice. Planets and Life: The Emerging Science of Astrobiology* (2007), pp. 292–312
- D.E. Dempsey, P.J. Langhorne, Geometric properties of platelet ice crystals. *Cold Reg. Sci. Technol.* **78**, 1–13 (2012)
- D.E. Dempsey, P.J. Langhorne, N.J. Robinson, M.J.M. Williams, T.G. Haskell, R.D. Frew, Observation and modeling of platelet ice fabric in McMurdo Sound, Antarctica. *J. Geophys. Res., Oceans* **115**(C1) (2010). <https://doi.org/10.1029/2008JC005264>

- D.J. Des Marais, J.A. Nuth III, L.J. Allamandola, A.P. Boss, J.D. Farmer, T.M. Hoehler, B.M. Jakosky, V.S. Meadows, A. Pohorille, B. Runnegar et al., The NASA astrobiology roadmap. *Astrobiology* **8**(4), 715–730 (2008)
- F. Deschamps, C. Sotin, Inversion of two-dimensional numerical convection experiments for a fluid with a strongly temperature-dependent viscosity. *Geophys. J. Int.* **143**(1), 204–218 (2000). <https://doi.org/10.1046/j.1365-246x.2000.00228.x>
- F. Deschamps, C. Sotin, Thermal convection in the outer shell of large icy satellites. *J. Geophys. Res., Planets* **106**(E3), 5107–5121 (2001)
- D. Dhingra, M.M. Hedman, R.N. Clark, P.D. Nicholson, Spatially resolved near infrared observations of Enceladus' tiger stripe eruptions from Cassini vims. *Icarus* **292**, 1–12 (2017). <https://doi.org/10.1016/j.icarus.2017.03.002>
- F. Dhooghe, J. De Keyser, K. Altwegg, C. Briois, H. Balsiger, J.J. Berthelier, U. Calmonte, G. Cessateur, M.R. Combi, E. Equeter et al., Halogens as tracers of protosolar nebula material in comet 67P/Churyumov–Gerasimenko. *Mon. Not. R. Astron. Soc.* **472**(2), 1336–1345 (2017)
- A.J. Dombard, G.W. Patterson, A.P. Lederer, L.M. Prockter, Flanking fractures and the formation of double ridges on Europa. *Icarus* **223**(1), 74–81 (2013). <https://doi.org/10.1016/j.icarus.2012.11.021>
- M.K. Dougherty, K.K. Khurana, F.M. Neubauer, C.T. Russell, J. Saur, J. Leisner, M.E. Burton, Identification of a dynamic atmosphere at Enceladus with the Cassini magnetometer. *Science* **311**(5766), 1406–1409 (2006)
- G. Durand, J. Weiss, V. Lipenkov, J.M. Barnola, G. Krinner, F. Parrenin, B. Delmonte, C. Ritz, P. Duval, R. Röthlisberger, M. Bigler, Effect of impurities on grain growth in cold ice sheets. *J. Geophys. Res., Earth Surf.* **111**(F1) (2006). <https://doi.org/10.1029/2005JF000320>
- D. Durante, D.J. Hemingway, P. Racioppa, L. Iess, D.J. Stevenson, Titan's gravity field and interior structure after Cassini. *Icarus* **326**, 123–132 (2019)
- W.B. Durham, L.A. Stern, Rheological properties of water ice—applications to satellites of the outer planets. *Annu. Rev. Earth Planet. Sci.* **29**(1), 295–330 (2001). <https://doi.org/10.1146/annurev.earth.29.1.295>
- P. Dutriex, C. Stewart, A. Jenkins, K.W. Nicholls, H.F.J. Corr, E. Rignot, K. Steffen, Basal terraces on melting ice shelves. *Geophys. Res. Lett.* **41**(15), 5506–5513 (2014)
- G.D. Egbert, R.D. Ray, Significant dissipation of tidal energy in the deep ocean inferred from satellite altimeter data. *Nature* **405**, 775 (2000). <https://doi.org/10.1038/35015531>
- S.A. Fagents, Considerations for effusive cryovolcanism on Europa: the post-Galileo perspective. *J. Geophys. Res., Planets* **108**(E12) (2003). <https://doi.org/10.1029/2003JE002128>
- S.A. Fagents, R. Greeley, R.J. Sullivan, R.T. Pappalardo, L.M. Prockter (Galileo SSI Team T), Cryomagnetic mechanisms for the formation of Rhadamanthys Linea, triple band margins, and other low-albedo features on Europa. *Icarus* **144**(1), 54–88 (2000). <https://doi.org/10.1006/icar.1999.6254>
- F.P. Fanale, Y.H. Li, E. De Carlo, C. Farley, S.K. Sharma, K. Horton, J.C. Granahan, An experimental estimate of Europa's "ocean" composition independent of Galileo orbital remote sensing. *J. Geophys. Res., Planets* **106**(E7), 14595–14600 (2001)
- R. Farber, J.C. Goodman, How quickly does drifting material traverse through Europa's ocean? *LPI Contrib.* **1774** 4059 (2014)
- R. Feistel, E. Hagen, On the GIBBS thermodynamic potential of seawater. *Prog. Oceanogr.* **36**(4), 249–327 (1995)
- H.J.S. Fernando, R. Chen, B.A. Ayotte, Development of a point plume in the presence of background rotation. *Phys. Fluids* **10**(9), 2369–2383 (1998)
- P.H. Figueredo, R. Greeley, Geologic mapping of the northern leading hemisphere of Europa from Galileo solid-state imaging data. *J. Geophys. Res.* **105**, 22629–22646 (2000)
- P.H. Figueredo, R. Greeley, Resurfacing history of Europa from pole-to-pole geological mapping. *Icarus* **167**, 287–312 (2004)
- P.H. Figueredo, F.C. Chuang, J.A. Rathbun, R.L. Kirk, R. Greeley, Geology and origin of Europa's Mitten feature (Murias Chaos). *J. Geophys. Res.* **107**, 5026 (2002)
- P.D. Fischer, M.E. Brown, K.P. Hand, Spatially resolved spectroscopy of Europa: the distinct spectrum of large-scale chaos. *Astron. J.* **150**(5), 164 (2015)
- A. Fortes, P. Grindrod, S. Trickett, L. Vočadlo, Ammonium sulfate on Titan: possible origin and role in cryovolcanism. *Icarus* **188**(1), 139–153 (2007). <https://doi.org/10.1016/j.icarus.2006.11.002>
- H.A. Fricker, S. Popov, I. Allison, N. Young, Distribution of marine ice beneath the Amery Ice Shelf. *Geophys. Res. Lett.* **28**, 2241–2244 (2001)
- E.J. Gaidos, F. Nimmo, Tectonics and water on Europa. *Nature* **405**, 637 (2000). <https://doi.org/10.1038/35015170>
- E. Gaidos, B. Lanoil, T. Thorsteinsson, A. Graham, M.L. Skidmore, S.K. Han, T. Rust, B. Popp, A viable microbial community in a subglacial volcanic crater lake, Iceland. *Astrobiology* **4**(3), 327–344 (2004)

- B. Galton-Fenzi, J.R. Hunter, R. Coleman, S.J. Marsland, R.C. Warner, Modeling the basal melting and marine ice accretion of the Amery Ice Shelf. *J. Geophys. Res.* **117**, C09031 (2012). <https://doi.org/10.1029/2012JC008214>
- P. Gao, D.J. Stevenson, Nonhydrostatic effects and the determination of icy satellites' moment of inertia. *Icarus* **226**(2), 1185–1191 (2013)
- T. Gastine, J. Wicht, J.M. Aurnou, Zonal flow regimes in rotating anelastic spherical shells: an application to giant planets. *Icarus* **225**, 156–172 (2013)
- T. Gastine, J. Wicht, J. Aubert, Scaling regimes in spherical shell rotating convection. *J. Fluid Mech.* **808**, 690–732 (2016)
- P. Geissler, R. Greenberg, G. Hoppa, A. McEwen, R. Tufts, C. Phillips, B. Clark, M. Ockert-Bell, P. Helfenstein, J. Burns, J. Veverka, R. Sullivan, R. Greeley, R. Pappalardo, J. Head, M. Belton, T. Denk, Evolution of lineaments on Europa: clues from Galileo Multispectral Imaging Observations. *Icarus* **135**(1), 107–126 (1998). <https://doi.org/10.1006/icar.1998.5980>
- C.R. German, A. Boetius, Robotics-based scientific investigations at an ice-ocean interface: first results from Nereid Under Ice in the Arctic. *LPI Contrib.* **2168**, 6002 (2019)
- C. Gissinger, L. Petidmange, A magnetically driven equatorial jet in Europa's ocean. *Nat. Astron.* **3**, 401–407 (2019)
- D.F. Gleeson, C. Williamson, S.E. Grasby, R.T. Pappalardo, J.R. Spear, A.S. Templeton, Low temperature S0 biomineralization at a supraglacial spring system in the Canadian High Arctic. *Geobiology* **9**(4), 360–375 (2011)
- D.F. Gleeson, R.T. Pappalardo, M.S. Anderson, S.E. Grasby, R.E. Mielke, K.E. Wright, A.S. Templeton, Biosignature detection at an Arctic analog to Europa. *Astrobiology* **12**(2), 135–150 (2012)
- C.R. Glein, J.H. Waite, The carbonate geochemistry of Enceladus' Ocean. *Geophys. Res. Lett.* **47**(3), e2019GL085885 (2020)
- C.R. Glein, F. Postberg, S.D. Vance, The geochemistry of Enceladus: composition and controls, in *Enceladus and the Icy Moons of Saturn* (University of Arizona Press, Tucson, 2018), pp. 39–56
- J.D. Goguen, B.J. Buratti, R.H. Brown, R.N. Clark, P.D. Nicholson, M.M. Hedman, R.R. Howell, C. Sotin, D.P. Cruikshank, K.H. Baines, K.J. Lawrence, J.R. Spencer, D.G. Blackburn, The temperature and width of an active fissure on Enceladus measured with Cassini vims during the 14 April 2012 south pole flyover. *Icarus* **226**(1), 1128–1137 (2013). <https://doi.org/10.1016/j.icarus.2013.07.012>
- K.M. Golden, S.F. Ackley, V.I. Lytle, The percolation phase transition in sea ice. *Science* **282**(5397), 2238–2241 (1998)
- K.M. Golden, H. Eicken, A.L. Heaton, J. Miner, D.J. Pringle, J. Zhu, Thermal evolution of permeability and microstructure in sea ice. *Geophys. Res. Lett.* **34**(16) (2007). <https://doi.org/10.1029/2007GL030447>
- D.L. Goldsby, D.L. Kohlstedt, Superplastic deformation of ice: experimental observations. *J. Geophys. Res., Solid Earth* **106**(B6), 11017–11030 (2001). <https://doi.org/10.1029/2000JB900336>
- D.B. Goldstein, M.M. Hedman, M. Manga, M. Perry, J. Spitale, B. Teolis, Eceladus plume dynamics: from surface to space, in *Enceladus and the Icy Moons of Saturn* (University of Arizona Press, Tucson, 2018), pp. 175–194
- M.P. Golombek, Constraints on the expansion of Ganymede and the thickness of the lithosphere. *J. Geophys. Res., Solid Earth* **87**(S01), A77–A83 (1982)
- M.P. Golombek, M.L. Allison, Sequential development of grooved terrain and polygons on Ganymede. *Geophys. Res. Lett.* **8**(11), 1139–1142 (1981)
- J.C. Goodman, E. Lenferink, Numerical simulations of marine hydrothermal plumes for Europa and other icy worlds. *Icarus* **221**, 970–983 (2012)
- J.C. Goodman, R.T. Pierrehumbert, Glacial flow of floating marine ice in “Snowball Earth”. *J. Geophys. Res., Oceans* **108**(C10), 3308 (2003)
- J.C. Goodman, G.C. Collins, J. Marshall, R.T. Pierrehumbert, Hydrothermal plume dynamics on Europa: implications for chaos formation. *J. Geophys. Res.* **109**, E03008 (2004)
- A.M. Grannan, M. Le Bars, D. Cebon, J.M. Aurnou, Experimental study of global-scale turbulence in a librating ellipsoid. *Phys. Fluids* **26**(12), 126601 (2014). <https://doi.org/10.1063/1.4903003>
- A.M. Grannan, B. Favier, M. Le Bars, J.M. Aurnou, Tidally forced turbulence in planetary interiors. *Geophys. J. Int.* **208**, 1690–1703 (2017)
- O. Grasset, M.K. Dougherty, A. Coustenis, E.J. Bunce, C. Erd, D. Titov, M. Blanc, A. Coates, P. Drossart, L.N. Fletcher et al., JUpiter ICy moons Explorer (JUICE): an ESA mission to orbit Ganymede and to characterise the Jupiter system. *Planet. Space Sci.* **78**, 1–21 (2013)
- R. Greeley, R. Sullivan, M.D. Coon, P.E. Geissler, B. Tufts, J.W. Head, R.T. Pappalardo, J.M. Moore, Terrestrial sea ice morphology: considerations for Europa. *Icarus* **135**(1), 25–40 (1998). <https://doi.org/10.1006/icar.1998.5977>

- R. Greenberg, P. Geissler, G.V. Hoppa, B.R. Tufts, D.D. Durda, R.T. Pappalardo, J.W. Head, R. Greeley, R. Sullivan, M.H. Carr, Tectonic processes on Europa: tidal stresses, mechanical response, and visible features. *Icarus* **135**, 64–78 (1998)
- R. Greenberg, G.V. Hoppa, B.R. Tufts, P. Geissler, J. Riley, Chaos on Europa. *Icarus* **141**, 263–286 (1999)
- S. Gulati, K. Richmond, C. Flesher, B.P. Hogan, A. Murarka, G. Kuhlmann, M. Sridharan, W.C. Stone, P.T. Doran, Toward autonomous scientific exploration of ice-covered lakes—field experiments with the ENDURANCE AUV in an Antarctic Dry Valley, in *2010 IEEE International Conference on Robotics and Automation* (IEEE Press, New York, 2010), pp. 308–315
- N.P. Hammond, E.M. Parmentier, A.C. Barr, Compaction and melt transport in ammonia-rich ice shells: implications for the evolution of Triton. *J. Geophys. Res., Planets* **123**(12), 3105–3118 (2018)
- L. Han, A.P. Showman, Thermo-compositional convection in Europa’s icy shell with salinity. *Geophys. Res. Lett.* **32**, L20201 (2005). <https://doi.org/10.1029/2005GL023979>
- L. Han, A.P. Showman, Implications of shear heating and fracture zones for ridge formation on Europa. *Geophys. Res. Lett.* **35**(3) (2008). <https://doi.org/10.1029/2007GL031957>
- L. Han, A.P. Showman, Coupled convection and tidal dissipation in Europa’s ice shell. *Icarus* **207**, 834–844 (2010)
- K.P. Hand, R.W. Carlson, Europa’s surface color suggests an ocean rich with sodium chloride. *Geophys. Res. Lett.* **42**(9), 3174–3178 (2015)
- K.P. Hand, R.W. Carlson, C.F. Chyba, Energy, chemical disequilibrium, and geological constraints on Europa. *Astrobiology* **7**(6), 1006–1022 (2007). <https://doi.org/10.1089/ast.2007.0156>
- K.P. Hand, C.F. Chyba, J.C. Priscu, R.W. Carlson, K.H. Nealson, Astrobiology and the potential for life on Europa, in *Europa* (University of Arizona Press, Tucson, 2009), pp. 589–629
- K.P. Hand, A.E. Murray, J.B. Garvin, W.B. Brinckerhoff, B.C. Christner, K.S. Edgett, B.L. Ehlmann, C. German, A.G. Hayes, T.M. Hoehler, S.M. Horst, J.I. Lunine, K.H. Nealson, C. Paranicas, B.E. Schmidt, D.E. Smith, A.R. Rhoden, M.J. Russell, A.S. Templeton, P.A. Willis, R.A. Yingst, C.B. Phillips, M.L. Cable, K.L. Craft, A.E. Hofmann, T.A. Nordheim, R.T. Pappalardo (the Project Engineering Team), Report of the Europa Lander Science Definition Team. Tech. rep. Jet Propulsion Laboratory, California Institute of Technology (2017)
- J. Hanley, J.B. Dalton III, V.F. Chevrier, C.S. Jamieson, R.S. Barrows, Reflectance spectra of hydrated chlorine salts: the effect of temperature with implications for Europa. *J. Geophys. Res., Planets* **119**(11), 2370–2377 (2014)
- C.J. Hansen, L.W. Esposito, A.I.F. Stewart, B. Meinke, B. Wallis, J.E. Colwell, A.R. Hendrix, K. Larsen, W. Pryor, F. Tian, Water vapour jets inside the plume of gas leaving Enceladus. *Nature* **456**, 477–479 (2008). <https://doi.org/10.1038/nature07542>
- C.J. Hansen, L.W. Esposito, K.M. Aye, J.E. Colwell, A.R. Hendrix, G. Portyankina, D. Shemansky, Investigation of diurnal variability of water vapor in Enceladus’ plume by the Cassini ultraviolet imaging spectrograph. *Geophys. Res. Lett.* **44**(2), 672–677 (2017). <https://doi.org/10.1002/2016GL071853>
- C.J. Hansen, L.W. Esposito, J.E. Colwell, A.R. Hendrix, G. Portyankina, A.I.F. Stewart, R.A. West, The composition and structure of Enceladus’ plume from the complete set of Cassini UVIS occultation observations. *Icarus* **344**, 113461 (2019)
- O. Hartkorn, J. Saur, Induction signals from Callisto’s ionosphere and their implications on a possible subsurface ocean. *J. Geophys. Res.* **122**(11), 11,677–11,697 (2017)
- H.C.F.C. Hay, I. Matsuyama, Numerically modelling tidal dissipation with bottom drag in the oceans of Titan and Enceladus. *Icarus* **281**, 342–356 (2017)
- H.C.F.C. Hay, I. Matsuyama, Nonlinear tidal dissipation in the subsurface oceans of Enceladus and other icy satellites. *Icarus* **319**, 68–85 (2019)
- L. Hays, L. Archenbach, J. Bailey, R. Barnes, J. Barros, C. Bertka, P. Boston, E. Boyd, M. Cable, I. Chen et al., *NASA Astrobiology Strategy* (National Aeronautics and Space Administration, Washington, 2015). NASA
- J.W. Head, R.T. Pappalardo, Brine mobilization during lithospheric heating on Europa: implications for formation of chaos terrain, lenticula texture, and color variations. *J. Geophys. Res., Planets* **104**(E11), 27143–27155 (1999). <https://doi.org/10.1029/1999JE001062>
- J.W. Head, R.T. Pappalardo, R. Sullivan, Europa: morphological characteristics of ridges and triple bands from Galileo data (E4 and E6) and assessment of a linear diapirism model. *J. Geophys. Res., Planets* **104**(E10), 24223–24236 (1999). <https://doi.org/10.1029/1998JE001011>
- M.M. Hedman, C.M. Gossmeier, P.D. Nicholson, C. Sotin, R.H. Brown, R.N. Clark, K.H. Baines, B.J. Buratti, M.R. Showalter, An observed correlation between plume activity and tidal stresses on Enceladus. *Nature* **500**, 182–184 (2013). <https://doi.org/10.1038/nature12371>
- M.M. Hedman, D. Dzingra, P. Nicholson, C. Hansen, G. Portyankina, S. Ye, Y. Dong, Spatial variations in the dust-to-gas ratio of Enceladus’ plume. *Icarus* **305**, 123–138 (2018). <https://doi.org/10.1016/j.icarus.2018.01.006>

- M.H. Heimpel, T. Gastine, J. Wicht, Simulation of deep-seated zonal jets and shallow vortices in gas giant atmospheres. *Nat. Geosci.* **9**(1), 19 (2015)
- P. Helfenstein, *Y-Shaped Discontinuity* (Springer, New York, 2014), pp. 1–5
- P. Helfenstein, E.M. Parmentier, Patterns of fracture and tidal stresses due to nonsynchronous rotation: implications for fracturing on Europa. *Icarus* **61**(2), 175–184 (1985)
- D.J. Hemingway, T. Mittal, Enceladus's ice shell structure as a window on internal heat production. *Icarus* (2019). <https://doi.org/10.1016/j.icarus.2019.03.011>
- D.J. Hemingway, F. Nimmo, H. Zebker, L. Iess, A rigid and weathered ice shell on Titan. *Nature* **500**, 550–552 (2013). <https://doi.org/10.1038/nature12400>
- M.C. Hendershott, Long waves and ocean tides, in *Evolution of Physical Oceanography*, ed. by B.A. Warren, C. Wunsch (MIT Press, Cambridge, 1981), pp. 292–341
- A.R. Hendrix, T.A. Hurford, L.M. Barge, M.T. Bland, J.S. Bowman, W. Brinckerhoff, B.J. Buratti, M.L. Cable, J. Castillo-Rogez, G.C. Collins, et al., The NASA roadmap to ocean worlds. *Astrobiology* **19**(1), 1–27 (2019)
- C.A. Hibbitts, T.B. McCord, G.B. Hansen, Distributions of CO<sub>2</sub> and SO<sub>2</sub> on the surface of Callisto. *J. Geophys. Res., Planets* **105**(E9), 22541–22557 (2000)
- C.A. Hibbitts, R.T. Pappalardo, G.B. Hansen, T.B. McCord, Carbon dioxide on Ganymede. *J. Geophys. Res., Planets* **108**(E5), 5036 (2003)
- P.F. Hoffman, D.P. Schrag, The snowball Earth hypothesis: testing the limits of global change. *Terra Nova* **14**(3), 129–155 (2002)
- D.L. Hogenboom, Magnesium sulfate-water to 400 MPa using a novel piezometer: densities, phase equilibria, and planetological implications. *Icarus* **115**(2), 258–277 (1995). <https://doi.org/10.1006/icar.1995.1096>
- D.L. Hogenboom, J.S. Kargel, G.J. Consolmagno, T.C. Holden, L. Lee, M. Buyounouski, The ammonia-water system and the chemical differentiation of icy satellites. *Icarus* **128**(1), 171–180 (1997)
- S.M. Howell, R.T. Pappalardo, Band formation and ocean-surface interaction on Europa and Ganymede. *Geophys. Res. Lett.* **45**(10), 4701–4709 (2018). <https://doi.org/10.1029/2018GL077594>
- S.M. Howell, R.T. Pappalardo, Can Earth-like plate tectonics occur in ocean world ice shells? *Icarus* **322**, 69–79 (2019)
- H.W. Hsu, F. Postberg, Y. Sekine, T. Shibuya, S.D. Kempf, M. Horányi, A. Juhász, N. Altobelli, K. Suzuki, Y. Masaki et al., Ongoing hydrothermal activities within Enceladus. *Nature* **519**(7542), 207 (2015)
- P.J. Hudleston, Structures and fabrics in glacial ice: a review. *J. Struct. Geol.* **81**, 1–27 (2015). <https://doi.org/10.1016/j.jsg.2015.09.003>
- T.A. Hurford, P. Helfenstein, J.N. Spitale, Tidal control of jet eruptions on Enceladus as observed by Cassini ISS between 2005 and 2007. *Icarus* **220**(2), 896–903 (2012)
- H. Hussmann, T. Spohn, Thermal-orbital evolution of io and Europa. *Icarus* **171**(2), 391–410 (2004)
- H. Hussmann, T. Spohn, K. Wiczekowski, Thermal equilibrium states of Europa's ice shell: implications for internal ocean thickness and surface heat flow. *Icarus* **156**, 143–151 (2002)
- H. Hussmann, F. Sohl, T. Spohn, Subsurface oceans and deep interiors of medium-sized outer planet satellites and large trans-neptunian objects. *Icarus* **185**, 258–273 (2006)
- H. Hussmann, C. Sotin, J.I. Lunine, Interiors and evolution of icy satellites, in *Treatise on Geophysics*, vol. 10, ed. by G. Schubert 2nd edn. (Elsevier, Amsterdam, 2015), pp. 605–635
- L. Iess, N.J. Rappaport, R.A. Jacobson, P. Racioppa, D.J. Stevenson, P. Tortora, J.W. Armstrong, S.W. Asmar, Gravity field, shape, and moment of inertia of Titan. *Science* **327**, 1367–1369 (2010)
- L. Iess, R.A. Jacobson, M. Ducci, D.J. Stevenson, J.I. Lunine, J.W. Armstrong, S.W. Asmar, P. Racioppa, N.J. Rappaport, P. Tortora, The tides of Titan. *Science* **337**, 457–459 (2012)
- L. Iess, D.J. Stevenson, M. Parisi, D. Hemingway, R.A. Jacobson, J.I. Lunine, F. Nimmo, J.W. Armstrong, S.W. Asmar, M. Ducci et al., The gravity field and interior structure of Enceladus. *Science* **344**(6179), 78–80 (2014)
- A.P. Ingersoll, S.P. Ewald, Decadal timescale variability of the Enceladus plumes inferred from Cassini images. *Icarus* **282**, 260–275 (2017). <https://doi.org/10.1016/j.icarus.2016.09.018>
- A.P. Ingersoll, A.A. Pankine, Subsurface heat transfer on Enceladus: conditions under which melting occurs. *Icarus* **206**(2), 594–607 (2010). <https://doi.org/10.1016/j.icarus.2009.09.015>
- R.A. Jacobson, P.G. Antreasian, J.J. Bordi, K.E. Criddle, R. Ionascu, J.B. Jones, R.A. Mackenzie, M.C. Meek, D. Parcher, F.J. Pelletier, et al., The gravity field of the Saturnian system from satellite observations and spacecraft tracking data. *Astron. J.* **132**(6), 2520 (2006)
- M.F. Jansen, The turbulent circulation of a Snowball Earth ocean. *J. Phys. Oceanogr.* **46**(6), 1917–1933 (2016)
- R. Jaumann, R.L. Kirk, R.D. Lorenz, R.M.C. Lopes, E. Stofan, E.P. Turtle, H.W. Keller, C.A. Wood, C. Sotin, L.A. Soderblom et al., Geology and surface processes on Titan, in *Titan from Cassini-Huygens* (Springer, Berlin, 2009), pp. 75–140

- A. Jenkins, The role of meltwater advection in the formulation of conservative boundary conditions at an ice-ocean interface. *J. Phys. Oceanogr.* **31**, 285–296 (2010)
- X. Jia, M.G. Kivelson, K.K. Khurana, W.S. Kurth, Evidence of a plume on Europa from Galileo magnetic and plasma wave signatures. *Nat. Astron.* **2**, 459–464 (2018). <https://doi.org/10.1038/s41550-018-0450-z>
- B.C. Johnson, R.Y. Sheppard, A.C. Pascuzzo, E.A. Fisher, S.E. Wiggins, Porosity and salt content determine if subduction can occur in Europa's ice shell. *J. Geophys. Res., Planets* **122**(12), 2765–2778 (2017)
- S.A. Johnston, L.G.J. Montési, Formation of ridges on Europa above crystallizing water bodies inside the ice shell. *Icarus* **237**, 190–201 (2014). <https://doi.org/10.1016/j.icarus.2014.04.026>
- B. Journaux, K. Kalousová, C. Sotin, G. Tobie, S.D. Vance, J. Saur, O. Bollengier, L. Noack, T. Rückriemen-Bez, T. Van Hoolst et al., High-pressure ices in large ocean worlds. *Space Sci. Rev.* **216**(1), 7 (2020)
- S.D. Kadel, S.A. Fagents, R. Greeley (GS Team), Trough-bounding ridge pairs on Europa: considerations for an endogenic model of formation, in *Lunar and Planetary Institute Science Conference Abstracts*, vol. 29 (1998), p. p 1078
- S.D. Kadel, F.C. Chuang, R. Greeley, J.M. Moore, Geological history of the Tyre region of Europa: a regional perspective on European surface features and ice thickness. *J. Geophys. Res., Planets* **105**(E9), 22657–22669 (2000). <https://doi.org/10.1029/1999JE001203>
- K. Kalousová, C. Sotin, Melting in high-pressure ice layers of large ocean worlds – implications for volatiles transport. *Geophys. Res. Lett.* **45**(16), 8096–8103 (2018). <https://doi.org/10.1029/2018GL078889>
- K. Kalousová, C. Sotin, Dynamics of Titan's high-pressure ice layer. *Earth. Planet. Sci. Lett.* (2020) <https://doi.org/10.1016/j.epsl.2020.116416>
- K. Kalousová, O. Souček, G. Tobie, G. Choblet, O. Čadek, Ice melting and downward transport of meltwater by two-phase flow in Europa's ice shell. *J. Geophys. Res., Planets* **119**, 532–549 (2014). <https://doi.org/10.1002/2013JE004563>
- K. Kalousová, O. Souček, G. Tobie, G. Choblet, O. Čadek, Water generation and transport below Europa's strike-slip faults. *J. Geophys. Res., Planets* **121**, 2444–2462 (2016). <https://doi.org/10.1002/2016JE005188>
- K. Kalousová, C. Sotin, G. Choblet, G. Tobie, O. Grasset, Two-phase convection in Ganymede's high-pressure ice layer – implications for its geological evolution. *Icarus* **299**, 133–147 (2018). <https://doi.org/10.1016/j.icarus.2017.07.018>
- J.S. Kargel, Brine volcanism and the interior structures of asteroids and icy satellites. *Icarus* **94**(2), 368–390 (1991)
- J.S. Kargel, J.Z. Kaye, J.W. Head III, G.M. Marion, R. Sassen, J.K. Crowley, O. Prieto-Ballesteros, S.A. Grant, D.L. Hogenboom, Europa's crust and ocean: origin, composition, and the prospects for life. *Icarus* **148**(1), 226–265 (2000)
- S.A. Kattenhorn, L.M. Prockter, Evidence for subduction in the ice shell of Europa. *Nat. Geosci.* **7**(10), 762 (2014)
- D.S. Kelley, J.A. Karson, D.K. Blackman, G.L. Früh-Green, D.A. Butterfield, M.D. Lilley, E.J. Olson, M.O. Schrenk, K.K. Roe, G.T. Lebon et al., An off-axis hydrothermal vent field near the Mid-Atlantic Ridge at 30 n. *Nature* **412**(6843), 145–149 (2001)
- S. Kempf, M. Horányi, H.W. Hsu, T.W. Hill, A. Juhász, H.T. Smith, Saturn's diffuse E ring and its connection with Enceladus, in *Enceladus and the Icy Moons of Saturn* (University of Arizona Press, Tucson, 2018), pp. 195–210
- R.R. Kerswell, Elliptical instability. *Annu. Rev. Fluid Mech.* **34**(1), 83–113 (2002). <https://doi.org/10.1146/annurev.fluid.34.081701.171829>
- R.R. Kerswell, W.V.R. Malkus, Tidal instability as the source for Io's magnetic signature. *Geophys. Res. Lett.* **25**(5), 603–606 (1998)
- N. Khawaja, F. Postberg, J. Hillier, F. Klenner, S. Kempf, L. Nölle, R. Reviol, R. Srama, Low mass organic compounds in Enceladean ice grains. *Mon. Not. R. Astron. Soc.* **489**(4), 5231–5243 (2019)
- K.K. Khurana, M.G. Kivelson, D.J. Stevenson, G. Schubert, C.T. Russell, R.J. Walker, C. Polanskey, Induced magnetic fields as evidence for subsurface oceans in Europa and Callisto. *Nature* **395**, 777–780 (1998)
- K.K. Khurana, M.G. Kivelson, C.T. Russell, Searching for liquid water in Europa by using surface observatories. *Astrobiology* **2**(1), 93–103 (2002)
- P.W. Kimball, E.B. Clark, M. Scully, K. Richmond, C. Flesher, L.E. Lindzey, J. Harman, K. Huffstutler, J. Lawrence, S. Lelievre et al., The ARTEMIS under-ice AUV docking system. *J. Field Robot.* **35**(2), 299–308 (2018)
- W.B.M. McKinnon, H. Melosh, Evolution of planetary lithospheres: evidence from multiringed structures on Ganymede and Callisto. *Icarus* **44**(2), 454–471 (1980). [https://doi.org/10.1016/0019-1035\(80\)90037-8](https://doi.org/10.1016/0019-1035(80)90037-8)
- E.S. Kite, A.M. Rubin, Sustained eruptions on Enceladus explained by turbulent dissipation in tiger stripes. *Proc. Natl. Acad. Sci.* **113**(15), 3972–3975 (2016). <https://doi.org/10.1073/pnas.1520507113>
- M.G. Kivelson, K.K. Khurana, M. Volwerk, The permanent and inductive magnetic moments of Ganymede. *Icarus* **157**, 507–522 (2002)

- M.W. Klaser, J. Gross, S. Tindall, R.W. Schlichte, C.J. Potter, Europa's ice tectonics: new insights from physical wax experiments with implications for subduction initiation and global resurfacing processes. *Icarus* **321**, 593–607 (2019)
- A. Kovacs, A.J. Gow, Brine infiltration in the McMurdo Ice Shelf, McMurdo Sound, Antarctica. *J. Geophys. Res.* **80**(15), 1957–1961 (1975)
- R.G. Kraus, L.E. Senft, S.T. Stewart, Impacts onto H<sub>2</sub>O ice: scaling laws for melting, vaporization, excavation, and final crater size. *Icarus* **214**, 724–738 (2011). <https://doi.org/10.1016/j.icarus.2011.05.016>
- O.L. Kuskov, V.A. Kronrod, Core sizes and internal structure of Earth's and Jupiter's satellites. *Icarus* **151**(2), 204–227 (2001)
- J. Kvorika, C. Cadek, G. Tobie, G. Choblet, Does Titan's long-wavelength topography contain information about subsurface ocean dynamics? *Icarus* **310**, 149–164 (2018)
- V. Lainey, O. Karatekin, J. Desmars, S. Charnoz, J.E. Arlot, N. Emelyanov, C. Le Poncin-Lafitte, S. Mathis, F. Remus, G. Tobie et al., Strong tidal dissipation in Saturn and constraints on Enceladus' thermal state from astrometry. *Astrophys. J.* **752**(1), 14 (2012)
- J. Lawrence, B.E. Schmidt, M.R. Meister, D. Dichek, C. Ramey, B. Hurwitz, A. Spears, A. Mullen, F.E. Bryson, J.J. Lutz et al., Life under ice: Antarctic Ocean world analogs with HROV icefin and RISE UP, in *AGUFM 2018* (2018). P21E-3402
- M. Le Bars, D. Cebbron, P. Le Gal, Flows driven by libration, precession, and tides. *Annu. Rev. Fluid Mech.* **47**, 163–193 (2015)
- C.M. Lee, D.L. Rudnick, Underwater gliders, in *Observing the Oceans in Real Time* (Springer, Berlin, 2018), pp. 123–139
- A. Lefevre, G. Tobie, G. Choblet, O. Čadek, Structure and dynamics of Titan's outer icy shell constrained from Cassini data. *Icarus* **237**, 16–28 (2014). <https://doi.org/10.1016/j.icarus.2014.04.006>
- D. Lemasquerier, A.M. Grannan, J. Vidal, D. Cébron, B. Favier M. Le Bars, J.M. Aurnou, Libration-driven flows in ellipsoidal shells. *J. Geophys. Res., Planets* **122**(9), 1926–1950 (2017)
- E.W. Lemmon, M.L. Huber, M.O. McLinden, NIST Standard Reference Database 23: Reference Fluid Thermodynamic and Transport Properties-REFPROP, Version 8.0. National Institute of Standards and Technology, Standard Reference Data Program, Gaithersburg (2007)
- E.L. Lewis, R.G. Perkin, Ice pumps and their rates. *J. Geophys. Res.* **91**, 11756–11762 (1986)
- N. Ligier, F. Poulet, J. Carter, R. Brunetto, F. Gourgéot, VLT/SINFONI observations of Europa: new insights into the surface composition. *Astron. J.* **151**(6), 163 (2016). <https://doi.org/10.3847/0004-6256/151/6/163>
- Y. Liu, W.R. Peltier, A carbon cycle coupled climate model of Neoproterozoic glaciation: Influence of continental configuration on the formation of a “soft snowball”. *J. Geophys. Res., Atmos.* **115**(D17) (2010). <https://doi.org/10.1029/2009JD013082>
- M.S. Longuet-Higgins, The eigenfunctions of Laplace's tidal equations over a sphere. *Philos. Trans. R. Soc. Lond. A* **262**(1132), 511–607 (1968). <https://doi.org/10.1098/rsta.1968.0003>
- R.P. Lowell, M. DuBose, Hydrothermal systems on Europa. *Geophys. Res. Lett.* **32**, L05202 (2005)
- J. Luan, Titan's dynamic love number implies stably-stratified ocean (2019). ArXiv preprint. [arXiv: 1905.03802](https://arxiv.org/abs/1905.03802)
- B.K. Lucchitta, Grooved terrain on Ganymede. *Icarus* **44**(2), 481–501 (1980)
- B.K. Lucchitta, L.A. Soderblom, The geology of Europa, in *Satellites of Jupiter*, ed. by D. Morrison (University of Arizona Press, Tucson, 1982), pp. 521–555
- J.I. Lunine, N. Artemieva, G. Tobie, Impact cratering on Titan: hydrocarbons versus water, in *Lunar and Planetary Science Conference, Lunar and Planetary Science Conference*, vol. 41 (2010), p. 1537
- J.I. Lunine, A. Coustenis, G. Mitri, G. Tobie, F. Tosi, Future exploration of Enceladus and other saturnian moons, in *Enceladus and the Icy Moons of Saturn* (University of Arizona Press, Tucson, 2018), pp. 453–468
- J.I. Lunine M.L. Cable, S.M. Hörst, M. Rahm, The astrobiology of Titan, in *Planetary Astrobiology*, ed. by V.S. Meadows, G. Arney, D. DesMarais, B.E. Schmidt (University of Arizona Press, Tucson, 2019). (In production)
- L.R.M. Maas, Wave attractors: linear yet nonlinear. *Int. J. Bifurc. Chaos* **15**(09), 2757–2782 (2005)
- B.A. Magee, J.H. Waite, Neutral gas composition of Enceladus' plume – model parameter insights from Cassini-INMS, in *Lunar and Planetary Institute Science Conference Abstracts*, vol. 48 (2017), p. 2974
- W.V.R. Malkus, Energy sources for planetary dynamos, in *Lectures on Solar and Planetary Dynamos*, ed. by M.R.E. Proctor, A.D. Gilbert (Cambridge University Press, Cambridge, 1994)
- M. Manga, C. Michaut, Formation of lenticulae on Europa by saucer-shaped sills. *Icarus* **286**, 261–269 (2017). <https://doi.org/10.1016/j.icarus.2016.10.009>
- M. Manga, A. Sinton, Formation of bands and ridges on Europa by cyclic deformation: Insights from analogue wax experiments. *J. Geophys. Res., Planets* **109**(E9) (2004). <https://doi.org/10.1029/2004JE002249>

- M. Manga, C.Y. Wang, Pressurized oceans and the eruption of liquid water on Europa and Enceladus. *Geophys. Res. Lett.* **34**(7) (2007). <https://doi.org/10.1029/2007GL029297>
- I. Matsuyama, Tidal dissipation in the oceans of icy satellites. *Icarus* **242**, 11–18 (2014)
- I. Matsuyama, M. Beuthe, H.C.F.C. Hay, F. Nimmo, S. Kamata, Ocean tidal heating in icy satellites with solid shells. *Icarus* **312**, 208–230 (2018)
- T.B. McCord, G. Teeter, G.B. Hansen, M.T. Sieger, T.M. Orlando, Brines exposed to Europa surface conditions. *J. Geophys. Res., Planets* **107**(E1) (2002). <https://doi.org/10.1029/2000JE001453>
- T.J. McDougall, P.M. Barker, *Getting Started with TEOS-10 and the Gibbs Seawater (GSW) Oceanographic Toolbox*. SCOR/IAPSO WG, vol. 127 (2011), p. 1–28
- W.B. McKinnon, Convective instability in Europa's floating ice shell. *Geophys. Res. Lett.* **26**, 951–954 (1999)
- W.B. McKinnon, On convection in ice I shells of outer solar system bodies, with detailed application to Callisto. *Icarus* **183**(2), 435–450 (2006). <https://doi.org/10.1016/j.icarus.2006.03.004>
- W.B. McKinnon, Effect of Enceladus's rapid synchronous spin on interpretation of Cassini gravity. *Geophys. Res. Lett.* **42**(7), 2137–2143 (2015)
- W.B. McKinnon, M.E. Zolensky, Sulfate content of Europa's ocean and shell: evolutionary considerations and some geological and astrobiological implications. *Astrobiology* **3**(4), 879–897 (2003)
- M. Meister, D. Dichek, A. Spears, B. Hurwitz, C. Ramey, J. Lawrence, K. Philleo, J. Lutz, J. Lawrence, B.E. Schmidt, Icefin: redesign and 2017 Antarctic field deployment, in *OCEANS 2018 MTS/IEEE Charleston* (IEEE Press, New York, 2018), pp. 1–5
- H.J. Melosh, *Impact Cratering: A Geologic Process* (Oxford University Press/Clarendon Press, New York/Oxford, 1989)
- H.J. Melosh, A.G. Ekholm, A.P. Showman, R.D. Lorenz, The temperature of Europa's subsurface water ocean. *Icarus* **168**, 498–502 (2004)
- L. Mével, E. Mercier, Large-scale doming on Europa: a model of formation of thea macula. *Planet. Space Sci.* **55**(7), 915–927 (2007). <https://doi.org/10.1016/j.pss.2006.12.001>
- C. Michaut, M. Manga, Domes, pits, and small chaos on Europa produced by water sills. *J. Geophys. Res., Planets* **119**(3), 550–573 (2014). <https://doi.org/10.1002/2013JE004558>
- J.A. Mikucki, P.A. Lee, D. Ghosh, A.M. Purcell, A.C. Mitchell, K.D. Mankoff, A.T. Fisher, S. Tulaczyk, S.P. Carter, M.R. Siegfried et al., Subglacial Lake Whillans microbial biogeochemistry: a synthesis of current knowledge. *Philos. Trans. R. Soc. Lond. A* **374**(2059), 20140290 (2016)
- J.W. Miles, On Laplace's tidal equations. *J. Fluid Mech.* **66**(2), 241–260 (1974). <https://doi.org/10.1017/S0022112074000176>
- K.E. Miller, C.R. Glein, J.H. Waite, S.J. Bolton, Using D/H ratio of water and volatile organics to constrain thermogenic processes inside ice-rock bodies, in *Lunar and Planetary Science Conference*, vol. 50 (2019)
- G. Mitri, A.P. Showman, Convective-conductive transitions and sensitivity of a convecting ice shell to perturbations in heat flux and tidal-heating rate: implications for Europa. *Icarus* **177**(2), 447–460 (2005). <https://doi.org/10.1016/j.icarus.2005.03.019>
- G. Mitri, M.T. Bland, A.P. Showman, J. Radebaugh, B. Stiles, R. Lopes, J.I. Lunine, R.T. Pappalardo, Mountains on Titan: Modeling and observations. *J. Geophys. Res., Planets* **115**(E10) (2010). <https://doi.org/10.1029/2010JE003592>
- G. Mitri, R. Meriggiola, A. Hayes, A. Lefevre, G. Tobie, A. Genova, J.I. Lunine, H. Zebker, Shape, topography, gravity anomalies and tidal deformation of Titan. *Icarus* **236**, 169–177 (2014)
- J. Monteux, G.S. Collins, G. Tobie, G. Choblet, Consequences of large impacts on Enceladus' core shape. *Icarus* **264**, 300–310 (2016). <https://doi.org/10.1016/j.icarus.2015.09.034>
- J.M. Moore, P.M. Schenk, L.S. Bruesch, E. Asphaug, W.B. McKinnon, Large impact features on middle-sized icy satellites. *Icarus* **171**(2), 421–443 (2004). <https://doi.org/10.1016/j.icarus.2004.05.009>
- L.N. Moresi, V.S. Solomatov, Numerical investigation of 2D convection with extremely large viscosity variations. *Phys. Fluids* **7**(9), 2154–2162 (1995). <https://doi.org/10.1063/1.868465>
- W.H. Munk, Once again: once again—tidal friction. *Prog. Oceanogr.* **40**(1), 7–35 (1997). [https://doi.org/10.1016/S0079-6611\(97\)00021-9](https://doi.org/10.1016/S0079-6611(97)00021-9). Part of special issue: Tidal Science In Honour of David E. Cartwright
- S.L. Murchie, J.W. Head, Geologic map of the Philus Sulcus (Jg-4) quadrangle of Ganymede. *U S Geol Surv Map I-1966* (1989)
- S.L. Murchie, J.W. Head, J.B. Plescia, Tectonic and volcanic evolution of dark terrain and its implications for the internal structure and evolution of Ganymede. *J. Geophys. Res., Solid Earth* **95**(B7), 10743–10768 (1990)
- A.E. Murray, F. Kenig, C.H. Fritsen, C.P. McKay, K.M. Cawley, R. Edwards, E. Kuhn, D.M. McKnight, N.E. Ostrom, V. Peng et al., Microbial life at -13 °C in the brine of an ice-sealed Antarctic lake. *Proc. Natl. Acad. Sci.* **109**(50), 20626–20631 (2012)

- K. Nagel, D. Breuer, T. Spohn, A model for the interior structure, evolution, and differentiation of Callisto. *Icarus* **169**(2), 402–412 (2004)
- M. Nakajima, A.P. Ingersoll, Controlled boiling on Enceladus: 1. Model of the vapor-driven jets. *Icarus* **272**, 309–318 (2016). <https://doi.org/10.1016/j.icarus.2016.02.027>
- A. Néri, F. Guyot, B. Reynard, C. Sotin, A carbonaceous chondrite and cometary origin for icy moons of Jupiter and Saturn. *Earth Planet. Sci. Lett.* **530**, 115920 (2020)
- F.M. Neubauer, The sub-Alfvénic interaction of the Galilean satellites with the Jovian magnetosphere. *J. Geophys. Res.* **103**(E9), 19843–19866 (1998)
- H.B. Niemann, S.K. Atreya, S.J. Bauer, G.R. Carignan, J.E. Demick, R.L. Frost, D. Gautier, J.A. Haberman, D.N. Harpold, D.M. Hunten, G. Israel, J.I. Lunine, W.T. Kasprzak, T.C. Owen, M. Paulkovich, F. Raulin, E. Raaen, S.H. Way The abundances of constituents of Titan's atmosphere from the GCMS instrument on the Huygens probe. *Nature* **438**, 779–784 (2005). <https://doi.org/10.1038/nature04122>
- H.B. Niemann, S.K. Atreya, J.E. Demick, D. Gautier, J.A. Haberman, D.N. Harpold, W.T. Kasprzak, J.I. Lunine, T.C. Owen, F. Raulin, Composition of Titan's lower atmosphere and simple surface volatiles as measured by the Cassini-Huygens probe gas chromatograph mass spectrometer experiment. *J. Geophys. Res., Planets* **115**(E12) (2010). <https://doi.org/10.1029/2010JE003659>
- F. Nimmo, B.G. Bills, Shell thickness variations and the long-wavelength topography of Titan. *Icarus* **208**(2), 896–904 (2010)
- F. Nimmo, E. Gaidos, Strike-slip motion and double ridge formation on Europa. *J. Geophys. Res., Planets* **107**(E4), 5 (2002)
- F. Nimmo, P.C. Thomas, R.T. Pappalardo, W.B. Moore, The global shape of Europa: constraints on lateral shell thickness variations. *Icarus* **191**, 183–192 (2007)
- F. Nimmo, B.G. Bills, P.C. Thomas, Geophysical implications of the long-wavelength topography of the saturnian satellites. *J. Geophys. Res., Planets* **116**(E11) (2011). <https://doi.org/10.1029/2011JE003835>
- F. Nimmo, C. Porco, C. Mitchell, Tidally modulated eruptions on Enceladus: Cassini iss observations and models. *Astron. J.* **148**(3), 46 (2014)
- F. Nimmo, D.P. Hamilton, W.B. McKinnon, P.M. Schenk, R.P. Binzel, C.J. Bierson, R.A. Beyer, J.M. Moore, S.A. Stern, H.A. Weaver et al., Reorientation of Sputnik Planitia implies a subsurface ocean on Pluto. *Nature* **540**(7631), 94–96 (2016)
- F. Nimmo, A.C. Barr, M. Běhouňková, W.B. McKinnon, The thermal and orbital evolution of Enceladus: observational constraints and models, in *Enceladus and the Icy Moons of Saturn*, ed. by P.M. Schenk et al. (University of Arizona Press, Tucson, 2018), pp. 79–94
- M. Ogawa, Two-stage evolution of the Earth's mantle inferred from numerical simulation of coupled magmatism-mantle convection system with tectonic plates. *J. Geophys. Res., Solid Earth* **119**(3), 2462–2486 (2014). <https://doi.org/10.1002/2013JB010315>
- C. O'Neill, F. Nimmo, The role of episodic overturn in generating the surface geology and heat flow on Enceladus. *Nat. Geosci.* **3**(2), 88–91 (2010)
- L. Paganini, G.L. Villanueva, L. Roth, A.M. Mandell, T.A. Hurford, K.D. Retherford, M.J. Mumma, A measurement of water vapour amid a largely quiescent environment on Europa. *Nat. Astron.* **4**, 266–272 (2020)
- R.T. Pappalardo, R.J. Sullivan, Evidence for separation across a gray band on Europa. *Icarus* **123**(2), 557–567 (1996). <https://doi.org/10.1006/icar.1996.0178>
- R.T. Pappalardo, J.W. Head, R. Greeley, R.J. Sullivan, C. Pilcher, G. Schubert, W.B. Moore, M.H. Carr, J.M. Moore, M.J.S. Belton, D.L. Goldsby, Geological evidence for solid-state convection in Europa's ice shell. *Nature* **391**, 365–368 (1998)
- R.T. Pappalardo, M.J.S. Belton, H.H. Breneman, M.H. Carr, C.R. Chapman, G.C. Collins, T. Denk, S. Fagents, P.E. Geissler, B. Giese et al., Does Europa have a subsurface ocean? Evaluation of the geological evidence. *J. Geophys. Res.* **104**(E10), 24015–24055 (1999)
- R.T. Pappalardo, G.C. Collins, J.W. Head, P. Helfenstein, T.B. McCord, J.M. Moore, L.M. Prockter, P.M. Schenk, J.R. Spencer, Geology of Ganymede, in *Jupiter*, ed. by F.D. Bagenal, T.E. Dowling, W.B. McKinnon (Cambridge University Press, Cambridge, 2004), pp. 363–396
- R.T. Pappalardo, S.D. Vance, F. Bagenal, B.G. Bills, D.L. Blaney, D.D. Blankenship, W.B. Brinckerhoff, J.E.P. Connerney, K.P. Hand, T.M. Hoehler et al., Science potential from a Europa lander. *Astrobiology* **13**(8), 740–773 (2013)
- C. Paranicas, J.F. Cooper, H.B. Garrett, R.E. Johnson, S.J. Sturmer, Europa's radiation environment and its effects on the surface, in *Europa* (University of Arizona Press, Tucson, 2009), pp. 529–544
- M.A. Pasek, R. Greenberg, Acidification of Europa's subsurface ocean as a consequence of oxidant delivery. *Astrobiology* **12**(2), 151–159 (2012)
- G.W. Patterson, G.C. Collins, J.W. Head, R.T. Pappalardo, L.M. Prockter, B.K. Lucchitta, J.P. Kay, Global geological mapping of Ganymede. *Icarus* **207**(2), 845–867 (2010)

- G.W. Patterson, S.A. Kattenhorn, P. Helfenstein, G.C. Collins, R.T. Pappalardo, The geology of Enceladus, in *Enceladus and the Icy Moons of Saturn* (University of Arizona Press, Tucson, 2018), pp. 95–126
- M. Pauer, S. Musiol, D. Breuer, Gravity signals on Europa from silicate shell density variations. *J. Geophys. Res., Planets* **115**(E12) (2010). <https://doi.org/10.1029/2010JE003595>
- D.A. Peddinti, A.K. McNamara, Dynamical investigation of a thickening ice-shell: Implications for the icy moon Europa. *Icarus* **329**, 251–269 (2019)
- J. Pedlosky, *Geophysical Fluid Dynamics* (Springer, New York, 1987)
- C.C. Porco, P. Helfenstein, P.C. Thomas, A.P. Ingersoll, J. Wisdom, R.A. West, G. Neukum, T. Denk, R. Wagner, T. Roatsch et al., Cassini observes the active south pole of Enceladus. *Science* **311**(5766), 1393–1401 (2006)
- C.C. Porco, D. DiNino, F. Nimmo, How the geysers, tidal stresses, and thermal emission across the south polar terrain of Enceladus are related. *Astron. J.* **148** (2014). <https://doi.org/10.1088/0004-6256/148/3/45>
- F. Postberg, S. Kempf, J. Hillier, R. Srama, S. Green, N. McBride, E. Grün, The E-ring in the vicinity of Enceladus: II. Probing the moon's interior—the composition of E-ring particles. *Icarus* **193**(2), 438–454 (2008). <https://doi.org/10.1016/j.icarus.2007.09.001>
- F. Postberg, S. Kempf, J. Schmidt, N. Brilliantov, A. Beinsen, B. Abel, U. Buck, R. Srama, Sodium salts in E-ring ice grains from an ocean below the surface of Enceladus. *Nature* **459**, 1098–1101 (2009). <https://doi.org/10.1038/nature08046>
- F. Postberg, J. Schmidt, J. Hillier, S.D. Kempf, R. Srama, A salt-water reservoir as the source of a compositionally stratified plume on Enceladus. *Nature* **474**(7353), 620 (2011)
- F. Postberg, R.N. Clark, C.J. Hansen, A.J. Coates, C.M.D. Ore, F. Scipioni, M.M. Hedman, J.H. Waite, Plume and surface composition of Enceladus, in *Enceladus and the Icy Moons of Saturn* (University of Arizona Press, Tucson, 2018a), pp. 129–162
- F. Postberg, N. Khawaja, B. Abel, G. Choblet, C.R. Glein, M.S. Gudipati, B.L. Henderson, H.W. Hsu, S. Kempf, F. Klenner, G. Moragas-Klostermeyer, B. Magee, L. Nölle, M. Perry, R. Reviol, J. Schmidt, R. Srama, F. Stolz, G. Tobie, M. Trieloff, J.H. Waite, Macromolecular organic compounds from the depths of Enceladus. *Nature* **558**, 564–568 (2018b). <https://doi.org/10.1038/s41586-018-0246-4>
- J.C. Priscu, B.C. Christner, Earth's icy biosphere, in *Microbial Diversity and Bioprospecting* (Am. Soc. Microbiol., Washington, 2004), pp. 130–145
- J.C. Priscu, C.H. Fritsen, E.E. Adams, S.J. Giovannoni, H.W. Paerl, C.P. McKay, P.T. Doran, D.A. Gordon, B.D. Lanoil, J.L. Pinckney, Perennial Antarctic lake ice: an oasis for life in a polar desert. *Science* **280**(5372), 2095–2098 (1998)
- L.M. Prockter, G.W. Patterson, Morphology and evolution of Europa's ridges and bands, in *Europa*, ed. by R.T. Pappalardo, W.B. McKinnon, K.K. Khurana (University of Arizona Press, Tucson, 2009), pp. 237–258
- L.M. Prockter, J.W. Head, R.T. Pappalardo, D.A. Senske, G. Neukum, R. Wagner, U. Wolf, J. Oberst, B. Giese, J.M. Moore et al., Dark terrain on Ganymede: geological mapping and interpretation of Galileo Regio at high resolution. *Icarus* **135**(1), 317–344 (1998)
- L.M. Prockter, P.H. Figueredo, R.T. Pappalardo, J.W. Head, G.C. Collins, Geology and mapping of dark terrain on Ganymede and implications for grooved terrain formation. *J. Geophys. Res., Planets* **105**(E9), 22519–22540 (2000)
- L.M. Prockter, J.W. Head III, R.T. Pappalardo, R.J. Sullivan, A.E. Clifton, B. Giese, R. Wagner, G. Neukum, Morphology of European bands at high resolution: a mid-ocean ridge-type rift mechanism. *J. Geophys. Res., Planets* **107**(E5), 4 (2002). <https://doi.org/10.1029/2000JE001458>
- L.C. Quick, B.D. Marsh, Heat transfer of ascending cryomagma on Europa. *J. Volcanol. Geotherm. Res.* **319**, 66–77 (2016). <https://doi.org/10.1016/j.jvolgeores.2016.03.018>
- L.C. Quick, L. Glaze, S.M. Baloga, Cryovolcanic emplacement of domes on Europa. *Icarus* **284**, 477–488 (2017). <https://doi.org/10.1016/j.icarus.2016.06.029>
- J.A. Rathbun, G.S.J. Musser, S.W. Squyres, Ice diapirs on Europa: implications for liquid water. *Geophys. Res. Lett.* **25**, 4157–4160 (1998)
- J. Requier, A. Trinh, S.A. Triana, V. Dehant, Internal energy dissipation in Enceladus's ocean from tides and libration and the role of inertial waves. *J. Geophys. Res., Planets* **124**, 2198–2212 (2019)
- R.T. Reynolds, S.W. Squyres, D.S. Colburn, C.P. McKay, On the habitability of Europa. *Icarus* **56**(2), 246–254 (1983)
- R.T. Reynolds, C.P. McKay, J.F. Kasting, Europa, tidally heated oceans, and habitable zones around giant planets. *Adv. Space Res.* **7**(5), 125–132 (1987)
- Y. Ricard, in *Physics of Mantle Convection. Treatise on Geophysics*, ed. by G. Schubert, D. Bercovici (Elsevier, Amsterdam, 2007), pp. 31–88
- M. Rieutord, Evolution of rotation in binaries: physical processes, in *Symposium-International Astronomical Union*, vol. 215 (Cambridge University Press, Cambridge, 2004), pp. 394–403

- M. Rieutord, B. Georgeot, L. Valdetaro, Inertial waves in a rotating spherical shell: attractors and asymptotic spectrum. *J. Fluid Mech.* **435**, 103–144 (2011)
- T. Roatsch, R. Jaumann, K. Stephan, P.C. Thomas, Cartographic mapping of the icy satellites using ISS and VIMS data, in *Saturn from Cassini-Huygens* (Springer, Berlin, 2009), pp. 763–781
- J.H. Roberts, The fluffy core of Enceladus. *Icarus* **258**, 54–66 (2015)
- J.H. Roberts, F. Nimmo, Tidal heating and the long-term stability of a subsurface ocean on Enceladus. *Icarus* **194**(2), 675–689 (2008)
- L. Roth, J. Saur, K.D. Retherford, D.F. Strobel, P.D. Feldman, M.A. McGrath, F. Nimmo, Transient water vapor at Europa's south pole. *Science* **343**(6167), 171–174 (2014). <https://doi.org/10.1126/science.1247051>
- M. Rovira-Navarro, M. Rieutord, T. Gerkema, L.R. Maas, W. van der Wal, B. Vermeersen, Do tidally-generated inertial waves heat the subsurface oceans of Europa and Enceladus? *Icarus* **321**, 126–140 (2019)
- T. Rückriemen, D. Breuer, T. Spohn, Top-down freezing in a Fe–FeS core and Ganymede's present-day magnetic field'. *Icarus* **307**, 172–196 (2018)
- M.J. Russell, A.E. Murray, K.P. Hand, The possible emergence of life and differentiation of a shallow biosphere on irradiated icy worlds: the example of Europa. *Astrobiology* **17**(12), 1265–1273 (2017)
- J. Saur, S. Duling, L. Roth, X. Jia, D.F. Strobel, P.D. Feldman, U.R. Christensen, K.D. Retherford, M.A. McGrath, F. Musacchio et al., The search for a subsurface ocean in Ganymede with Hubble Space Telescope observations of its auroral ovals. *J. Geophys. Res.* **120**(3), 1715–1737 (2015)
- P.M. Schenk, W.B. McKinnon, Fault offsets and lateral crustal movement on Europa: evidence for a mobile ice shell. *Icarus* **79**(1), 75–100 (1989). [https://doi.org/10.1016/0019-1035\(89\)90109-7](https://doi.org/10.1016/0019-1035(89)90109-7)
- P.M. Schenk, J.M. Moore, Volcanic constructs on Ganymede and Enceladus: Topographic evidence from stereo images and photoclinometry. *J. Geophys. Res., Planets* **100**(E9), 19009–19022 (1995)
- P.M. Schenk, E.P. Turtle, Europa's impact craters: probes of the icy shell, in *Europa*, ed. by R.T. Pappalardo, W.B. McKinnon, K.K. Khurana (University of Arizona Press, Tucson, 2009), pp. 181–198
- P.M. Schenk, W.B. McKinnon, D. Gwynn, J.M. Moore, Flooding of Ganymede's bright terrains by low-viscosity water-ice lavas. *Nature* **410**(6824), 57 (2001)
- P.M. Schenk, C.R. Chapman, K. Zahnle, J.M. Moore, Ages and interiors: the cratering record of the Galilean satellites, in *Jupiter: The Planet, Satellites and Magnetosphere*, vol. 2 (Cambridge University Press, Cambridge, 2004), p. 427
- N. Schilling, F.M. Neubauer, J. Saur, Time-varying interaction of Europa with the Jovian magnetosphere: constraints on the conductivity of Europa's subsurface ocean. *Icarus* **192**, 41–55 (2007)
- B.E. Schmidt, The astrobology of Europa and the Jovian Moons, in *Planetary Astrobiology*, ed. by V.S. Meadows, G. Arney, D. DesMarais, B.E. Schmidt (University of Arizona Press, Tucson, 2020), p. 185
- J. Schmidt, N. Brilliantov, F. Spahn, S. Kempf, Slow dust in Enceladus' plume from condensation and wall collisions in tiger stripe fractures. *Nature* **451**, 685–688 (2008). <https://doi.org/10.1038/nature06491>
- B.E. Schmidt, D.D. Blankenship, G.W. Patterson, P.M. Schenk, Active formation of chaos terrain over shallow subsurface water on Europa. *Nature* **479**, 502–505 (2011)
- B.E. Schmidt, J.D. Lawrence, M.R. Meister, D.J.G. Dicheck, B.C. Hurwitz, A. Spears, A.D. Mullen, P.M. Washam, F.E. Bryson, E. Quartini et al., Europa in our backyard: under ice robotic exploration of Antarctic analogs *LPI Contrib.* **2326**, 1065 (2020)
- R.W. Schmitt, Double diffusion in oceanography. *Annu. Rev. Fluid Mech.* **26**(1), 255–285 (1994)
- G. Schubert, J.D. Anderson, T. Spohn, W.B. McKinnon, Interior composition, structure and dynamics of the Galilean satellites, in *Jupiter: The Planet, Satellites and Magnetosphere*, (2004), pp. 281–306
- F. Scipioni, P. Schenk, F. Tosi, E. D'Aversa, R. Clark, J.P. Combe, C.D. Ore, Deciphering sub-micron ice particles on Enceladus surface. *Icarus* **290**, 183–200 (2017). <https://doi.org/10.1016/j.icarus.2017.02.012>
- Y. Sekine, T. Shibuya, F. Postberg, H.W. Hsu, K. Suzuki, Y. Masaki, T. Kuwatani, M. Mori, P.K. Hong, M. Yoshizaki, S. Tachibana, S. Sirono, High-temperature water-rock interactions and hydrothermal environments in the chondrite-like core of Enceladus. *Nat. Commun.* **6**, 8604 (2015). <https://doi.org/10.1038/ncomms9604>
- L.E. Senft, S.T. Stewart, Modeling the morphological diversity of impact craters on icy satellites. *Icarus* **214**, 67–81 (2011). <https://doi.org/10.1016/j.icarus.2011.04.015>
- SESAME program selections, Scientific Exploration Subsurface Access Mechanism for Europa (SESAME) Abstracts of selected proposals (NNH18ZDA001N) (2019). <https://nspires.nasaprs.com/external/viewrepositorydocument/cmdocumentid=664490/solicitationId=%7B24ACEF00-C2AE-6179-001F-C9E1BB025436%7D/viewSolicitationDocument=1/SESAME%20Abstracts.pdf>
- M. Seufert, J. Saur, F.M. Neubauer, Multi-frequency electromagnetic sounding of the Galilean moons. *Icarus* **214**(2), 477–494 (2011)

- T. Shank, C. German, C. Machado, A. Bowen, J. Drazen, P. Yancey, A. Jamieson, A. Rowden, M. Clark, T. Heyl et al., Ocean worlds analog systems in the hadal ocean: systematic examination of pressure, food supply, topography, and evolution on hadal life, in *Ocean Worlds*, vol. 2085 (2018)
- E.M. Shoemaker, B.K. Lucchitta, D.E. Wilhelms, J.B. Plescia, S.W. Squyres, The geology of Ganymede, in *Satellites of Jupiter*, ed. by D. Morrison (University of Arizona Press, Tucson, 1982), pp. 435–520
- A.P. Showman, R. Malhotra, Tidal evolution into the Laplace resonance and the resurfacing of Ganymede. *Icarus* **127**(1), 93–111 (1997). <https://doi.org/10.1006/icar.1996.5669>
- S.E. Smrekar, P. Lognonné, T. Spohn, W.B. Banerdt, D. Breuer, U. Christensen, V. Dehant, M. Drilleau, W. Folkner, N. Fuji et al., Pre-mission InSights on the interior of Mars. *Space Sci. Rev.* **215**(1) (2018). <https://doi.org/10.1007/s11214-018-0563-9>
- K.M. Soderlund, Ocean dynamics of outer solar system satellites. *Geophys. Res. Lett.* **46**(15), 8700–8710 (2019)
- K.M. Soderlund, M.H. Heimpel, E.M. King, J.M. Aurnou, Turbulent models of ice giant internal dynamics: dynamos, heat transfer, and zonal flows. *Icarus* **224**, 97–113 (2013)
- K.M. Soderlund, B.E. Schmidt, J. Wicht, D.D. Blankenship, Ocean-driven heating of Europa's icy shell at low latitudes. *Nat. Geosci.* **7**, 16–19 (2014)
- F. Sohl, T. Spohn, D. Breuer, K. Nagel, Implications from Galileo observations on the interior structure and chemistry of the Galilean satellites. *Icarus* **157**, 104–119 (2002)
- F. Sohl, H. Hussmann, B. Schwentker, T. Spohn, R.D. Lorenz, Interior structure models and tidal Love numbers of Titan. *J. Geophys. Res., Planets* **108**(E12), 5130 (2003)
- C. Sotin, J.W. Head, G. Tobie, Tidal heating of upwelling thermal plumes and the origin of lenticulae and chaos melting. *Geophys. Res. Lett.* **29**(8), 1233 (2002). <https://doi.org/10.1029/2001GL013884>
- C. Sotin, G. Tobie, J. Wahr, W.B. McKinnon, Tides and tidal heating on Europa, in *Europa*, ed. by R.T. Pappalardo, W.B. McKinnon, K.K. Khurana (University of Arizona Press, Tucson, 2009)
- O. Souček, J. Hron, M. Běhounková, O. Čadek, Effect of the tiger stripes on the deformation of Saturn's moon Enceladus. *Geophys. Res. Lett.* **43**(14), 7417–7423 (2016). <https://doi.org/10.1002/2016GL069415>
- O. Souček, M. Běhounková, O. Čadek, J. Hron, G. Tobie, G. Choblet, Tidal dissipation in Enceladus' uneven, fractured ice shell. *Icarus* **328**, 218–231 (2019). <https://doi.org/10.1016/j.icarus.2019.02.012>
- B.S. Southworth, S. Kempf, J. Schmidt, Modeling Europa's dust plumes. *Geophys. Res. Lett.* **42**(24), 10,541–10,548 (2015). <https://doi.org/10.1002/2015GL066502>
- B.S. Southworth, S. Kempf, J. Spitale, Surface deposition of the Enceladus plume and the zenith angle of emissions. *Icarus* **319**, 33–42 (2019). <https://doi.org/10.1016/j.icarus.2018.08.024>
- F. Spahn, J. Schmidt, N. Albers, M. Hörning, M. Makuch, M. Seiß, S. Kempf, R. Srama, V. Dikarev, S. Helfert, G. Moragas-Klostermeyer, A.V. Krivov, M. Sremčević, A.J. Tuzzolino, T. Economou, E. Grün, Cassini dust measurements at Enceladus and implications for the origin of the E ring. *Science* **311**(5766), 1416–1418 (2006). <https://doi.org/10.1126/science.1121375>
- W.B. Sparks, K.P. Hand, M.A. McGrath, E. Bergeron, M. Cracraft, S.E. Deustua, Probing for evidence of plumes on Europa with HST/STIS. *Astrophys. J.* **829**(2), 121 (2016)
- W.B. Sparks, B.E. Schmidt, M.A. McGrath, K.P. Hand, J.R. Spencer, M. Cracraft, S.E. Deustua, Active cryovolcanism on Europa? *Astrophys. J. Lett.* **839**(2), L18 (2017)
- N.A. Spaun, J.W. Head, G.C. Collins, L.M. Prockter, R.T. Pappalardo, Conamara Chaos Region, Europa: reconstruction of mobile polygonal ice blocks. *Geophys. Res. Lett.* **25**(23), 4277–4280 (1998)
- N.A. Spaun, J.W. Head, R.T. Pappalardo et al. (GS Team), Scalloped depressions on Ganymede from Galileo (G28) very high resolution imaging, in *Lunar and Planetary Science Conference*, vol. 32 (2001)
- J.R. Spencer, F. Nimmo, A.P. Ingersoll, T.A. Hurford, E.S. Kite, A.R. Rhoden, J. Schmidt, C.J.A. Howett, Plume origins and plumbing: from ocean to surface, in *Enceladus and the Icy Moons of Saturn* (University of Arizona Press, Tucson, 2018), pp. 163–174
- J.N. Spitale, T.A. Hurford, A.R. Rhoden, E.E. Berkson, S.S. Platts, Curtain eruptions from Enceladus' south-polar terrain. *Nature* **521**, 57–60 (2015). <https://doi.org/10.1038/nature14368>
- T. Spohn, G. Schubert, Oceans in the icy Galilean satellites of Jupiter? *Icarus* **161**(2), 456–467 (2003)
- G. Steinbrügge, D.M. Schroeder, M.S. Haynes, H. Hussmann, C. Grima, D.D. Blankenship, Assessing the potential for measuring Europa's tidal Love number  $h_2$  using radar sounder and topographic imager data. *Earth Planet. Sci. Lett.* **482**, 334–341 (2018)
- W.C. Stone, B. Hogan, V. Siegel, S. Lelievre, C. Flesher, Progress towards an optically powered cryobot. *Ann. Glaciol.* **55**(65), 2–13 (2014)
- R. Sullivan, R. Greeley, K. Homan, J. Klemaszewski, M.J.S. Belton, M.H. Carr, C.R. Chapman, R. Tufts, J.W. Head, R. Pappalardo, J. Moore, P. Thomas (the Galileo Imaging Team), Episodic plate separation and fracture infill on the surface of Europa. *Nature* **391**, 371–373 (1998). <https://doi.org/10.1038/34874>
- R. Tajeddine, K.M. Soderlund, P.C. Thomas, P. Helfenstein, M.M. Hedman, J.A. Burns, P.M. Schenk, True polar wander of Enceladus from topographic data. *Icarus* **295**, 46–60 (2017)

- R.S. Taubner, K. Olsson-Francis, S.D. Vance, N.K. Ramkissoon, F. Postberg, J.P. de Vera, A. Antunes, E.C. Casas, Y. Sekine, L. Noack et al., Experimental and simulation efforts in the astrobiological exploration of exoceans. *Space Sci. Rev.* **216**(1), 9 (2020)
- B.D. Teolis, M.E. Perry, C.J. Hansen, J.H. Waite, C.C. Porco, J.R. Spencer, C.J.A. Howett, Enceladus plume structure and time variability: comparison of Cassini observations. *Astrobiology* **17**(9), 926–940 (2017). <https://doi.org/10.1089/ast.2017.1647>
- P.C. Thomas, J.A. Burns, P. Helfenstein, S. Squyres, J. Veverka, C. Porco, E.P. Turtle, A. McEwen, T. Denk, B. Giese et al., Shapes of the saturnian icy satellites and their significance. *Icarus* **190**(2), 573–584 (2007)
- P.C. Thomas, R. Tajeddine, M.S. Tiscareno, J.A. Burns, J. Joseph, T.J. Loredò, P. Helfenstein, C.C. Porco, Enceladus's measured physical libration requires a global subsurface ocean. *Icarus* **264**, 37–47 (2016)
- R.E. Thomson, J.R. Delaney, Evidence for a weakly stratified European ocean sustained by seafloor heat flux. *J. Geophys. Res.* **106**, 12355–12365 (2001)
- G. Tobie, G. Choblet, C. Sotin, Tidally heated convection: constraints on Europa's ice shell thickness. *J. Geophys. Res.* **108**(E11), 5124 (2003). <https://doi.org/10.1029/2003JE002099>
- G. Tobie, O. Grasset, J.I. Lunine, A. Mocquet, C. Sotin, Titan's internal structure inferred from a coupled thermal-orbital model. *Icarus* **175**(2), 496–502 (2005). <https://doi.org/10.1016/j.icarus.2004.12.007>
- G. Tobie, J.I. Lunine, C. Sotin, Episodic outgassing as the origin of atmospheric methane on Titan. *Nature* **440**(7080), 61 (2006)
- G. Tobie, O. Čadež, C. Sotin, Solid tidal friction above a liquid water reservoir as the origin of the south pole hotspot on Enceladus. *Icarus* **196**(2), 642–652 (2008)
- B.J. Travis, J. Palguta, G. Schubert, A whole-moon thermal history model of Europa: impact of hydrothermal circulation and salt transport. *Icarus* **218**, 1006–1019 (2012)
- S.K. Trumbo, M. Brown, K.P. Hand, Sodium chloride on the surface of Europa. *Sci. Adv.* **5**(6), eaaw7123 (2019)
- B. Tufts, R. Greenberg, G. Hoppa, P. Geissler, Lithospheric dilation on Europa. *Icarus* **146**(1), 75–97 (2000). <https://doi.org/10.1006/icar.2000.6369>
- E.P. Turtle, Finite-element modeling of large impact craters: Implications for the size of the Vredefort structure and the formation of multiple ring craters. Ph.D. dissertation, Univ. of Arizona, Tucson (1998)
- E.P. Turtle, E. Pierazzo, Thickness of a European ice shell from impact crater simulations. *Science* **294**, 1326–1328 (2001). <https://doi.org/10.1126/science.1062492>
- E.P. Turtle, H.J. Melosh, C.B. Phillips, Tectonic modeling of the formation of European ridges, in *EOS Trans. AGU*, vol. 79 (1998), p. F541
- E.P. Turtle, J.W. Barnes, M.G. Trainer, R.D. Lorenz, S.M. MacKenzie, K.E. Hibbard, et al. Dragonfly: exploring Titan's prebiotic organic chemistry and habitability. *LPI Contrib.* **1964**, 1958 (2017)
- R.H. Tyler, Strong ocean tidal flow and heating on moons of the outer planets. *Nature* **456**, 770–773 (2008)
- R.H. Tyler, Ocean tides heat Enceladus. *Geophys. Res. Lett.* **36**(15), L15205 (2009). <https://doi.org/10.1029/2009GL038300>
- R.H. Tyler, Comparative estimates of the heat generated by ocean tides on icy satellites in the outer Solar System. *Icarus* **243**(Suppl. C), 358–385 (2014). <https://doi.org/10.1016/j.icarus.2014.08.037>
- T. Van Hoolst, R.M. Baland, A. Trinh, The diurnal libration and interior structure of Enceladus. *Icarus* **277**, 311–318 (2016)
- S.D. Vance, J.M. Brown, Layering and double-diffusion style convection in Europa's ocean. *Icarus* **177**, 506–514 (2005)
- S.D. Vance, J.M. Brown, Thermodynamic properties of aqueous MgSO<sub>4</sub> to 800 MPa at temperatures from –20 to 100 °C and concentrations to 2.5 mol kg<sup>–1</sup> from sound speeds, with applications to icy world oceans. *Geochim. Cosmochim. Acta* **110**, 176–189 (2013)
- S.D. Vance, J.C. Goodman, The structure and evolution of Europa's ocean and ice shell in the presence of aqueous MgSO<sub>4</sub>. *LPI Contrib.* **1719**, 1877 (2013)
- S.D. Vance, M. Melwani Daswani, Serpentine and the search for life beyond Earth. *Philos. Trans. - Royal Soc., Math. Phys. Eng. Sci.* **378**(2165), 20180421 (2020). <https://doi.org/10.1098/rsta.2018.0421>
- S.D. Vance, J. Harnmeijer, J. Kimura, H. Hussmann, B. DeMartin, J.M. Brown, Hydrothermal systems in small ocean planets. *Astrobiology* **7**(6), 987–1005 (2007)
- S.D. Vance, M. Bouffard, M. Choukroun, C. Sotin, Ganymede's internal structure including thermodynamics of magnesium sulfate oceans in contact with ice. *Planet. Space Sci.* **96**, 62–70 (2014)
- S.D. Vance, K.P. Hand, R.T. Pappalardo, Geophysical controls of chemical disequilibria in Europa. *Geophys. Res. Lett.* **43**(10), 4871–4879 (2016)
- S.D. Vance, S. Kedar, M.P. Panning, S.C. Stähler, B.G. Bills, R.D. Lorenz, H.H. Huang, W.T. Pike, J.C. Castillo, P. Lognonné et al., Vital signs: seismology of icy ocean worlds. *Astrobiology* **18**(1), 37–53 (2018). <https://doi.org/10.1089/ast.2016.1612>

- S.D. Vance, M.P. Panning, S. Stahler, F. Cammarano, B.G. Bills, G. Tobie, S. Kamata, S. Kedar, C. Sotin, W.T. Pike, R.D. Lorenz, H.H. Huang, J.M. Jackson, B. Banerdt, Geophysical investigations of habitability in ice-covered ocean worlds. *J. Geophys. Res.* **123**, 180–205 (2018)
- S.D. Vance, L.M. Barge, S.S.S. Cardoso, J.H.E. Cartwright, Self-assembling ice membranes on Europa: brinicle properties, field examples, and possible energetic systems in icy ocean worlds. *Astrobiology* **19**(5), 685–695 (2019)
- A.K. Verma, J.L. Margot, Expected precision of Europa Clipper gravity measurements. *Icarus* **314**, 35–49 (2018)
- T.H. Vu, R. Hodyss, M. Choukroun, P.V. Johnson, Chemistry of frozen sodium–magnesium–sulfate–chloride brines: implications for surface expression of Europa’s ocean composition. *Astrophys. J. Lett.* **816**(2), L26 (2016)
- J.H. Waite, H. Niemann, R.V. Yelle, W.T. Kasprzak, T.E. Cravens, J.G. Luhmann, R.L. McNutt, W.H. Ip, D. Gell, V. De La Haye, I. Müller-Wodarg, B. Magee, N. Borggren, S. Ledvina, G. Fletcher, E. Walter, R. Miller, S. Scherer, R. Thorpe, J. Xu, B. Block, K. Arnett, Ion neutral mass spectrometer results from the first flyby of Titan. *Science* **308**(5724), 982–986 (2005). <https://doi.org/10.1126/science.1110652>
- J.H. Waite, M.R. Combi, W.H. Ip, T.E. Cravens, R.L. McNutt, W.T. Kasprzak, R.V. Yelle, J.G. Luhmann, H.B. Niemann, D. Gell, B.A. Magee, Cassini ion and neutral mass spectrometer: Enceladus plume composition and structure. *Science* **311**(5766), 1419–1422 (2006)
- J.H. Waite, W.S. Lewis, B.A. Magee, J.I. Lunine, W.B. McKinnon, C.R. Glein, O. Mousis et al., Liquid water on Enceladus from observations of ammonia and 40 ar in the plume. *Nature* **460**(7254), 487 (2009)
- J.H. Waite, C.R. Glein, R.S. Perryman, B.D. Teolis, B.A. Magee, G. Miller, J. Grimes, M.E. Perry, K.E. Miller, A. Bouquet, J.I. Lunine, T. Brockwell, S.J. Bolton, Cassini finds molecular hydrogen in the Enceladus plume: evidence for hydrothermal processes. *Science* **356**(6334), 155–159 (2017). <https://doi.org/10.1126/science.aai8703>
- C.C. Walker, B.E. Schmidt, Ice collapse over trapped water bodies on Enceladus and Europa. *Geophys. Res. Lett.* **42**(3), 712–719 (2015). <https://doi.org/10.1002/2014GL062405>
- S.G. Warren, R.E. Brandt, T.C. Grenfell, C.P. McKay, Snowball Earth: ice thickness on the tropical ocean. *J. Geophys. Res.* **107**(C10), 3167 (2002)
- J. Weertman, On the sliding of glaciers. *J. Glaciol.* **3**(21), 33–38 (1957)
- M.B. Weller, L. Fuchs, T.W. Becker, K.M. Soderlund, Convection in thin shells of icy satellites: effects of latitudinal surface temperature variations. *J. Geophys. Res., Planets* (2019). <https://doi.org/10.1029/2018JE005799>
- E.H. Wilson, S.K. Atreya, Sensitivity studies of methane photolysis and its impact on hydrocarbon chemistry in the atmosphere of Titan. *J. Geophys. Res., Planets* **105**(E8), 20263–20273 (2000). <https://doi.org/10.1029/1999JE001221>
- A. Wilson, R.R. Kerswell, Can libration maintain Enceladus’s ocean? *Earth Planet. Sci. Lett.* **500**, 41–46 (2018). <https://doi.org/10.1016/j.epsl.2018.08.012>
- T.W. Wilson, L.A. Ladino, P.A. Alpert, M.N. Breckels, I.M. Brooks, J. Browse, S.M. Burrows, K.S. Carlsaw, J.A. Huffman, C. Judd, W.P. Kilhau, R.H. Mason, G. McFiggans, L.A. Miller, J.J. Nájera, E. Polishchuk, S. Rae, C.L. Schiller, M. Si, J.V. Temprado, T.F. Whale, J.P.S. Wong, O. Wurl, J.D. Yakobi-Hancock, J.P.D. Abbatt, J.Y. Aller, A.K. Bertram, D.A. Knopf, B.J. Murray, A marine biogenic source of atmospheric ice-nucleating particles. *Nature* **525**, 234–238 (2015). <https://doi.org/10.1038/nature14986>
- D.P. Winebrenner, W.T. Elam, P.M.S. Kintner, S. Tyler, J.S. Selker, Clean, logistically light access to explore the closest places on Earth to Europa and Enceladus, in *AGU Fall Meeting Abstracts* (2016)
- S.K. Yeoh, T.A. Chapman, D.B. Goldstein, P.L. Varghese, L.M. Trafton, On understanding the physics of the Enceladus south polar plume via numerical simulation. *Icarus* **253**, 205–222 (2015). <https://doi.org/10.1016/j.icarus.2015.02.020>
- K. Zaeny, J. Mueller, T. Costa, T. Cwik, A. Gray, W. Zimmerman, P. Chow, F. Rehnmark, G. Adams, SLUSH: Europa hybrid deep drill, in *2018 IEEE Aerospace Conference* (IEEE Press, New York, 2018), pp. 1–14
- K.J. Zahnle, D.G. Korycansky, C.A. Nixon, Transient climate effects of large impacts on Titan. *Icarus* **229**, 378–391 (2014). <https://doi.org/10.1016/j.icarus.2013.11.006>
- P. Zhu, G.E. Manucharyan, A.F. Thompson, J.C. Goodman, S.D. Vance, The influence of meridional ice transport on Europa’s ocean stratification and heat content. *Geophys. Res. Lett.* **44**, 5969–5977 (2017). <https://doi.org/10.1002/2017GL072996>
- C. Zimmer, K.K. Khurana, M.G. Kivelson, Subsurface oceans on Europa and Callisto: constraints from Galileo magnetometer observations. *Icarus* **147**, 329–347 (2000)
- M.Y. Zolotov, Aqueous fluid composition in CI chondritic materials: chemical equilibrium assessments in closed systems. *Icarus* **220**(2), 713–729 (2012)
- M.Y. Zolotov, J.S. Kargel, On the chemical composition of Europa’s icy shell, ocean, and underlying rocks, in *Europa*, vol. 431 (University of Arizona Press, Tucson, 2009)

- M.Y. Zolotov, E. Shock, Composition and stability of salts on the surface of Europa and their oceanic origin. *J. Geophys. Res.* **106**(E12), 32815–32827 (2001)
- M.Y. Zolotov, E.L. Shock, Energy for biologic sulfate reduction in a hydrothermally formed ocean on Europa. *J. Geophys. Res., Planets* **108**(E4) (2003). <https://doi.org/10.1029/2002JE001966>
- M.Y. Zolotov, E.L. Shock, A model for low-temperature biogeochemistry of sulfur, carbon, and iron on Europa. *J. Geophys. Res., Planets* **109**(E6) (2004). <https://doi.org/10.1029/2003JE002194>
- I.A. Zotikov, V.S. Zagorodnov, J.V. Raikovsky, Core drilling through the Ross Ice Shelf (Antarctica) confirmed basal freezing. *Science* **207**(4438), 1463–1465 (1980)